Decision Feedback Scheme for Spatial Modulation

by

Mir Rejaul Karim

B.Sc. (Electrical Engineering), Islamic University of Technology, 2015

Thesis Submitted in Partial Fulfillment of the
Requirements for the Degree of
Master of Applied Science

in the
School of Engineering Science
Faculty of Applied Sciences

SIMON FRASER UNIVERSITY
Spring 2019

Approval

Name:	**Mir Rejaul Karim**
Degree:	**Master of Applied Science**
Title:	**Decision Feedback Scheme for Spatial Modulation**
Examining Committee:	**Chair:** **Parvaneh Saeedi** Associate Professor
	Paul Ho Senior Supervisor Professor
	Rodney Vaughan Supervisor Professor
	Daniel Lee Internal Examiner Professor
Date Defended/Approved:	January 25, 2019

Abstract

Spatial Modulation (SM) is a newly developed Multiple Input Multiple Output (MIMO) technique where the antenna/spatial constellation is used as an information carrying unit in addition to the modulation constellation. Traditional SM techniques rely on periodic insertion of the pilot symbols to estimate the channel state information; however, it reduces the effective throughput. A differential SM (DSM) technique was developed to circumvent the need of channel estimation altogether. However, the computational complexity of the DSM increases exponentially with the increase of antennas and becomes impractical even for a moderate antenna array. In this scenario a novel clustering based decision feedback (CB-DFB) scheme is proposed in this thesis which similar to DSM does not require any pilot symbols, and yet has a very low complexity. A generalized CB-DFB scheme is later proposed which further overcomes the constraints of traditional SM techniques and increases the overall throughput.

Keywords: Spatial Modulation; Clustering; Decision Feedback; Maximum Likelihood

Acknowledgements

I would like to express my deepest gratitude to my senior supervisor, Dr. Paul Ho, for his patient guidance and counselling throughout my master studies. I have learnt so much from him during this duration which has helped me not only in my academic life but also to grow as a person. I would like to thank my supervisor, Dr. Rodney Vaughan, for his time to time guidance and for keeping me up to date with the innovations and technologies happening in the telecom industry. Special thanks to Dr. Daniel Lee for examining and reviewing this thesis, and Dr. Parvaneh Saeedi for chairing the thesis defense.

In addition, thanks to my lovely wife who has been with me throughout this journey. Without her constant support, love, and care, I would not be where I am today.

Table of Contents

List of Tables

List of Figures

List of Acronyms

5G	Fifth Generation
ABER	Average Bit Error Rate
AWGN	Additive White Gaussian Noise
BEP	Bit Error Probability
BER	Bit Error Rate
BS	Base Stations
BTS	Base Transceiver Station
CA	Clustering Algorithm
CB	Clustering Based
CDF	Cumulative Density Function
CIR	Channel Impulse Response
CSI	Channel State Information
DFB	Decision Feedback
DSM	Differential Spatial Modulation
EE	Energy Efficiency
GDFB	Generalized Decision Feedback
IAS	Inter Antenna Synchronization
ICI	Inter-channel Interference
IID	Independent and Identically Distributed
LTE	Long-Term Evolution
LTE-A	Long Term Evolution-Advanced
MAD	Multiply And Add
MIMO	Multiple-Input-Multiple-Output
ML	Maximum Likelihood
MLE	Maximum Likelihood Estimation
MRC	Maximum Ratio Combining
MSE	Mean Squared Error
NC	Non Coherent
NMSE	Normalized Mean Squared Error
PDF	Probability Density Function

PEP	Pairwise Error Probability
PSK	Phase Shift Keying
PSM	Pilot-aided Spatial Modulation
QoS	Quality of Service
RA	Receive Antenna
RF	Radio Frequency
S/P	Serial to Parallel
SISO	Single Input Single Output
SM	Spatial Modulation
SNR	Signal to Noise Ratio
SSK	Space Shift Keying
TA	Transmit Antenna
WiMAX	Worldwide Interoperability for Microwave Access

List of Symbols

Symbol	Definition
$\mathbf{H}$	$N_r \times N_t$ Channel Matrix
$\lvert\ \rvert$	Absolute Value
$\arg\max(\cdot)$	Argument of the Maxima
$\arg\min(\cdot)$	Argument of the Minima
avg	Average
$\log_2$	Binary Logarithm
N_B	Block Size
σ_h^2	Channel Variance
$\mathbf{h}$	Channel Vector
eff	Effective
$\hat{x}$	Estimate of x
$E(\cdot)$	Expected Value
$x!$	Factorial of x
$\lfloor \cdot \rfloor$	Floor Operation
iff	If and Only If
$\mathrm{Im}\{\cdot\}$	Imaginary part of a complex number
$(\cdot)^H$	Hermitian Transpose
min	Minimum
$\mathbf{N}$	Noise Matrix
σ_n^2	Noise Variance
$\mathbf{n}$	Noise Vector
$\binom{n}{\alpha}$	Number of Combinations of the Elements of Vector n taken α at a time
N_I	Number of Iterations
N_{MAD}	Number of Multiply And Add

N_r	Number of Receive Antennas
N_t	Number of Transmit Antennas
$P_{e,bit}$	Probability of Bit Error Rate
$\mathrm{Re}\{\cdot\}$	Real Part of a Complex Number
R_x	Receive Antenna
$\mathbf{Y}$	Received Signal Matrix
$\|\cdot\|_F$	Frobenius Norm
$\mathbf{y}$	Received Signal Vector
SW	RF Switch
S	Set of Modulation Symbols
M	Size of Modulation Constellation
η	Throughput
$trace(x)$	Sum of the diagonal elements of matrix x
B	Total Number of Bit Per Encoding Block
T_x	Transmit Antenna
σ_e^2	Variance of Error

Chapter 1.

Introduction

Mobile communication has been one of the most successful technological innovations in modern history. The main challenge of future mobile communication is to achieve a balance between throughput and energy efficiency. The increasing energy cost and carbon footprint of operational cellular network has motivated both network operators and regulatory bodies to develop innovative solutions for improving energy efficiency in cellular systems. Since throughput is directly linked to the notion of Shannon Capacity [1], it has been considered the key performance indictor fueling the design and optimization of wireless communication systems until recently. This resulted in the design of most of the transmission technologies which is based on diverse factors, such as throughput, QoS, availability, scalability etc., without paying specific attention to energy consumption. These transmission schemes can only achieve energy savings at the cost of severe performance or throughput degradation. Therefore, it is still paramount to have a power efficient, low-complexity scheme that also satisfies the target throughput requirements.

WiMAX and LTE-A physical layer standards heavily depend on the use of MIMO technology to achieve their desired output. Future wireless communications systems including the 5G cellular networks will also rely on MIMO communications techniques. Large scale antenna system or massive MIMO has been considered as one of the core technologies for the upcoming 5G standard [2]. In simple terms, the capacity of MIMO systems is proportional to $\min\{N_t, N_r\}$ under favorable propagation conditions [3], where N_t is the number of transmit antennas and N_r is the number of receive antennas. However, the theoretical limit can only be achieved provided that the channel information is available in both the transmitter and receiver side, the transmit-receive links are satisfactorily independent, and also the Signal to Noise Ratio (SNR) needs to be sufficiently high [3]. Under those favorable conditions the throughput may be increased

linearly by increasing the number of antennas. As a result, the MIMO techniques can provide high data rates without increasing the spectrum utilization and transmit power.

However, in practice, MIMO systems needs a combination of associative circuits such as power amplifiers, RF chains, mixers, synthesizers, filters etc., which significantly increase the circuit power dissipation at the base stations (BS) [4]. This indicates that the design of energy efficient MIMO communications systems for multi user multicell network is a reasonably open research problem. Hence, while the throughput of MIMO communications is widely recognized, the energy efficiency (EE) potential of MIMO communications is still a challenge [5]. Hereafter, new transmission techniques have to be developed that are capable of creating an attractive trade-off between throughput and energy efficiency, rather than aiming for throughput optimization only.

1.1. From MIMO to SM

In MIMO all the transmit antennas are active at any time instant. Both multiplexing and transmit diversity gains can be obtained using MIMO techniques by appropriately choosing the transmission/precoding matrices. Activating all the antennas at the same time provides a high throughput but this doesn't necessarily lead to EE. In comparison with single antenna transmission system, MIMO achieves higher data rates and improved error performance at the cost of the following things. It increases the signal processing complexity which is caused by simultaneously transmitting many data streams. It requires a more rigorous synchronization among the transmit antennas (TA) to exploit the benefit of space-time coded and multiuser MIMO transmissions. MIMO needs multiple RF chains at the transmitter to be able to simultaneously transmit many data streams, which do not goes with Moore's Law and make the transmitter bulky [6]. It also requires independent power amplifiers for each RF chain, which dissipate majority of the power consumed at the transmitter, since they are power inefficient due to stringent linearity requirements of the state-of-the-art phase/amplitude modulations [4].

Summarizing, the common pitfalls among MIMO systems are[7]

I. Inter-channel Interference (ICI): This is introduced by superimposing independent information sequence to be transmitted by multiple antennas.

II. Inter-Antenna Synchronization (IAS): In the Vertical Bell Laboratories layered space time (V-BLAST) [8] and Orthogonal Space Time Block Codes (OSTBC) [9] architectures it is assumed that all symbols are transmitted at the same time. That makes IAS a fundamental requirement to avoid performance degradation which results in making increased transmitter overhead [10].

III. Radio Frequency (RF) chains: The inexpensiveness of deploying multiple antenna elements and the feasibility of the required digital signal processing made possible by increasing industrial growth has made us go towards MIMO. But the necessary RF elements are not as simple to implement [11]. The required RF chains are bulky and expensive.

Furthermore, several transceiver designs require the number of receive antennas to be greater than the number of transmit antennas, which could be a limiting factor due to economical reasons on mobile handsets. These issues make the practical implementations of MIMO schemes demanding, especially in mobile stations as the necessary hardware and digital signal processing require significant energy.

This shows a major challenge for next generation MIMO aided cellular networks, as it needs to design multiantenna transmission schemes with a limited number of active RF chains aiming for reducing the complexity, to relax inter antenna synchronization requirements, and inter channel interference, as well as the signal processing complexity at the receiver, while aiming for improving the EE. At this point, single-RF MIMO design is emerging as a strong contender [6]. The main idea behind the single-RF MIMO is to realize the gains of MIMO communications with the aid of many antenna elements, of which a single or at most a few antenna elements are active at the transmitter at any modulation instant [12]. The motivation behind the multi-RF to single-RF shift in MIMO

design originates from the consideration that large number of TAs may be accommodated at the BSs bearing in mind that the complexity and power consumption of MIMO communications are mainly determined by the number of simultaneously 'active' TAs, i.e., by the number of active RF chains[13].

Considering these factors Spatial Modulation (SM) has recently established itself as a promising concept which belongs to the single-RF large scale MIMO wireless systems family, while exploiting the multiple antennas in a novel fashion compared to the state-of-the-art high complexity and power hungry classic MIMOs [14].

1.2. Spatial Modulation Techniques

The spatial modulation (SM) principle is known in the literature in various forms, such as Information Guided Channel Hopping (IGCH) [15], Spatial Modulation (SM) [16], Space Shift Keying (SSK) [17] , Quadrature Space Shift Keying [18], Space Time Block Coded Spatial Modulation (STBC-SM) [19] and Differential Spatial Modulation (DSM) [20]. Although different from one another all this transmission technologies share the same fundamental working principle, which makes them unique with respect to conventional modulation schemes.

1.2.1. Space Shift Keying (SSK)

SSK is the simplest form of spatial modulation techniques even though it was proposed after SM [16]. In SSK modulation technique, the spatial domain is solely exploited to convey information [7], [21]. SSK modulation exploits the location specific property of the wireless channel for data modulation, meaning the data are transmitted through spatial symbols only, and the transmitted signal is unmodulated RF signal considered to indicate the spatial index of the active transmit antenna. In SSK, only one antenna remains active during transmission hence only one RF chain is required for the data transmission. The main idea here is the transmitted symbol itself doesn't contain any information rather the location of the transmit antenna carries information. As only one antenna remains active during transmission, the receiver sees a different Channel Impulse

Response (CIR) on any transmit to receive wireless link [21]. It has been shown that the CIRs are the points of the spatial-constellation diagram, and that the Bit Error Probability (BEP) depends on the distance among these points [17]. An example of SSK modulation for 1 bit/interval transmission for a two transmit antenna system is given by Table 1.1 [7].

Antenna/Spatial bit	Active Antenna Index	Modulation bit	Modulation symbol	Equivalent Signal Vector
0	1	0	+1	$[+1 \quad 0]^T$
1	2	0	+1	$[0 \quad +1]^T$

Table 1.1: Example of SSK Mapper Rule

In this simple SSK scheme, there is one information bit being transmitted per modulation interval and this bit, called the antenna/spatial bit, is used to select which of the two antennas to activate. Given that there are two available antennas, so the signal vectors of this SSK lies in a 2-dimensional signal space. No matter which antenna is selected, the same modulation (channel) symbol of +1 (corresponding to a modulation bit of "0") will be transmitted, resulting in the transmitted signal vectors in the last column. The non-zero entry in each of these signal vectors corresponds to the +1 symbol being transmitted by the selected antenna while the "0" entry corresponds to the non-active antenna. Later on, when we discussed the more general SM, we will show how the non-zero entry in each signal vector varies with the modulation bits in that interval.

However, due to its inherent working principle, the major criticism about the adoption of SSK modulation in realistic propagation environments is its robustness to the imperfect knowledge of the wireless channel at the receiver [22]. In particular, SSK modulation is much more sensitive to channel estimation errors than conventional systems.

1.2.2. Spatial Modulation (SM)

SM is the first proposed technique among the set of spatial-domain based modulation techniques and most existing methods are derived based on it [16]. The idea to modulate data bits in the spatial index of transmit antennas were suggested for the first time when proposing SM [16], [23]. In the previous illustration of SSK, we assume that

the modulation symbol transmitted by the selected antenna is always +1, i.e. there is no modulation happening at the antenna at all. However, in the case of SM, modulation takes place on top of exploiting the spatial domain, resulting in a higher throughput. As an example, consider the 2-antenna example in Table 1.1 again, but this time we add a modulation bit, m, so that we can impose BPSK modulation onto the selected antenna. The mapping of the binary 2-tuple (b, m) onto equivalent (antenna index, modulation symbol), and the equivalent signal vectors is shown in Table 1.2. This SM scheme has a throughput of 2 bits per interval, double that of the SSK scheme in Table 1.1.

Antenna/Spatial bit, b	Active Antenna index	Modulation bit, m	Modulation symbol	Equivalent signal vector
0	1	0	+1	$[+1 \quad 0]^T$
0	1	1	-1	$[-1 \quad 0]^T$
1	2	0	+1	$[0 \quad +1]^T$
1	2	1	-1	$[0 \quad -1]^T$

Table 1.2: Example of SM Mapper Rule

We summarize in Fig. 1.1 the difference between SSK and the more general SM. Also shown in figure is conventional spatial multiplexing and Alamouti Space-Time block code (STBC) scheme. In the spatial multiplexing scheme, S1 and S2 are the modulation symbols sent over Antenna 1 and 2 respectively. On the other hand, in the Alamouti STBC scheme, S1 and S2 are the modulation symbols transmitted by the two antennas in the first interval, and -S2* and S1* are those transmitted in the second interval. As for SM, S1 and S2 are the modulation and antenna/spatial bit respectively with the former bit being used to select a +1 or -1 symbol from a BPSK constellation. Lastly, for SSK scheme, S2 is the antenna/spatial bit and there is no modulation bit.

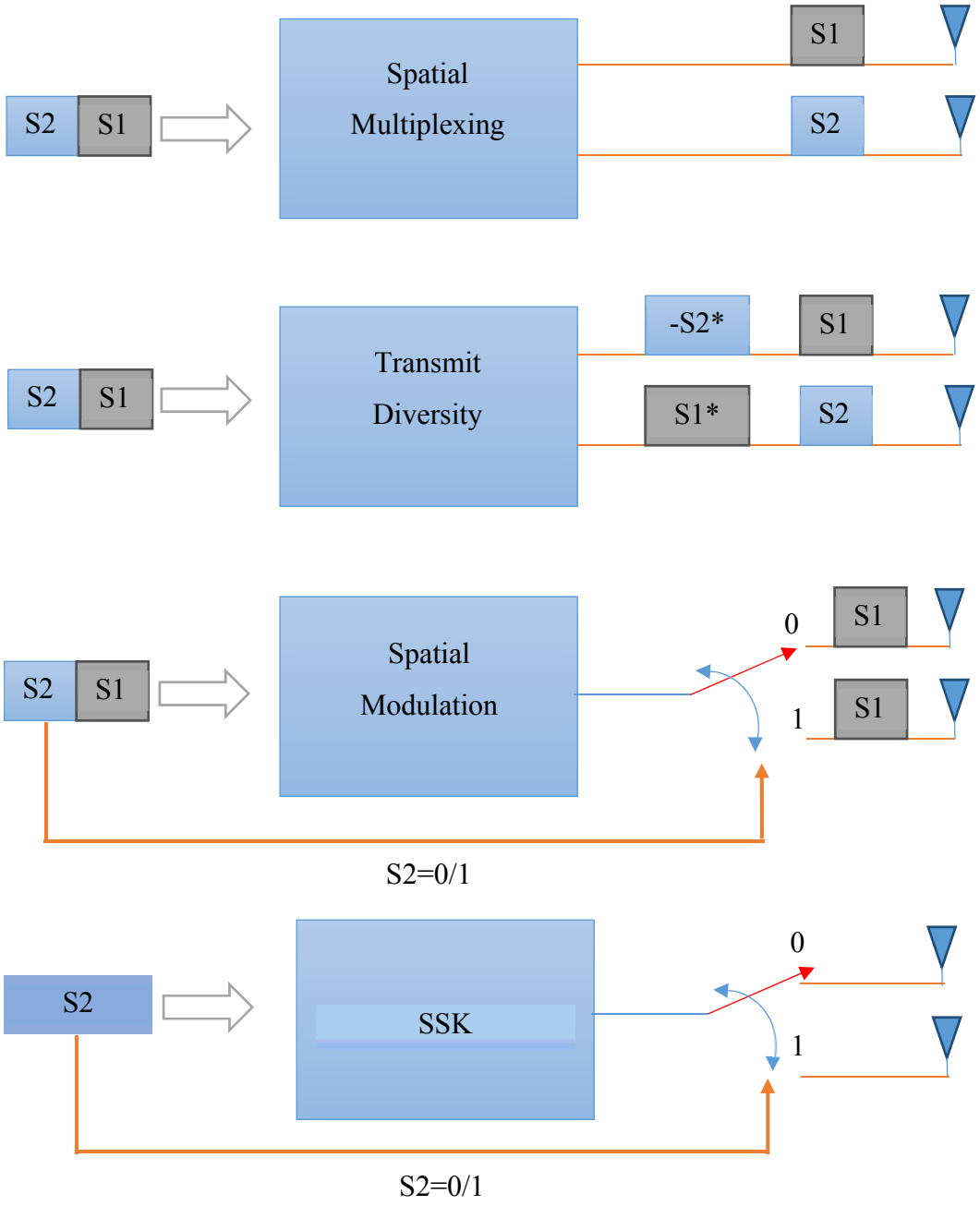

Fig. 1.1: Illustration of MIMO concepts: Spatial Multiplexing, Transmit Diversity, Spatial Modulation (SM), and Space Shift Keying (SSK)

1.2.3. Space Time Block Coded Spatial Modulation (STBC-SM)

Space time block coded spatial modulation or STBC-SM presented in [19] which combines the SM-MIMO concept with the Alamouti code [9] for the sake of proposing a modulation scheme that can take advantage of the multiplexing gain of SM and the

second order diversity of Alamouti code [13]. This proposes pairs of transmit antenna chosen from the spatial-constellation diagram to transmit the Alamouti code. Second order diversity is guaranteed by the appropriate optimization of the spatial constellation diagram. Some rotation angles are introduced to this end for ensuring both the maximum diversity order and coding gain. Numerical results show that it provides better performance than state-of-the-art space time coded MIMO schemes at the cost of larger number of TAs without increasing the number of RF chains.

The problem imposed by STBC-SM is that the maximum normalized throughput of one can only be fully achieved by Alamouti's 2 X 2 STBC, hence in order to improve the throughput of STBC-SM, an increased number of antennae should be employed, which would impose a higher complexity. Besides, this scheme requires at least two RF chains whereas traditional SM techniques require only one.

1.2.4. Detection of Spatial Modulation

The SM format was illustrated earlier in Table 1.1, Table 1.2 and Fig. 1.1. Specifically, the last columns in the two tables provide the effective signal vectors. When the transmitted SM goes through the wireless channel, each component in the signal vector will experience random channel gain. Owing to different spatial positions occupied by the transmit antenna in the antenna array, these random gains are statistically independent and the collection of channel gains from any specific transmit antenna to all the receive antennas forms the signature pattern for that antenna. It should be noted that even though we are considering mobile communications, the channel can be considered static because the mobility is very low in relation to the data rates. This represents the fundamental working principle of SM, since at any time instant only one transmit antenna is active, so only one particular signal pattern will actually be received at a time, making it distinguishable from other patterns. It is obvious from this working mechanism that, especially for SSK modulation [7], the wireless channel plays the role of a "modulation unit", by introducing a distinct fingerprint that makes the signal emitted by distinct transmit antennas distinguishable at the receiver.

The receiver exploits the random modulation introduced by the wireless channel for signal detection. In order to detect the transmitted signal from the noisy received signal, the receiver must know the channel impulse response of all the transmit to receive wireless link beforehand [7], [16], [19]. Usually this information is obtained via channel estimation. According to Maximum Likelihood (ML) principle the receiver computes the Euclidean distance between the received signal and the set of possible signals obtained via combined digital-channel modulation and chooses the closest one. In this way all the bits in the transmitted block can be decoded and the original bit stream recovered. In short, SM transports information by exploiting the location specific property of the wireless channel.

1.2.5. Differential Spatial Modulation (DSM)

The above schemes are based on perfect channel knowledge at the receiver. However, it may not always be easy to acquire perfect CSI at the receiver. Although pilot aided techniques [24] had been proposed for this purpose, however, they lead to a significant drop in throughput. As a result, Differential Spatial Modulation (DSM) [25], [26] is proposed which entirely avoids the need of channel state information (CSI) at the transmitter or receiver. To perform differential detection in DSM, it is required transmissions in different intervals be grouped in blocks, and that different antennas are activated in different intervals within the same block [20]. The scheme performs fairly well for small number of antenna system model but for higher number of transmit antenna DSM becomes unfeasible due to its exponential complexity growth with the increase of number of transmit antennas. In addition, the block structure described above (which is a form of coding) leads to a loss of throughput especially for a large number of antennas.

1.3. Advantages and Disadvantages of Spatial Modulation Techniques

Summarizing the above discussions, SM provides the following potential advantages compared to state-of-the-art MIMO communications.

I. Compared to conventional MIMO solutions, such as V-BLAST [8] and Alamouti space-time schemes [27], SM entirely avoids ICI, and only requires a single RF chain at the transmitter. This is due to the working mechanism of SM where only a single transmit antenna is switched on for data transmission while all the other antennas are kept silent.

II. The spatial constellation in SM introduces a multiplexing gain in the spatial domain that increases logarithmically with the increase of number of transmit antenna. This results in an absolute increase of the throughput by a factor of $\log_2(N_t)$ without any bandwidth expansion.

III. The receiver design is inherently simpler than the V-BLAST scheme [28]. Since complicated interference cancellation algorithm are not required to cope with the ICI, it can provide ML optimum performance at a single stream decoding complexity [17].

IV. Due to single antenna transmission, SM can be implemented using a single RF chain with one or more RF switches and several inactive TAs, which is inexpensive and easy to deploy. In [43] the cost of employing a RF chain is shown to be at around 180 USD and the cost of a RF switch at around 2-3 USD. Thus, implementation of a single RF chain can reduce the hardware cost significantly compared to traditional MIMO where the number of RF chains equals the number of TA elements.

V. Since the multiplexing gain is achieved by a single RF-source, SM reduces the total consumed power required for the same RF output power. Various independent research have recently unveiled that conventional MIMO may be less power efficient than single antenna transmission if the total power (RF and circuit) is taken into account [29], [30]. More specifically, it is shown that the power dissipation inefficiency originates from the increased amount of power dissipated by all the independent RF chains that are needed in conventional MIMO communications. In [31] it is shown that for massive MIMO the actual power consumption associated

with supporting hundreds of TAs will be determined by the economy scale in manufacturing hundreds of RF chains, up/down converters, analog/digital converters, etc., as well as by the development of highly parallel and dedicated hardware for baseband signal processing. In this context, SM-MIMO transmission has the potential of representing a win-win alternative to the circuit power inefficiency of conventional MIMO systems and to the technological challenge of implementing hundreds of small low power RF chains and power amplifiers. Also, in case of SM, the power dissipation is independent of the number of TAs and this results in significant EE gains.

These are the important advantages of Spatial Modulation techniques. However, some fundamental trade-offs are-

I. At least two transmit antenna are required to exploit the SM concept. Since some TA elements remain inactive in every channel use SM offers a lower throughput than conventional MIMO for the same number of TA elements. Thus SM requires a larger number of transmit antennas to achieve the same throughput capacity as multiplexed MIMO [13].

II. Due to its specific encoding mechanism, the active TA in a SM changes in almost every channel use. As a consequence, a single RF implementation needs a sufficiently fast RF switch operating at the symbol rate to minimize switching loses. Thus, high speed RF switches constitute a critical part of the transmitter design. Fortunately, several example of RF switches capable of switching at nanosecond or even at sub nanosecond speeds with insertion loss and good isolation properties are available in the literature for a wide range of frequency band [32].

III. The operational wireless communication channel requires the transmitted signal to obey a well-defined spectral mask. More specifically, the transmitted signals are usually designed to have a flat spectrum in the pass band for improving the energy efficiency, as well as a fast roll off in the

stop band in order to reduce the out of band interference and to enhance the associated coexistence capabilities. To this end, appropriate shaping filters have to be used before transmission. Commonly adopted shaping filters satisfying the Nyquist criterion are bandwidth-limited and hence have infinite duration impulse responses. On the other hand, spatial modulation encoding based on a symbol-time switching mechanism is better suited for time limited pulse shapes [7] , which results in a bandwidth expansion. Thus, in SM systems, pulse shaping should be realized with the objective of striking a balance between a limited time duration and a practical bandwidth occupancy in order to ease the implementation of the switching mechanism while meeting the practical coexistence requirements. Fortunately, various methods are available in the literature for generating practical time and bandwidth-limited pulse shaping filters [21].

IV. The efficiency of SM depends on the radio environment which is termed in the large-scale MIMO literature as favorable propagation. Briefly, this implies that the channel impulse responses of the transmit to receive links are sufficiently different from each other [27]. In fact, the channel impulse responses represent the unique points of the spatial constellation diagram, which implies that the more different they are, the easier for the demodulator to distinguish them. On the contrary when multiple transmit antennas are located at the same spatial location space, then the size of the spatial constellation is one and no data can be conveyed through spatial symbols. Thus, a lack of scattering in the propagation environment may result in a poor error probability and EE. However, adequate transmit processing such as orthogonal pulse shaping, is capable of alleviating those problems [22]. Furthermore, the routinely encountered practical design issues of conventional MIMO communications, such as RF power imbalance may no longer be a serious problem in SM, since they in fact assist in making the channel impulse responses more different from each other.

V. Demodulation of SM is complicated in the sense that it either requires pilot-aided channel estimation [24] or differential detection [20], [25]. The former leads to drop in throughput, especially when there is a large number of antennas. On the other hand, the latter has a complexity that grows exponentially with the number of antennas, making DSM impractical even for a moderate antenna array.

1.4. Contribution of This Thesis

An objective of this thesis is to devise a low-complexity coherent SM scheme that does not require the periodic transmission of pilot symbols for channel estimation purpose. Specifically, a novel Clustering Based Decision Feedback (CB-DFB) coherent detection scheme is proposed. The idea works as follows. The spatial modulator first emits one reference symbol for each transmit antenna at the beginning of the communication session. These symbols are sent only once, just like the initial reference symbols in a DSM. The received vectors associated with these reference symbols are then used to form the initial centroids (channel estimates) of the clustering based receiver. Subsequent received vectors in the same data packet, with modulation symbols removed through non-linear processing, are then used to form clusters based on the minimum distance criterion. Centroids (or channel estimates) are then updated based on the members in the same clusters and this process is repeated until convergence occur or until a fixed number of iterations. At this point, fine channel estimates are obtained which can be used for coherent detection.

The CB-DFB scheme performs quite similar to other recognized spatial modulation techniques in terms of the Bit Error Rate (BER). The BER of CB-DFB scheme is compared with that of DSM and similar outcomes are obtained. However, in complexity comparison CB-DFB scheme outperforms DSM by substantial margin, as the complexity of the CB-DFB scheme grows linearly with the increase in number of transmit antennas, whereas it grows exponentially in case of DSM. This makes implementing a large number of antennas feasible, and this translates into an increase in throughput.

The CB-DFB scheme mentioned above is further extended to obtain a Clustering Based Generalized Decision Feedback (CB-GDFB) scheme that overcomes the constraint in SM whereby the number of transmit antennas has to be a power of two. In the proposed CB-GDFB scheme, two (can be more) out of all the transmit antennas are activated at any time instant and the single-RF property of SM is also maintained by sending the same modulation symbol through both active antennas. CB-GDFB can be deployed to increase the overall throughput by base-two logarithm of the number of antenna combinations. It also reduces the number of transmit antennas as well as initial reference symbols required for the same throughput. It is shown that for the same throughput, CB-GDFB performs nearly the same as CB-DFB, but with significant reduction in the number of transmit antennas and initial reference symbols.

1.5. Outline of the Thesis

The thesis is organized as follows. Chapter 1 provides a literature review of different MIMO technologies and brief introduction to SM. The detailed signal and system model of a coherent (i.e. non-differentially encoded) SM system and a discussion of the encoding and detection process in a DSM system is then presented in Chapter 2. In Chapter 3 a novel coherent SM scheme called CB-DFB based on decision feedback and the clustering algorithm is subsequently proposed to resolve the complexity issue of DSM. Chapter 4 focuses on the generalized CB-DFB scheme which further overcomes the constraint of a traditional SM system and increases the overall throughput. Finally, conclusion of the thesis research is provided in Chapter 5, together with suggestions for further research.

Chapter 2.

Signal and System Models

The objective of this chapter is to describe the basic components of a generic Spatial Modulation (SM) system operating in a Rayleigh flat fading channel. A thorough discussion of the Differential Spatial Modulation (DSM), briefly addressed in Chapter 1, is also provided in the later part of this chapter. It has been shown that the DSM scheme becomes impractical for a large antenna array due to its very high receiver complexity. A new scheme will be proposed in the following chapter to overcome this drawback of the DSM scheme while maintaining its advantages.

2.1. Spatial Modulation (SM)

As mentioned earlier in Chapter 1, the first proposed spatial modulation technique was exclusively called 'Spatial Modulation (SM)' [16] [23] and most existing methods are derived as special or generalized cases from it. SM is the first technique to utilize both spatial and signal constellation. Fig. 2.1 illustrates the key components of a spatial modulation system: the transmitter (with 4 antennas), the wireless channel, and the receiver (with one antenna). This is followed by Fig. 2.2 where a slightly more detailed system is presented with notations for signals that appear at different points in the system.

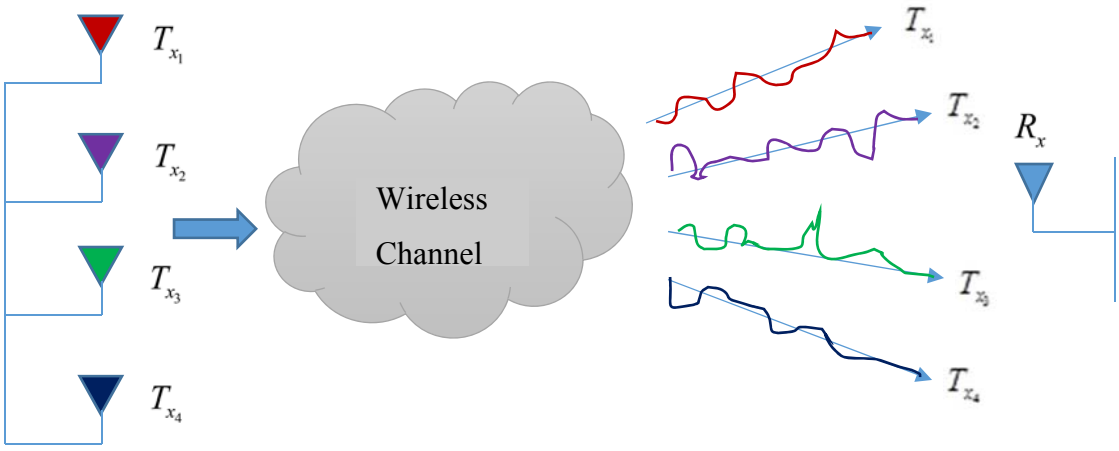

Fig. 2.1: Spatial Modulation communication channels for a 4x1 system model

2.1.1. Transmitter

The modulation process in SM can be visualized as follows. The incoming data bits shifted onto the modulator in blocks of η bits, where the first $\log_2(N_t)$ bits are called the antenna/spatial bits and the remaining $\log_2(M)$ bits are called the modulation bits, i.e.

$$\eta = \log_2(N_t) + \log_2(M) \tag{2.1}$$

where N_t, is the number of transmit antennas and M is the size of modulation constellation. According to Fig. 2.2, the data block to be transmitted in the k-th interval is denoted as $\mathbf{q}(k)$, which is a string of "0" and "1". The first $\log_2(N_t)$ bits in each block is used to select and activate one antenna among the set of N_t antennas using the RF switch while the remaining $\log_2(M)$ bits are used to select a symbol from a $M-QAM$ / PSK constellation $S = \{S_1, S_2, \cdots, S_M\}$, where S_i is the i-th point in the constellation. For example, in BPSK, $S = \{+1, -1\}$ while for QPSK/4QAM, the signal set is $\{\frac{1}{\sqrt{2}}(\pm 1 \pm j)\}$

where j is the unit complex number. Note that if S_t is the complex symbol emitted by the baseband modulator, then the actual transmitted RF signal by the selected antenna is

$$X_{RF} = \mathrm{Re}\{S_t\}\cos(\omega_c t) + \mathrm{Im}\{S_t\}\sin(\omega_c t) \tag{2.2}$$

where ω_c is the carrier frequency in radian per second. For convenience and conciseness though, we will adopt complex baseband notation throughout the thesis.

To better explain the modulation process, lets consider the following example. Assuming a system with $N_t = 4$ antenna with QPSK/4QAM modulation $(M = 4)$. The number of data bits per encoding interval is thus $\eta = 4$ bits, where the first two bits are used to select one of the 4 antennas and the last two are used to pick a symbol from the QPSK constellation $S = \left\{\frac{1}{\sqrt{2}}(\pm 1 \pm j)\right\}$. Without loss of generality, the encoding rule for this system is shown in Table 2.1. According to this encoding table, when the input data in any given interval is $\mathbf{q} = \begin{bmatrix} 0 & 1 & 1 & 0 \end{bmatrix}^T$, the antenna index selected by the first two bits (0,1) is $l = 2$, and modulation symbol selected by the last two bits of (1,0) is $S_3 = -\frac{1}{\sqrt{2}} - \frac{j}{\sqrt{2}}$. The resultant complex signal vector is

$$\mathbf{x} = \begin{bmatrix} 0 & -\frac{1}{\sqrt{2}} - \frac{j}{\sqrt{2}} & 0 & 0 \end{bmatrix}^T \tag{2.3}$$

and the corresponding transmitted RF signal vector is

$$X_{RF}(t) = \frac{-\cos(\omega_c t)}{\sqrt{2}} - \frac{\sin(\omega_c t)}{\sqrt{2}} \tag{2.4}$$

The fact that the signal vector is only non-zero in the second row means the RF signal is sent from Antenna 2.

In general, when the encoding rule and the input data determine that I-th antenna and the J-th modulation symbol are to be selected, the effective signal vector is of the form

$$x = S_J U_I \tag{2.5}$$

where U_I is an all-zero vector except in its I-th position where it has a value of 1, and S_J is the J-th complex symbol of the signal constellation.

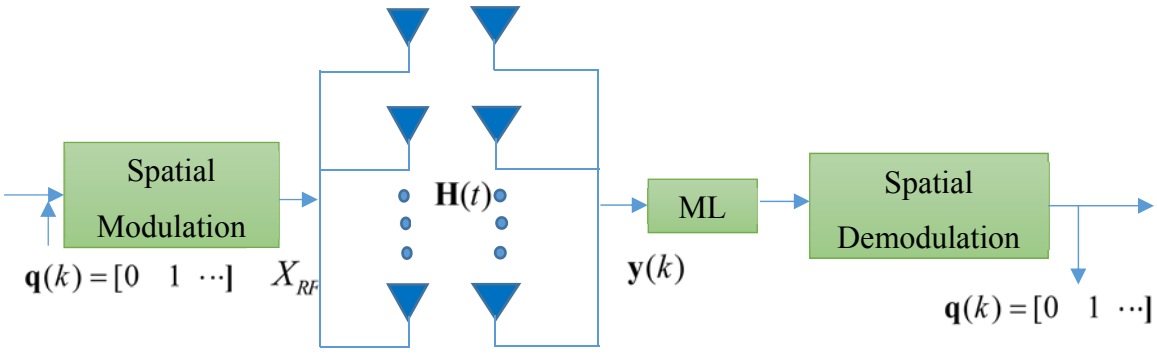

Fig. 2.2: Simplified Spatial Modulation System Model

Bits	Spatial bits	Antenna index	Modulation bits	Symbols
0000	00	1	00	$\frac{1}{\sqrt{2}}(+1+j)$
0001	00	1	01	$\frac{1}{\sqrt{2}}(-1+j)$
0010	00	1	10	$\frac{1}{\sqrt{2}}(+1-j)$
0011	00	1	11	$\frac{1}{\sqrt{2}}(-1-j)$
0100	01	2	00	$\frac{1}{\sqrt{2}}(+1+j)$
0101	01	2	01	$\frac{1}{\sqrt{2}}(-1+j)$

Bits	Spatial bits	Antenna index	Modulation bits	Symbols
0110	01	2	10	$\frac{1}{\sqrt{2}}(+1-j)$
0111	01	2	11	$\frac{1}{\sqrt{2}}(-1-j)$
1000	10	3	00	$\frac{1}{\sqrt{2}}(+1+j)$
1001	10	3	01	$\frac{1}{\sqrt{2}}(-1+j)$
1010	10	3	10	$\frac{1}{\sqrt{2}}(+1-j)$
1011	10	3	11	$\frac{1}{\sqrt{2}}(-1-j)$
1100	11	4	00	$\frac{1}{\sqrt{2}}(+1+j)$
1101	11	4	01	$\frac{1}{\sqrt{2}}(-1+j)$
1110	11	4	10	$\frac{1}{\sqrt{2}}(+1-j)$
1111	11	4	11	$\frac{1}{\sqrt{2}}(-1-j)$

Table 2.1: SM mapping table for $N_t = 4$ and 4-QAM modulation

2.1.2. The Wireless Channel as a Modulation Unit

The RF signal in (2.2), or equivalently the corresponding baseband complex signal vector (2.3) is transmitted over a Rayleigh flat fading channel. The N_r wireless links between the n-th transmit antennas and N_r received antennas is denoted as $\mathbf{h}_n = [h_{n,1}, h_{n,2}, ..., h_{n,N_r}]^T$, where $h_{n,m}$ is the complex channel gain in the link between the n-th transmit and the m-th receive antenna, and $[\bullet]^T$ denotes matrix transpose. Since the channel is assumed to be flat Rayleigh, each channel gain is a zero mean complex Gaussian random variance with a variance of $\sigma_h^2 = \frac{1}{2}E\left[\left|h_{n,m}\right|^2\right]$, where $E[\cdot]$ is the expectation operator, $|\cdot|$ is the magnitude of a complex number. Furthermore, the

different gains in all the signal vectors are statistically independent and identically distributed (iid). Note also that the set of channel vectors $\mathbf{H} = \{\mathbf{h}_1, \mathbf{h}_2, ..., \mathbf{h}_{N_t}\}$ forms the channel constellation.

In addition to fading, the channel also introduces additive white Gaussian noise (AWGN), $\mathbf{n} = \left[n_1, n_2, ..., n_{N_r} \right]^T$, where n_m is the complex Gaussian noise at the m-th receive antenna. The different noise terms are iid with zero mean and a variance of $\sigma_n^2 = \frac{1}{2} E\left[|n_m|^2 \right]$. Let $\mathbf{h}_{TX}$ and S_{TX} denotes in general the transmit antenna/spatial symbols and modulation symbols respectively, where it is understood that these are chosen from sets H and S respectively. If I-th antenna and J-th modulation symbol are selected for transmission, then the received signal vector is

$$\mathbf{y} = \mathbf{h}_{TX} S_{TX} + \mathbf{n} \tag{2.6}$$

It is evident from the above equation that, except for the noise term, SM is essentially a product modulation scheme whereby the effective signal at the receiver is the multiplication of the vector channel symbol $\mathbf{h}_{TX}$ by the scalar modulation symbol S_{TX}. As one would intuitively expect, the more different the channel symbols are, the more reliable is the SM scheme. Since these are random vectors, this means the more statistically independent $\mathbf{h}_m$-s are, the better the performance. This statistical independency can be achieved in practice if the different antennas are spaced far apart enough.

2.1.3. Maximum Likelihood Estimation of SM

The receiver exploits the unique fingerprint introduced by the wireless channel for retrieving the information bits. The receiver is assumed to be aware of the N_t channel impulse responses. Since the actual channel impulse response that is received in each channel use depends on the index of the active TA, the demodulator performs an exhaustive search among all possible combinations of channel impulse responses and

modulation symbols, and makes a decision in favor of the hypothesis that is most likely, using a ML receiver. Specifically, the ML receiver determines the pair of $(\mathbf{h}_n, S_m)$, $n = 1, 2, ..., N_t$, $m = 1, 2, ..., M$ that maximizes the conditional probability density function (pdf)

$$p(\mathbf{y} \mid (\mathbf{h}_n, S_m)) = \frac{1}{\pi^{N_t}} \exp(-\left\|\mathbf{y} - \mathbf{h}_n S_m\right\|_F^2) \tag{2.7}$$

that is performing the maximization

$$(\hat{\mathbf{h}}_{TX}, \hat{S}_{TX}) = \arg \max_{\substack{\mathbf{h}_n \in H \\ S_m \in S}} p(\mathbf{y} \mid S_m, \mathbf{h}_n) \tag{2.8}$$

and arriving at the decisions $\hat{\mathbf{h}}_{TX}$ and $\hat{S}_{TX}$ that are at the receiver's estimates of the transmitted channel and modulation symbol respectively. Note that $\left\|\cdot\right\|_F$ is the Frobenius norm of a vector. Given that the exponential function in (2.7) decreases monotonically with $\left\|y - \mathbf{h}_n S_m\right\|_F^2$, maximizing the conditional pdf in (2.8) is thus equivalent to minimizing the square distance

$$(\hat{\mathbf{h}}_{TX}, \hat{S}_{TX}) = \arg \min_{\substack{\mathbf{h}_n \in H \\ S_m \in S}} \left\|\mathbf{y} - \mathbf{h}_n S_m\right\|_F^2 \tag{2.9}$$

The estimated spatial and modulation symbols are then used to retrieve the transmitted data bits by inversing the mapping procedure considered at the transmitter.

As pointed out by Jeganathan et al. in [17], the ML detector in (2.9) is optimal for equiprobable modulation and channel symbols. On the other hand the maximum ratio combining (MRC) based receiver proposed in [16] is sub-optimal. The difference between the two is that the ML detector performs joint detection of the channel and modulation symbols while the MRC receiver detects the two separately. It was shown that SM with ML detection outperforms SM with MRRC detection. As such, we will adopt the ML detector in (2.9), where applicable, in this thesis.

2.2. Differential Spatial Modulation

The ML detector in the previous section requires channel state information (CSI) to function properly. While this can be achieved using pilot symbols [24], the insertion of these symbols into the data stream reduces the effective throughput of transmission. As such differential spatial modulation or DSM is proposed to circumvent this problem of needing pilot symbols to generate the CSI at the receiver[20], [25], [33]. Through differential encoding on the transmitter side, the differential detector in DSM is able to use the received signal in previous interval as CSI for detecting the symbol in the current interval. Below is brief review of DSM.

In a nutshell, DSM is a block encoding scheme, whereby the number of signaling intervals in a DSM block is N_t , the number of transmit antennas. The DSM encoding rules are [20]

I. To comply with the SM format, one and only one antenna can be active in any given interval within a DSM block.

II. To enable differential encoding and detection of the antenna/spatial symbols, each antenna is activated once and only once within a DSM block.

III. To enable differential encoding and detection of the modulation symbols, the signal constellation is restricted to an equal energy M-ary phase shift keying (PSK).

IV. The DSM symbol is a $N_t \times N_t$ space-time matrix with the rows representing the different transmit antennas and the columns representing the different signaling intervals within the same DSM block. Because of Rules I and II, there is one and only one non-zero entry in each row and each column in a DSM symbol. Fundamentally, if the PSK modulation effect is ignored, each DSM symbol is a permutation matrix, and it is well known that permutation matrices

have a closure property and the product of a permutation matrix with its transpose is the identity matrix. These properties make differential encoding and detection in DSM possible.

To further clarify this modulation format, let's consider the case of $N_t = 4$. Assuming that Antennas 1, 3, 2, and 4 are used in intervals 1, 2, 3, and 4 to transmit the BPSK symbols +1, -1, -1, +1 respectively in the k-th encoding block, then the corresponding space-time data symbol is

$$\mathbf{C}_k = \mathbf{A}_k \mathbf{S}_k = \begin{bmatrix} +1 & 0 & 0 & 0 \\ 0 & 0 & -1 & 0 \\ 0 & -1 & 0 & 0 \\ 0 & 0 & 0 & +1 \end{bmatrix} \tag{2.10}$$

where

$$\mathbf{A}_k = \begin{bmatrix} 1 & 0 & 0 & 0 \\ 0 & 0 & 1 & 0 \\ 0 & 1 & 0 & 0 \\ 0 & 0 & 0 & 1 \end{bmatrix} \tag{2.11}$$

is the ST- antenna/spatial symbol and

$$\mathbf{S}_k = \begin{bmatrix} +1 & 0 & 0 & 0 \\ 0 & -1 & 0 & 0 \\ 0 & 0 & -1 & 0 \\ 0 & 0 & 0 & +1 \end{bmatrix} \tag{2.12}$$

is the modulation symbol of this encoding block. Here, $\mathbf{S}_k$ is a diagonal matrix whose diagonal entries are +1, -1, -1, and +1 respectively. It should be clear that the antenna/spatial symbol is example of a permutation matrix of size 4 and that $\mathbf{A}_k \mathbf{A}_k^H = \mathbf{I}_4$, an identity matrix of size 4. In DSM, the data symbol $\mathbf{C}_k$ is not actually transmitted. Instead it is differentially encoded into

$$\mathbf{X}_k = \mathbf{X}_{k-1}\mathbf{C}_k \tag{2.13}$$

for transmission purpose, where $\mathbf{X}_{k-1}$ and $\mathbf{X}_k$ represent respectively the previous and current transmitted ST symbols.

For further illustration purpose, a mapping table for DSM system with $N_t = 3$ and without any modulation information is shown in Table 2.2 below.

Antenna/Spatial Bits	Antenna/Spatial Symbol in DSM
00	$\begin{bmatrix} 1 & 0 & 0 \\ 0 & 1 & 0 \\ 0 & 0 & 1 \end{bmatrix}$
01	$\begin{bmatrix} 0 & 1 & 0 \\ 1 & 0 & 0 \\ 0 & 0 & 1 \end{bmatrix}$
11	$\begin{bmatrix} 0 & 0 & 1 \\ 1 & 0 & 0 \\ 0 & 1 & 0 \end{bmatrix}$
10	$\begin{bmatrix} 0 & 0 & 1 \\ 0 & 1 & 0 \\ 1 & 0 & 0 \end{bmatrix}$
Not used	$\begin{bmatrix} 1 & 0 & 0 \\ 0 & 0 & 1 \\ 0 & 1 & 0 \end{bmatrix}$
Not used	$\begin{bmatrix} 0 & 1 & 0 \\ 0 & 0 & 1 \\ 1 & 0 & 0 \end{bmatrix}$

Table 2.2: DSM mapping table for $N_t = 3$

Notice that for $N_t = 3$, there are 6 permutation matrices of size 3. However, only 4 are being used as antenna matrices, corresponding to 2 bits of information. In general, without any elaborate encoding, the number of antenna/spatial bits that can be transmitted per block with N_t antenna is

$$N_b = \lfloor \log_2(N_t!) \rfloor \tag{2.14}$$

where $\lfloor \cdot \rfloor$ denotes integer floor, and ! denotes factorial. The number of permutation matrices that will be discarded is thus $(N_t!) - 2^{\lfloor \log_2(N_t!) \rfloor}$. Lexicographically larger permutations are discarded for ease of implementation of permutation index mapping [20]. For DSM, the order in which the transmit antennas will be activated follows some index mapping procedure. Two types of index mapping were presented in DSM. One is look up table method as presented in Table 2.2 and the other is permutation method. The look up table method is only feasible for small values of N_t, as the table grows exponentially with the number of transmit antennas. The permutation method is required for large values of N_t which follows the Lehmer Code [20].

In addition to the N_b antenna/spatial bits stated above, each encoding block contains another $N_s = N_t \log_2(M)$ bits for overlaying M-ary PSK modulation on top of the antenna/spatial symbol, bringing the total number of bits per block to

$$B = \lfloor \log_2(N_t!) \rfloor + N_t \log_2(M) \tag{2.15}$$

As a result, the throughput of DSM is B / N_t, or

$$\eta_{DSM} = \frac{1}{N_t} \lfloor \log_2(N_t!) \rfloor + \log_2(M) \tag{2.16}$$

per signaling interval. In summary, the transmission process in DSM consists of the following steps. First, the $\lfloor \log_2(N_t!) \rfloor$ antenna/spatial bits in each block are used to select an antenna/spatial symbol $\mathbf{A}_k$ from the encoding table. The remaining $N_t \log_2(M)$ modulation are mapped into a (matrix) modulation symbol $\mathbf{S}_k = diag(s_{k,1}, s_{k,2}, ..., s_{k,N_t})$, where $\mathbf{S}_k$ is a diagonal matrix with $s_{k,1}, s_{k,2}, ..., s_{k,N_t}$ as entries, and the $S_{k,m}, m = 1, 2, ..., N_t$ are complex symbols from M-ary PSK constellation. The product of $\mathbf{A}_k$ and $\mathbf{S}_k$ is then used to form the space-time data symbol $\mathbf{C}_k = \mathbf{A}_k \mathbf{S}_k$. The transmitted DSM symbol is

obtained via differential encoding of $\mathbf{C}_k$ into $\mathbf{X}_k=\mathbf{X}_{k-1}\mathbf{C}_k$ as per (2.8), where $\mathbf{X}_{k-1}$ and $\mathbf{X}_k$ are respectively the previous and current transmitted ST symbols. Finally, the non-zero entries in the columns of $\mathbf{X}_k$ are sent in succession from signaling intervals $N_t k$ to $N_t(k+1)-1$ using the antennas specified in the antenna/spatial symbol. This process is repeated until the end of transmission.

The received signal for the k-th encoding block is

$$\mathbf{Y}_k=\mathbf{H}\mathbf{X}_k+\mathbf{N}_k \tag{2.17}$$

where

$$\mathbf{H}=\left[\mathbf{h}_1,\mathbf{h}_2,...,\mathbf{h}_{N_t}\right]$$

is the $N_r \times N_t$ channel matrix comprising all the N_t channel symbols, and N_k is a $N_r \times N_t$ AWGN matrix whose entries are iid complex Gaussian rv's with zero mean and variance σ_n^2. Upon receiving $\mathbf{Y}_k$ and its predecessor $\mathbf{Y}_{k-1}$, the DSM receiver will make a ML decision on the space-time data symbol $\mathbf{C}_k$. The decision rule is (2.7)

$$\begin{aligned}\hat{\mathbf{C}}_k &= \arg\min_{\forall \mathbf{C}\in C} \left\|\mathbf{Y}_k-\mathbf{Y}_{k-1}\mathbf{C}\right\|_F^2 \\ &= \arg\min_{\forall \mathbf{C}\in C} trace\{(\mathbf{Y}_k-\mathbf{Y}_{k-1}\mathbf{C})^H(\mathbf{Y}_k-\mathbf{Y}_{k-1}\mathbf{C})\} \\ &\equiv \arg\max_{\forall \mathbf{C}\in C} \{\mathrm{Re}(\mathbf{Y}_k^H\mathbf{Y}_{k-1}\mathbf{C})\}\end{aligned} \tag{2.18}$$

where F stands for Frobenius norm, $\mathbf{C}$ is the set of all space-time symbols, and the minimization (or maximization in the last line) is over the all members of $\mathbf{C}$. Note that the last line in the decision rule has a familiar structure of a differential detector, although all signals are now in matrix from. Now, the reason why this differential detector works can be explained as follow. Since $\mathbf{Y}_k=\mathbf{H}\mathbf{X}_k+\mathbf{N}_k$, $\mathbf{Y}_{k-1}=\mathbf{H}\mathbf{X}_{k-1}+\mathbf{N}_{k-1}$, and $\mathbf{X}_k=\mathbf{X}_{k-1}\mathbf{C}_k$, we can see that if the noise term $\mathbf{N}_{k-1}$ is negligible, then $\mathbf{Y}_k$ is approximately

$$\mathbf{Y}_k = \mathbf{H}\mathbf{X}_{k-1}\mathbf{C}_k + \mathbf{N}_k \approx \mathbf{Y}_{k-1}\mathbf{C}_k + \mathbf{N}_k \tag{2.19}$$

Given that $\mathbf{N}_k$ is small, the approximation suggests that a square-distance type detector can be used to recover $\mathbf{C}_k$ from $\mathbf{Y}_k$ and $\mathbf{Y}_{k-1}$ as per (2.18). Indeed, one can prove that the detector in (2.18) is optimal. Fig. 2.3 provides a canonical depiction of this differential detector.

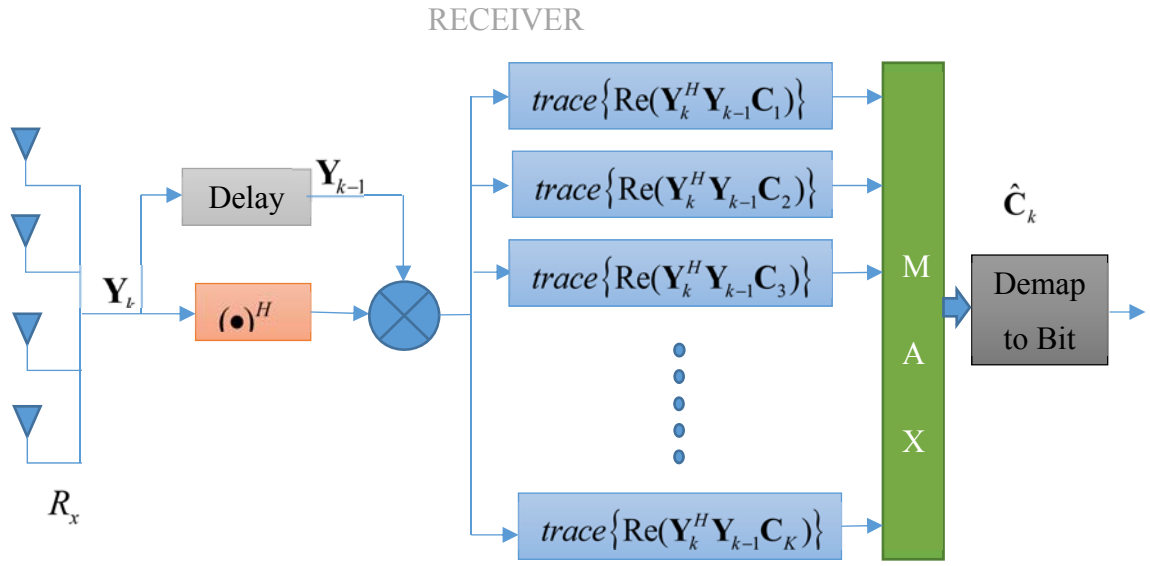

Fig. 2.3: Receiver diagram of DSM model

It is evident from (2.19) and Fig. 2.3 that differential detector does not need to know any of the channel symbols, i.e. the matrix $\mathbf{H}$, to detect the transmitted symbol $\mathbf{C}_k$. However, this nice feature of DSM comes at the expense of a high decoding complexity. Recall from (2.15) that there are altogether $B = \lfloor \log_2(N_t!) \rfloor + N_t \log_2(M)$ bits per encoding block. As a result, the total number of hypothesis is

$$N_c = 2^B = M^{N_t} 2^{\lfloor \log_2(N_t!) \rfloor} \tag{2.20}$$

and the differential detector has thus a computation complexity that grows exponentially with the number of transmit antennas. Furthermore, given that $\mathbf{Y}_k$ and $\mathbf{Y}_{k-1}$ are matrices

of size $N_r \times N_t$ and $\mathbf{C}$ is a square matrix of size N_t, the number of multiply-and-add (MAD) required to compute each matrix product in (2.18) is

$$N_{MAD} = (N_r \times N_t)N_t + N_t^3 = N_t^2(N_r + N_t) \tag{2.21}$$

where $(N_r \times N_t)N_t$ and N_t^3 are respectively the number of MADs required to compute $\mathbf{Y}_k^H \mathbf{Y}_{k-1}$ and $\mathbf{Y}_k^H \mathbf{Y}_{k-1}\mathbf{C}$ from $\mathbf{Y}_k^H$, $\mathbf{Y}_{k-1}$, and $\mathbf{C}$. Finally, the total number of MADs over N_C hypothesis is

$$N_{total} = N_C N_{MAD} = M^{N_t} 2^{\lfloor \log_2(Nt!) \rfloor} N_t^2(N_t + N_r) \tag{2.22}$$

As an example, let us consider a DSM system with 4 transmit and 4 receive antennas, and $M = 2$ or BPSK modulation. This system has a throughput of $\eta_{DSM} = 2$ bits per signaling interval as per (2.16) or $B = 8$ bits per DSM encoding block. As a result, there are $N_C = 256$ hypotheses for the data symbol C_k, each requiring $N_{MAD} = 128$ MADs for a total of $N_{total} = 32,768$ MADs per encoding block, or $4,096$ MADs per bit of information. When the numbers of transmit and receive antennas increase to $N_t = 8$ and $N_r = 8$ while keeping $M = 2$, these numbers increase to $B = 23$, $N_C = 8,388,608$, $N_{MAD} = 1024$, $N_{total} = 8.59 \times 10^9$, or 3.73×10^8 MADs per bit of information. It becomes evident that DSM is not suitable for a system with relatively large number of transmit antennas! In the later chapter of this thesis, a novel clustering based decision feedback (CB-DFB) based SM scheme is proposed to overcome this bottleneck in DSM while maintaining the nice feature of no CSI at the receiver. As it will be shown, this new scheme enables us to deploy a larger number of transmit antennas than DSM, leading to better BER performance and/or throughput.

Chapter 3.

Clustering Based Decision Feedback Coherent Detection for Spatial Modulation

We reviewed in Chapter 2 the basic structures of spatial modulation (SM) with coherent detection and differential spatial modulation (DSM). We found that while coherent SM provides a better performance than DSM, this is achieved at the expense of a loss in throughput because in practice, coherent detection can only be achieved by transmitting pilot symbols periodically. While DSM can circumvent the need of pilot symbols, it may lead to a very high receiver complexity, especially with a large number of transmit antennas. In this chapter, a novel receiver for SM that maintains the spirit of DSM of not requiring pilot symbols and yet has very low complexity is proposed. The core of this receiver is the clustering algorithm (CA) [Section 3.2], a technique used in signal processing, machine learning, data mining, etc. to group together similar data points. Specifically, we use the CA, in conjunction with non-linear processing to remove the modulation symbols, to identify all the spatial/channel symbols in SM. These channel estimates are then fed back to a coherent detector for optimal detection of both the spatial and the modulation symbols. We will refer to this novel receiver as Clustering-based Decision Feedback Spatial Modulation (CB-DFB SM).

3.1. System Model of CB-DFB SM

The system model of the proposed CB-DFB SM is similar to what we have discussed in Chapter 2, i.e. it consists of a transmitter, wireless channel and a receiver. The transmitter and receiver together form a $N_t \times N_r$ MIMO system with a static Rayleigh flat fading channel in between, where N_t and N_r are respectively the number of transmit and receive antennas. The information to be conveyed is separately carried by the antenna/spatial constellation and the modulation constellation as in (2.1). The size of spatial constellation is the number of transmit antennas, N_t, while the size of the modulation constellation is M.

In the proposed CB-DFB SM scheme, transmission starts with N_t pilot or initial reference symbols as shown in Fig. 3.1, one for each transmit antenna. These initial reference symbols are unmodulated, and they serve as the initial centroids of the clustering algorithm based detector. It should be emphasized that unlike conventional pilot-aided methods where training symbols are inserted periodically [24], the initial reference symbols in the proposed CB-DFB SM system are sent only once, and are thus referred to as "one-shot" reference symbols in Fig. 3.1. It is also interesting to point out that the number of initial reference symbols that is required in the proposed CB-DFB system is exactly the number of initial reference symbols needed in DSM [20]. Thus, from this point of view, the proposed CB-DFB scheme is consistent with DSM in its ability to detect the transmitted space-time information with minimal loss in throughput.

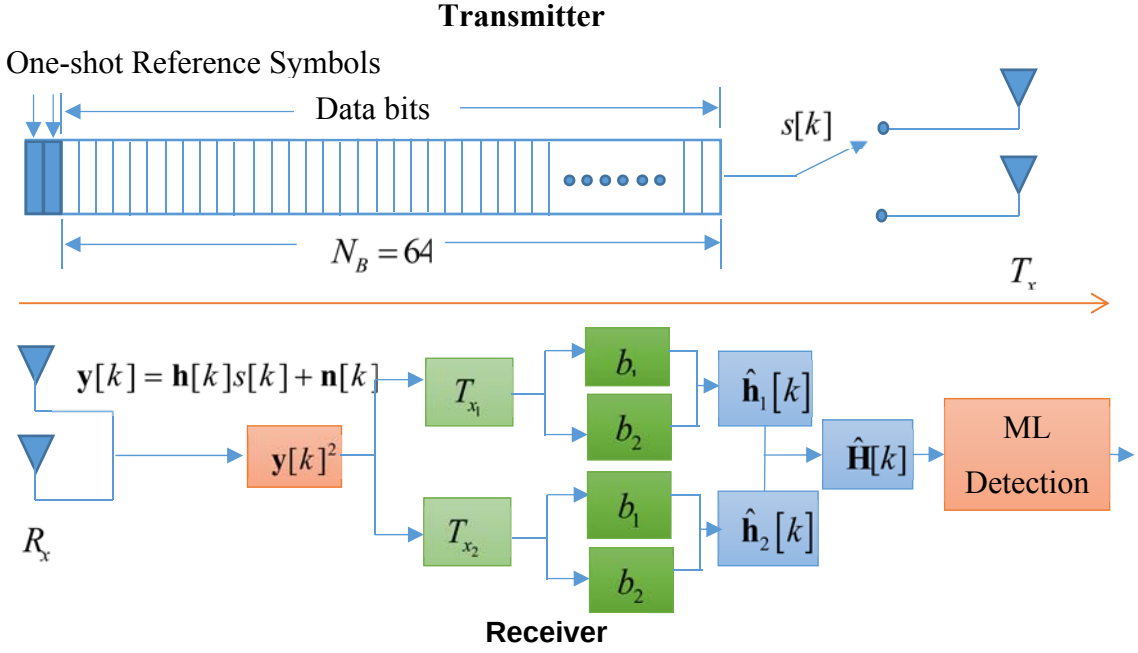

Fig. 3.1: CB-DFB SM system model with $N_t = 2$ and BPSK modulation

During the data transmission phase, the incoming serial bit stream is converted to parallel streams using a η-bit serial to parallel (S/P) converter; $\eta = \log_2(N_t) + \log_2(M)$. The first $\log_2(N_t)$ streams carry the antenna/spatial bits, while the remaining $\log_2(M)$ streams carry the modulation bits, where M is the size of the modulation. For example, in the case of $N_t = 2$ and $M = 2$, there is one stream of antenna/spatial data and one

stream of modulation data, and the four possible combinations of antenna/spatial and modulation bits are summarized in Table 3.1. Note that the notation of the equivalent signal vectors in the last column of this table follows that in Table 2.1.

Incoming Bits	Antenna/Spatial bit	Antenna index	Modulation bit	Modulation Symbol	Equivalent signal vector
$[0 \quad 0]$	0	1	0	$+1$	$[+1 \quad 0]^T$
$[0 \quad 1]$	0	1	1	-1	$[-1 \quad 0]^T$
$[1 \quad 0]$	1	2	0	$+1$	$[0 \quad +1]^T$
$[1 \quad 1]$	1	2	1	-1	$[0 \quad -1]^T$

Table 3.1: Example of a CB-DFB SM Scheme and its mapping rule for $N_t = 2$.

In Chapter 2, we used S_{TX} to denote in general the modulation symbol selected by the modulation bits in a signalling interval, and used $\mathbf{h}_{TX}$ to denote the vector containing the channel gains between the selected transmit antenna and all the receive antennas. We modeled the different channel gains as being iid complex Gaussian random variable with zero mean and a variance of σ_h^2. As for the modulation symbol S_{TX}, it is chosen randomly from a M-ary PSK constellation $S \triangleq \left\{ S_m = e^{j2\pi m/M}; m = 1, 2, ..., M \right\}$.

Furthermore, we stated in Eqn. (2.4) that the received vector is $\mathbf{y} = \mathbf{h}_{TX} S_{TX} + \mathbf{n}$, where $\mathbf{n}$ is the noise vector seen at the receiver. The different components of $\mathbf{n}$ are iid complex Gaussian random variables with zero mean and unit variance. In this Chapter, we generalize this signal notation to include transmissions at different time intervals as follows:

$$\mathbf{y}[k] = \mathbf{h}[k] s[k] + \mathbf{n}[k]; \quad k = 0, 1, 2, ..., N_B - 1 \quad \text{(data symbols)} \qquad (3.1)$$

where $\mathbf{h}[k] \in H \triangleq \left\{ \mathbf{h}_1, \mathbf{h}_2, ..., \mathbf{h}_{N_t} \right\}$, $s[k] \in S \triangleq \left\{ S_1, S_2, ..., S_M \right\}$, and $\mathbf{n}[k]$ are respectively the spatial symbol, modulation symbol, and noise vector in the k-th signalling interval, and N_B is the block size used in the proposed clustering-based detector. Here the received

signal $\mathbf{y}[k]$, the spatial symbol $\mathbf{h}[k]$, and noise vector $\mathbf{n}[k]$are vectors with a dimension of $N_r \times 1$. As for the initial reference symbols mentioned above, they are unmodulated, i.e. $s[k]=1,$ and transmitted from Antenna 1 to N_t at times $-N_t$ to -1 in that order. As a result

$$\mathbf{y}[k]=\mathbf{h}_{k+N_t+1}+\mathbf{n}[k];\quad k=-N_t,-1 \quad \text{(initial reference symbols)} \tag{3.2}$$

It is clear from (3.2) that in the absence of noise, the received pilot signals are simply the channel/spatial symbols.

3.2. Clustering Algorithms for Data Detection and Channel Estimation

Consider the received signal in Eqn. (3.1). The signal component $\mathbf{h}[k]s[k]$ is the product of the modulation symbol and the channel symbol. The detection of these symbols requires knowledge of the entire set of channel gains $\mathbf{H} \triangleq \left\{\mathbf{h}_1, \mathbf{h}_2, ..., \mathbf{h}_{N_t}\right\}$. While the initial reference symbols in Eqn. (3.2) give us some partial channel state information (CSI), they are not accurate enough for reliable detection. In this section, we detail an accurate channel estimation strategy based on the clustering algorithm.

3.2.1. Non-linear Processing to remove Modulation

Let the ℓ-th component of the received signal in Eqn. (3.1) be

$$y[\ell,k]=h[\ell,k]s[k]+n\left[\ell,k\right]. \tag{3.3}$$

Since $s[k]$ is an *M*-ary PSK symbol of the form $e^{j2\pi m/M}$ for some integer *m*, it means the $s^M[k]=1$ no mater what $s[k]$ is. As a consequence, the *M*-th power of $y[\ell,k]$ is $y^M[\ell,k]\approx h^M[\ell,k]$ when $n[\ell,k]$ is small. This suggests that

$$\mathbf{y}^M[0],\mathbf{y}^M[1],...,\mathbf{y}^M[N_B-1], \tag{3.4}$$

the M-th powers of the received vectors in signalling intervals 0 to $N_B - 1$, are noisy versions of

$$\mathbf{h}_1^M, \mathbf{h}_2^M, ..., \mathbf{h}_{N_t}^M, \tag{3.5}$$

the M-th powers of the channel/spatial symbols. Note that throughout this thesis, the M-th power of the vector **v** is defined as a vector whose entrees are the M-th powers of the corresponding entrees in **v**. Now, if the block size N_B is sufficiently large, there will be multiple noisy copies of $\mathbf{h}_m^M$, $m = 1, 2, ..., M$, in the set of $\mathbf{y}^M[k]$, $k = 0, 1, ..., N_B - 1$. This means if we can isolate the individual subsets, we can

1. detect the antenna/spatial bits in the k-th interval, $k = 0, 1, ..., N_B - 1$, by simply knowing which subset $\mathbf{y}^M[k]$ belongs to;

2. detect the modulation bits by realizing that the received vectors in those intervals detected in Step 1 above to be associated with the n-th antenna must be noisy versions of

$$\mathbf{h}_n s[1], \mathbf{h}_n s[2], ..., \mathbf{h}_n s[M]. \tag{3.6}$$

The channel/spatial symbol $\mathbf{h}_n$ is a vector of $N_r \times 1$ dimension. As we are going to show later on, the same algorithm used to detect the antenna/spatial bits in Step 1 can be used in Step 2 to detect the modulation bits. Furthermore, since the decisions on the transmit antennas are used to determine the modulation bits, the proposed receiver is a decision-feedback receiver. Finally, decision feedback will also be employed to derive accurate channel estimates for final coherent detection; refer to Section 3.3.

3.2.2. The Clustering Algorithm

In this thesis, the clustering algorithm (CA) is used to detect both the antenna/spatial bits and the modulation bits. These decisions could be final, or they will be used in a decision-aided channel estimator for making the final decisions.

Algorithm 1: (Initial) Detection of the Antenna/Spatial Symbols

The CA-based receiver detects the antenna/spatial symbols from the M-th power of the received signals in (3.4) as follows:

1. Set the iteration counter to $I = 0$. The initial centroids of the CA are set to the M-th powers of the received pilot signals in (3.2). These initial centroids are denoted as $\mathbf{c}_1[I], \mathbf{c}_2[I], ..., \mathbf{c}_{N_t}[I]$, where

$$\mathbf{c}_n[I] = \mathbf{y}^M[n - N_t - 1]; \quad n = 1, 2, ..., N_t \ . \tag{3.7}$$

   Initially, the membership sets or clusters, Φ_n, $n = 1, 2, ..., N_t$, associated with these centroids are empty.

2. For each $\mathbf{y}^M[k]$ in (3.4), determine which centroid in (3.7) it is closest to using the square Euclidean distance norm and update the membership sets. Specifically, set

$$\mathbf{y}^M[k] \to \Phi_J \text{ iff } J = \underbrace{\arg\min}_{n=1,2,...,N_t} \left\{ \left| \mathbf{y}^M[k] - \mathbf{c}_n[I] \right|^2 \right\}, \tag{3.8}$$

   where $\to$ denotes assigning a membership in a group.

3. Once Step 2 is completed for all the $\mathbf{y}^M[k]$s, increase the iteration counter I by 1 and update the centroids to

$$\mathbf{c}_n[I] = avg\left\{\Phi_n\right\} \tag{3.9}$$

   where $\text{avg}\left\{\Phi_n\right\}$ means taking the average of all the members associated with the n-th centroid.

4. Repeat Step 3 until convergence or for a fixed number of iterations. At this point, the receiver decides that the n-th antenna was activated in interval *k* if $\mathbf{y}^M[k]$ belongs to the n-th cluster Φ_n.

5. Generate the sets $\Psi_1, \Psi_2, ..., \Psi_{N_t}$ according to the following: if $\mathbf{y}^M[k]$ belongs to Φ_n, then $\mathbf{y}[k]$ belongs to Ψ_n, i.e. the members in Ψ_n are the M-th roots of the corresponding members in Φ_n.

It can not be emphasized more that this CA-based receiver is able to associate the different clusters to their respective antennas because of the initial reference symbols in (3.2).

Algorithm 2: (Initial) Detection of the Modulation Symbols

Once the antenna/spatial symbols are detected using the procedure described above, the receiver proceeds to detect the modulation symbols. Once again, the CA is employed. The procedure is as follows:

1. Set antenna/cluster number to $J = 1$.

2. Set the iteration counter to $I = 0$ and set the initial centroids to be

$$\mathbf{d}_m[I] = \mathbf{y}[J - N_t - 1]S_m; \quad m = 1, 2, ..., M, \tag{3.10}$$

where $S_m = e^{j2\pi m/M}$ is the m-th point in the modulation constellation. In the absence of noise, these initial centroids are the channel vector $\mathbf{h}_J$ multiplied by the different modulation symbols. Let $\Lambda_1, \Lambda_2, ..., \Lambda_M$ denote the clusters associated with these centroids. These clusters are empty at this stage.

3. For each member $\mathbf{y}[k]$ in the group Ψ_J (see Step 5 in the previous procedure), determine which centroid in (3.10) it is closest to using the square Euclidean distance norm and update the membership sets. Specifically, set

$$\mathbf{y}[k] \to \Lambda_K \text{ iff } K = \underbrace{\arg\min}_{m=1,2,...,M} \left\{ \left| \mathbf{y}[k] - \mathbf{d}_m[I] \right|^2 \right\} \tag{3.11}$$

4. Once Step 3 is completed for all members in the group Ψ_J increase the iteration counter *I* by 1 and update the centroids to

$$\mathbf{d}_m[I] = \text{avg}\{\Lambda_m\};\ m = 1, 2, ..., M \tag{3.12}$$

where $\text{avg}\{\Lambda_m\}$ means taking the average of all the members in the cluster Λ_m.

5. Repeat Step 4 until convergence or for a fixed number of iterations. At this point, the receiver decides that the *m*-th modulation was transmitted in interval *k* (via antenna *J*) if $\mathbf{y}[k]$ belongs to Λ_m (and Ψ_J).

6. Perform decision-aided channel estimation according to

$$\hat{\mathbf{h}}_J = \frac{\sum_{m=1}^{M}\left(\sum_{i=1}^{n_m}\boldsymbol{\lambda}_{m,i}\right)S_m^*}{n_1 + n_2 + ... + n_M} \tag{3.13}$$

where $\boldsymbol{\lambda}_{m,i}$, $i = 1, 2, ..., n_m$, are members of the cluster Λ_m, and the multiplication of Λ_m by S_m^* represents modulation removal.

7. Increase the antenna counter *J* by 1 and repeat steps 2 to 6 until all antenna groups are exhausted.

Note that the set of channel estimates obtained in (3.13) can be used in a decision-aided coherent detector for making final decisions on both the spatial and modulation symbols.

As an illustrative example, let us consider the case of $N_t = 2$ transmit antennas, a block size of $N_B = 64$, and BPSK modulation; refer to Table 3.1 for the corresponding encoding rule. According to Algorithm 1, the steps in detecting the antenna/spatial bits are:

I. Initially we set the iteration counter to $I = 0$ and the two initial centroids to $\mathbf{c}_1[I] = \mathbf{y}^2[-2]$ and $\mathbf{c}_2[I] = \mathbf{y}^2[-1]$ as per Eqn. (3.7). The empty clusters associated with those centroids are Φ_1 and Φ_2.

II. For each $\mathbf{y}^2[k]$, $k = 0,1,...,63$, determine which of $\mathbf{c}_1[I]$ and $\mathbf{c}_2[I]$ is closer to $\mathbf{y}^2[k]$ as per (3.8) and update the clusters Φ_1 and Φ_2 accordingly.

III. Once all the $\mathbf{y}^2[k]$s are examined, increase the iteration counter to $I = I + 1$ and update the centroids to $\mathbf{c}_1[I] = avg\{\Phi_1\}$ and $\mathbf{c}_2[I] = avg\{\Phi_2\}$ as per (3.9).

IV. Repeat Step III until there is no more switching of members between the two clusters. The receiver decides either antenna 1 or antenna 2 was activated in interval k depending on whether $\mathbf{y}^2[k]$ belongs to Φ_1 or Φ_2.

V. The sets Ψ_1 and Ψ_2 are generated by checking whether $\mathbf{y}^2[k]$ belongs to Φ_1 or Φ_2. Specifically, if $\mathbf{y}^2[k]$ belongs to Φ_1, assign $\mathbf{y}[k]$ to Ψ_1; else assign $\mathbf{y}[k]$ to Ψ_2.

Without loss of generality, let us assume at the end of Steps IV and V in the above procedure, $\mathbf{y}^2[0], \mathbf{y}^2[1], ..., \mathbf{y}^2[35]$ were found to belong to Φ_1 while $\mathbf{y}^2[36], \mathbf{y}^2[37], ..., \mathbf{y}^2[63]$ were found to belong to Φ_2. The receiver then decides (preliminarily) that the antenna/spatial bits in the first 36 intervals are "0" and those in the remaining 28 intervals are "1". Furthermore, the sets Ψ_1 contains $\mathbf{y}[0], \mathbf{y}[1], ..., \mathbf{y}[35]$ while the set Ψ_2 contains $\mathbf{y}[36], \mathbf{y}[37], ..., \mathbf{y}[63]$. At this point, the receiver proceeds to detect (preliminarily) the modulation bits according to Algorithm 2 as follows (Step I below incorporates both Steps 1 and 2 in the original algorithm):

I. Consider first Antenna 1 and its cluster Ψ_1 provided by Algorithm 1. Initially, we set the iteration counter to $I = 0$ and the initial centroids to

$\mathbf{d}_1[I] = \mathbf{y}[-2]S_1$, and $\mathbf{d}_2[I] = \mathbf{y}[-2]S_2$ as per Eqn. (3.10), where $S_1 = -1$ and $S_2 = +1$. The clusters, Λ_1 and Λ_2, associated with $\mathbf{d}_1[I]$ and $\mathbf{d}_2[I]$ are empty at this point.

II. For each $\mathbf{y}[k]$ in the group Ψ_1, determine which of $\mathbf{d}_1[I]$ and $\mathbf{d}_2[I]$, $\mathbf{y}[k]$ is closer to and update the clusters Λ_1, and Λ_2 accordingly as per Eqn. (3.11).

III. Once all the members of Ψ_1 are placed in their respective clusters, increase iteration counter to $I = I + 1$ and update the centroids to $\mathbf{d}_1[I] = \text{avg}\{\Lambda_1\}$ and $\mathbf{d}_2[I] = \text{avg}\{\Lambda_2\}$ as per (3.12).

IV. Repeat Step II and III until convergence or for a fixed number of iterations. At this stage, the receiver makes decisions on the modulation bits. Specifically, if $\mathbf{y}[k]$ belongs to Λ_1, the receiver decides that a -1 was transmitted in the k-th interval through antenna 1, else it decides that a +1 was transmitted. Continue with our hypothetical example where Antenna 1 was determined being activated in the first 36 intervals. If we further assume that out of these 36 intervals, it was determined that $\mathbf{y}[0], \mathbf{y}[1], ..., \mathbf{y}[15]$ belongs to Λ_1 while $\mathbf{y}[16], \mathbf{y}[17], ..., \mathbf{y}[35]$ belong to Λ_2, this means the (preliminary) decisions are that the -1 modulation symbol was transmitted by Antenna 1 in the first 16 intervals while the +1 symbol was transmitted by the same antenna in the next 20 intervals.

V. After detecting all the modulation bits in cluster Ψ_1, decision aided channel estimation is performed as per Eqn. (3.13). Using the above hypothetical example again, the data-aided channel estimate obtained for the first transmit antenna is $\hat{\mathbf{h}}_1 = \frac{1}{36}\left(\left(\sum_{k=0}^{15} \mathbf{y}[k]\right)\cdot(-1) + \left(\sum_{k=16}^{35} \mathbf{y}[k]\right)\cdot(+1)\right)$ where $\lambda_{1,i} = \mathbf{y}[i-1],\ i = 1,2,....,16$, and $\lambda_{2,i} = \mathbf{y}[i+15],\ i = 1,2,....,20$. Note that with

BPSK modulation, the modulation symbols equal to their respective complex conjugates.

VI. Repeat all the above steps for Antenna 2 and its cluster Ψ_2. The results are the (preliminary) decisions on the modulation symbols transmitted by that antenna and the corresponding channel estimate $\hat{\mathbf{h}}_2$.

3.3. Coherent Detection

Two clustering algorithms were presented in the last section to detect the antenna/spatial symbols and the modulation symbols in a SM system. The first algorithm performs non-coherent detection of the antenna usages after non-linear processing of the received signals while the second algorithm performs decision feedback detection of the modulation symbols by considering all different rotations of the detected channel vectors. Like DSM, the proposed CB-DFB SM scheme requires only N_t reference symbols at the beginning to provide raw channel estimates. As opposed to a pilot-aided system, it does not require any periodic insertion of training symbols nor does it require a computationally intensive receiver to detect the data in a DSM. Another nice feature of the proposed CA based receiver is its ability to generate channel estimates once the modulation symbols are detected. Intuitively, the channel estimates obtained as per (3.13) will be very accurate as long as the preliminary decisions on the antenna/spatial and modulation symbols are reasonably accurate. This suggests a data-aided coherent detector can be used to improve the reliability of the receiver. This receiver makes a joint detection of the antenna/spatial symbol $\mathbf{h}[k]$ and the modulation symbol $s[k]$ using the channel estimates $\hat{\mathbf{H}} \triangleq \left\{\hat{\mathbf{h}}_1, \hat{\mathbf{h}}_2, ..., \hat{\mathbf{h}}_{N_t}\right\}$ in (3.13) based on the ML principle, as follows:

$$(\hat{\mathbf{h}}[k], \hat{s}[k]) = \arg \min_{\substack{\hat{\mathbf{h}} \in \hat{H} \\ S_m \in S}} \left\| \mathbf{y}[k] - \hat{\mathbf{h}}_n S_m \right\|_F^2 \tag{3.14}$$

It should be clear this coherent detector is practically identical to the ideal coherent detector in (2.7) except that it uses the estimated channel vectors instead of the actual

ones. For the $N_t = 2, M = 2$ examples in the last section, the receiver computes the metrics $M_{1,+1} = \left\| \mathbf{y}[k] - \hat{\mathbf{h}}_1 \right\|_F^2$, $M_{1,-1} = \left\| \mathbf{y}[k] + \hat{\mathbf{h}}_1 \right\|_F^2$, $M_{2,+1} = \left\| \mathbf{y}[k] - \hat{\mathbf{h}}_2 \right\|_F^2$, and $M_{2,-1} = \left\| \mathbf{y}[k] + \hat{\mathbf{h}}_2 \right\|_F^2$ for the four combinations of antenna/spatial symbol (1 or 2) and modulation symbol (-1 or +1) and selects the one which is the smallest. For example, if $M_{2,+1}$ is the smallest amongst the four, then the data-aided coherent detector decides that $\hat{\mathbf{h}}[k] = \mathbf{h}_2$, $\hat{s}[k] = +1$.

3.4. Channel Estimation Error and Analytical BER Bound

Channel estimation plays a vital role in any coherent detection process. The mean-square-error (MSE) and the normalized mean-square error (NMSE) are two important indicators of the channel estimator's performance. The MSE of data-aided channel estimator in (3.13) is

$$MSE = E\left[\left\| \mathbf{H} - \hat{\mathbf{H}} \right\|_F^2 \right] \tag{3.15}$$

where $\mathbf{H} = \left[\mathbf{h}_1, \mathbf{h}_2, ..., \mathbf{h}_{N_t} \right]$ and $\hat{\mathbf{H}} = \left[\hat{\mathbf{h}}_1, \hat{\mathbf{h}}_2, ..., \hat{\mathbf{h}}_{N_t} \right]$ are the channel matrix and its estimate respectively, $E[\cdot]$ is the expected value operator and $\|\cdot\|_F$ stands for the Frobenius norm. The normalized MSE, on the other hand is MSE divided by the actual channel power, $\|\mathbf{H}\|_F^2$ and is written as,

$$NMSE = \frac{E\left[\left\| \mathbf{H} - \hat{\mathbf{H}} \right\|_F^2 \right]}{\left\| \mathbf{H} \right\|_F^2}. \tag{3.16}$$

Ideally, one would like to obtain an analytical expression for the MSE and the NMSE. Unfortunately, because of the non-linear processing and decision feedback mechanisms

in the proposed receiver, it is not possible to obtain such analytical results. As such only simulation results are presented.

We first show in Fig. 3.2 and Fig. 3.3 the simulated MSE as per Eqn. (3.15) and NMSE as per Eqn. (3.16) of the channel estimates in (3.13), as functions of the signal-to-noise ratio (SNR) in dB, for a $N_t = 2, N_r = 2$ (2×2) and a $N_t = 4, N_r = 4$ (4×4) configuration. Both systems employ BPSK. In the simulation, the variance of each complex gain term in **H** was set to σ_h^2 while the variance of each component in the noise vector $\mathbf{n}[k]$ in (3.1) and (3.2) was set to 1. The SNR is thus simply defined as $10\log\sigma_h^2$ (dB). It is observed from Fig. 3.2 that the MSEs as per Eqn. (3.15) of both the 2×2 and the 4×4 systems reach their respective "steady state" values at large enough SNRs. With the increase of SNR values, the MSE values decrease and after reaching SNR of around 10 dB, the MSE values for both systems reach their steady state values, which are around 10^{-1} . Since the noise variance used in the simulation was 1, this means if we treat the MSE as noise, there will only be minor degradation in the performance because of imperfect channel estimation. Another interesting observation from the two figures is that, while the 2×2 system exhibits a higher steady state MSE than the 4×4 antenna, the opposite is true when the NMSE is considered instead. As shown in Fig. 3.3, the

difference is about 5 dB at a NMSE of 10^{-5}. This result is consistent with the intuitive belief that a larger number of antennas leads to a better performance.

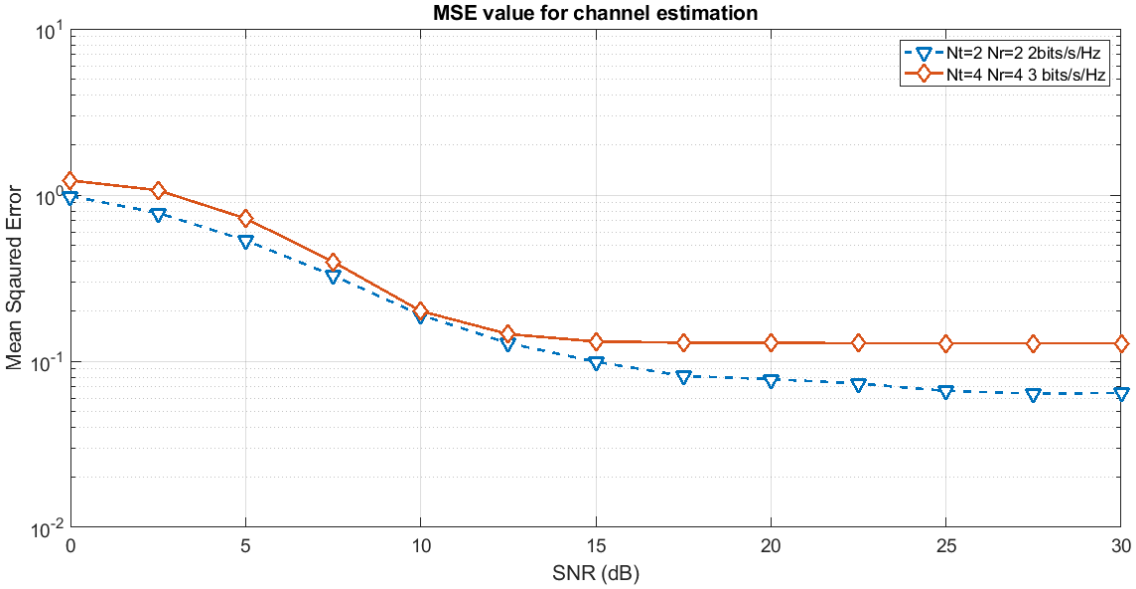

Fig. 3.2: Mean Squared Error Comparisons of channel estimation for $N_t = 2, N_r = 2$ vs $N_t = 4, N_r = 4$ CB-DFB system models

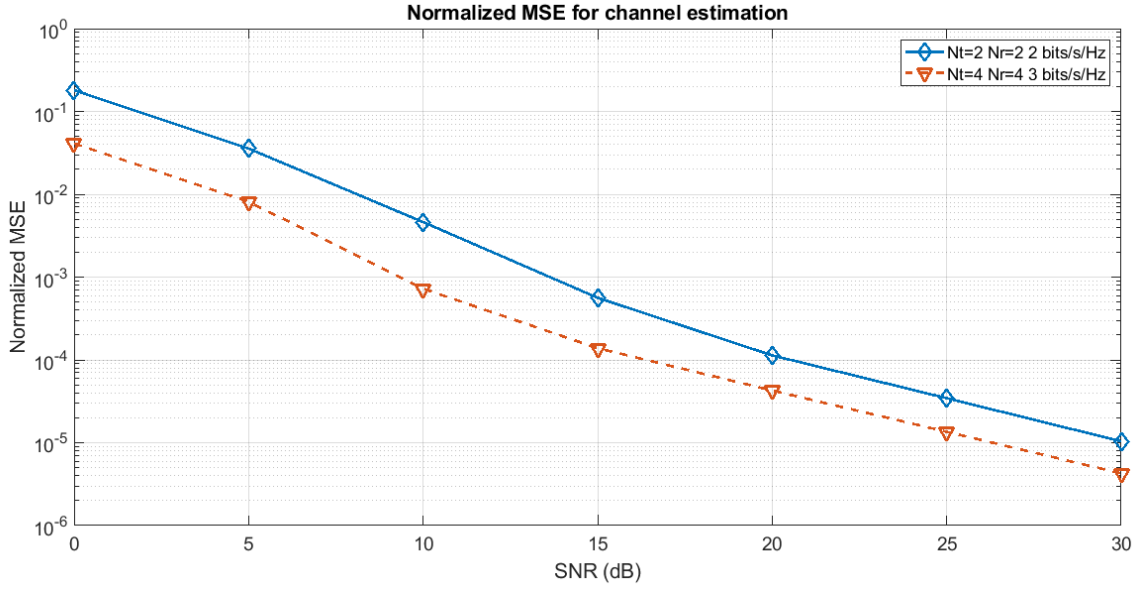

Fig. 3.3: Normalized MSE comparisons of channel estimation for $N_t = 2, N_r = 2$ and $N_t = 4, N_r = 4$ CB-DFB system models.

The effect of modulation on the MSE and NMSE of the proposed CB-DFB SM system is considered in Fig. 3.4 and Fig. 3.5. Specifically, the antenna configuration is set

to $N_t = 2, N_r = 4$ (2×4) while the modulation can be either BPSK or QPSK. It is observed from the two figures that the MSE and the NMSE are substantially higher in QPSK at low SNR, for example 10 times higher at a SNR of 10 dB. However, at SNR of 25 dB or beyond, both BPSK and QPSK attain the same steady state MSE of 6×10^{-2} and the same NMSE. The poorer performance of QPSK at low SNR can be attributed to the fact that QPSK requires a 4-th power nonlinear processing in (3.4) as opposed to a square-law processing for BPSK. When noise level is high (i.e. at low SNR), a higher order non-linear processing will amplify the noise when compared to a lower-order non-linear processing. On the other hand, when the noise level is low (i.e. high SNR), noise amplification due to non-linear processing becomes insignificant.

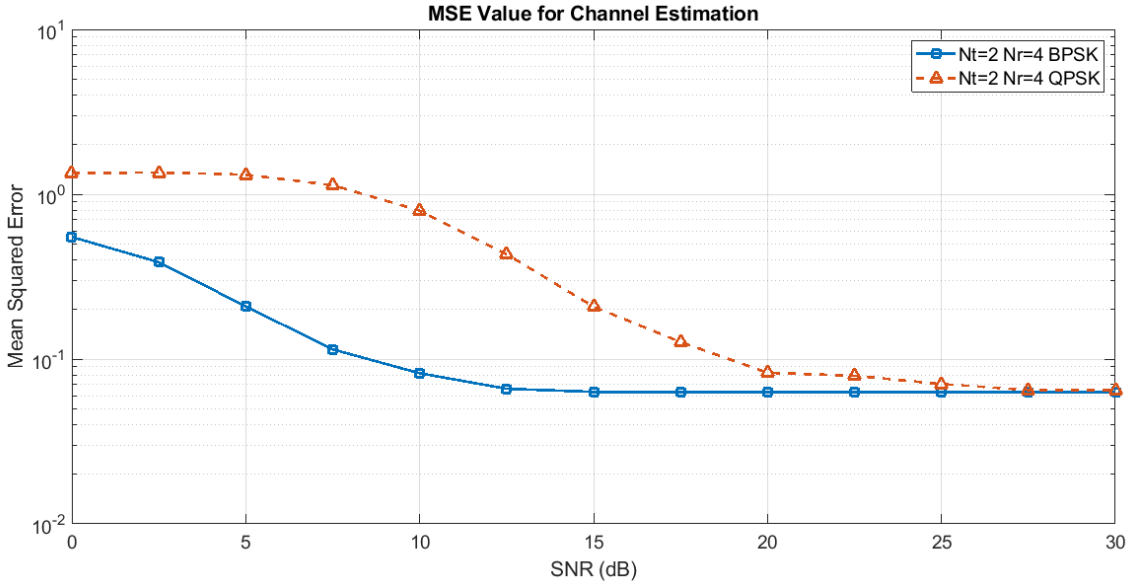

Fig. 3.4: **Mean Squared Error comparisons of channel estimation for $N_t = 2$ and $N_r = 4$, BPSK vs QPSK CB-DFB systems**

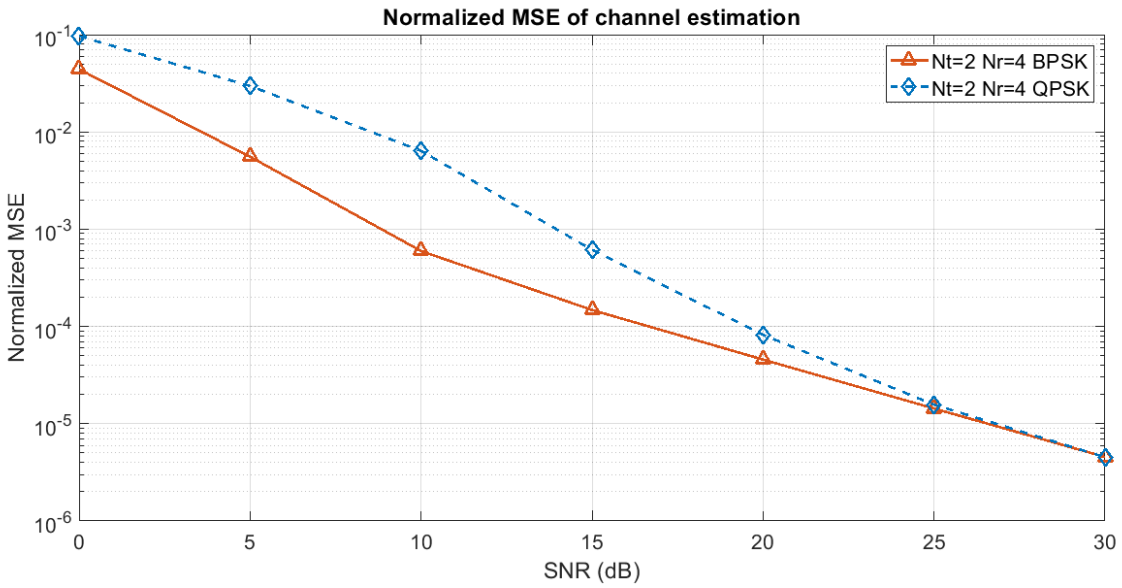

Fig. 3.5: Normalized MSE comparisons of channel estimation for $N_t = 2, N_r = 4$ CB-DFB systems with different modulations.

The reason why we consider the mean-square channel estimation error is that it directly affects the bit error rate (BER) performance of the proposed CB-DFB SM scheme. Specifically, analytical expressions for the Union Bound on the average BER (ABER) of SM with coherent detection were derived in [17] for a Rayleigh flat fading channel with additive white Gaussian noise (AWGN) and Gaussian channel estimation error. The results from [17] are reproduced in Appendix, with the structure of the union bound given by

$$P_{e,bit} \le \sum_{l=1}^{N_t} \sum_{t=1}^{M} \sum_{\hat{l}=1}^{N_t} \sum_{\hat{t}=1}^{M} \frac{e_{\hat{l},\hat{t}}^{l,t} \Pr((\mathbf{h}_l, s_t) \to (\mathbf{h}_{\hat{l}}, s_{\hat{t}}))}{N_t M} \quad . \tag{3.17}$$

In the above equation, $\mathbf{h}_l$ and s_t denote respectively the transmitted antenna/spatial and modulation symbols respectively, $\Pr((\mathbf{h}_l, s_t) \to (\mathbf{h}_{\hat{l}}, s_{\hat{t}}))$ denotes the Pairwise Error Probability (PEP) of deciding on the pair $(\mathbf{h}_{\hat{l}}, s_{\hat{t}})$ when $(\mathbf{h}_l, s_t)$ is transmitted, and $e_{\hat{l},\hat{t}}^{l,t}$ is the number of bits in error associated with the pairwise error event . It should be emphasized that the PEP is a function of the MSE. The detail calculation can be referred to Appendix.

The ABER as per Eqn. (3.17) of a $N_t = 2, N_r = 1$ and a $N_t = 2, N_r = 2$ systems are shown in Fig. 3.6. Both systems employ BPSK modulation and both has a throughput of 2 bits/interval. Also included in the figure are the simulated BERs of the two systems. In generating the ABER curves, we simply substituted the simulated MSE of the two systems into the analytical expressions in Appendix. It is observed from Fig. 3.6 that the ABER and the simulated BER agree with each other. Specifically, the union bound in (3.17) is very tight at large SNR. Also notice that the union bounds can have a BER higher than 0.5 and that is because for low SNR values the bound is loose. The main conclusion that can be drawn from these results is that the channel estimation error can be modelled as Gaussian.

Fig. 3.7 repeats the same exercise in Fig. 3.6 for 4 transmit antennas and 1 and 2 receive antennas. Again, the modulation is BPSK. Just like in Fig. 3.5, it is observed that using the simulated MSE in the ABER equation in (3.17) generates a tight upper bound on the BER at large SNR.

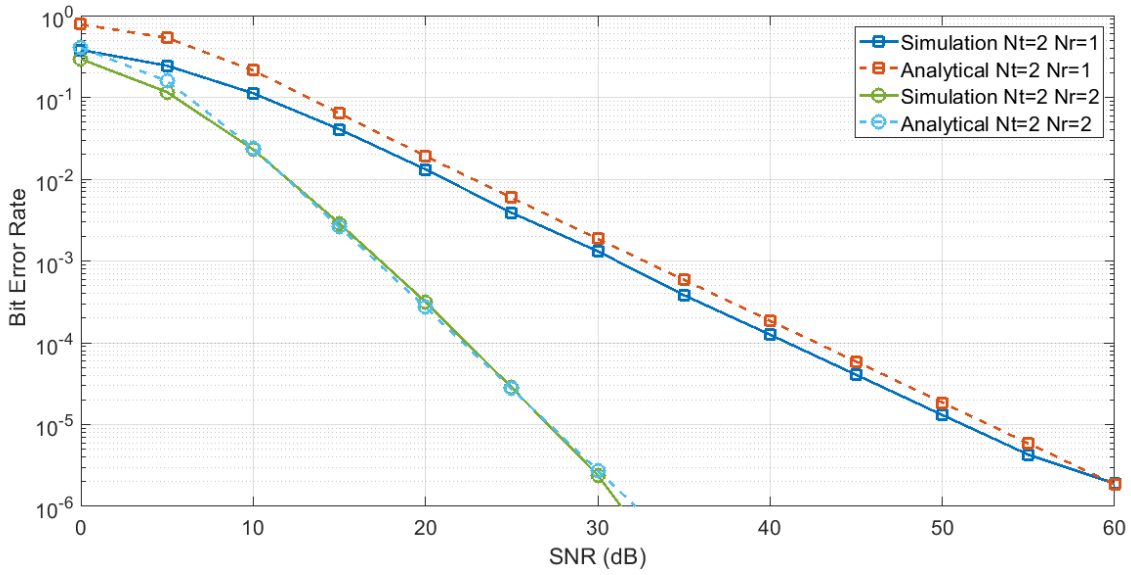

Fig. 3.6: BER comparison of analytical bound vs simulation result for CB-DFB schemes with $N_t = 2, N_r = 1$ and $N_t = 2, N_r = 2$.

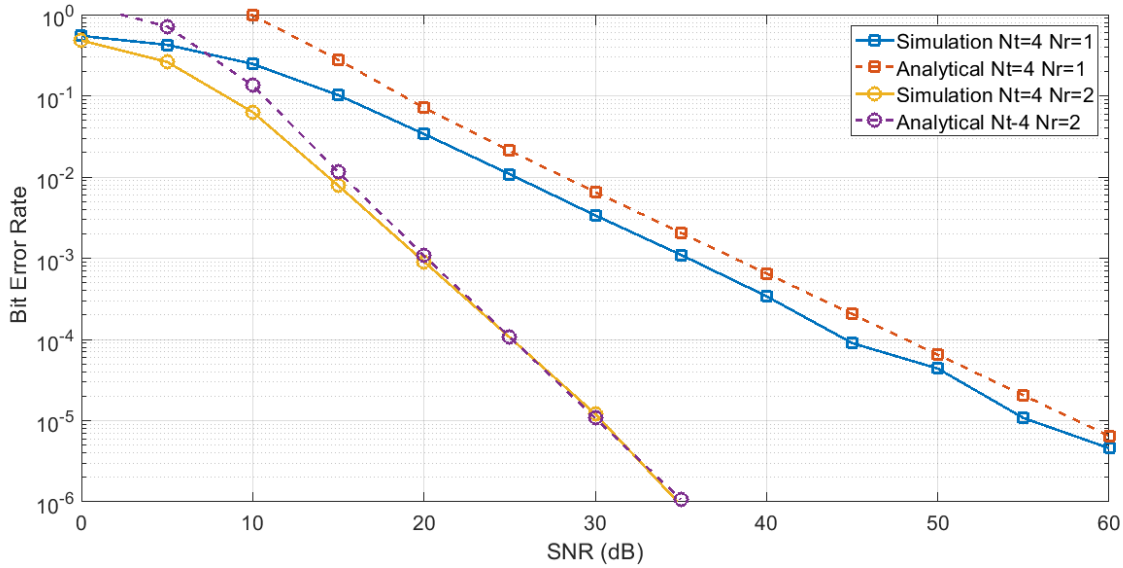

Fig. 3.7: BER comparison of analytical bound vs Simulation result of CB-DFB schemes with $N_t = 4, N_r = 1$ and $N_t = 4, N_r = 2$.

3.5. Throughput and BER Results

Throughput or bandwidth efficiency refers to the information rate that can be transmitted over a given bandwidth in a specific communication system. Throughout this thesis, the system throughput is measured in bits/interval. As shown in (2.1), the throughput of the proposed CB-DFB scheme is

$$\eta_{CB-DFB} = \lfloor \log_2(N_t) \rfloor + \log_2(M). \tag{3.18}$$

This equation suggests that to reach the desired throughput, we can increase the number of transmit antenna, N_t, and/or increase the order of modulation M. As an example, for a basic $N_t = 2$ CB-DFB system with BPSK ($M = 2$) modulation constellation, the throughput as per (3.18) is $\eta_{CB-DFB} = 1 + 1 = 2$ bits/interval. If we want to increase the throughput to 3 bits/interval, we can increase the number of transmit antenna to $N_t = 4$ while keeping the order of the PSK modulation constellation at $M = 2$. Alternatively, we can keep the number of antennas at $N_t = 2$, while increasing the order of the PSK modulation constellation to $M = 4$, i.e. QPSK. As will be shown by the BER results below, it seems that a scheme with a higher number of transmit antennas and a lower

modulation order is preferred over a scheme with a smaller number of transmit antennas but a higher modulation order.

3.5.1. BER Results

In this section, we compare the BER performance of the proposed CB-DFB scheme against DSM [20], [25] and conventional pilot aided spatial modulation (PSM) [24] in a flat Rayleigh fading channel with additive white Gaussian noise. The BERs of these schemes will be plotted as functions of the SNR (in dB). The transmit power is constraint, i.e. the transmit power is divided among active transmit antennas. As only one transmit antenna remains active at any time instant, the per-antenna power constraint equals total transmit power constraint. As discussed earlier, both CB-DFB and DSM uses the same number of initial reference symbols and both do not require periodic reference symbol insertions as in PSM.

CB-DFB vs DSM

We first compare the proposed CB-DFB scheme with DSM for different antenna and modulation configurations at various throughput.

Fig. 3.8 compares the BER performance between CB-DFB and DSM using $N_t = 2, N_r = 1, 2, 4$ transmit antennas. The target throughput is 2 bits/interval. In case of CB-DFB, BPSK modulation was used as per Eqn. (3.18). However, for DSM, the two signaling intervals in each encoding period uses different modulations: BPSK in the first time interval and QPSK in the second time interval. Note that if BPSK is used in both intervals of the encoding periods in DSM, the throughput will only be 1.5 bits/interval. It can be noticed from the figure that the BER performance of the CB-DFB scheme is quite similar to the DSM. However, as it will be shown later on, the computational complexity of CB-DFB is much simpler. It is also observed from the figure that the number of receive antennas should be equal or higher than the number of transmit antennas to extract the maximum potential of SM.

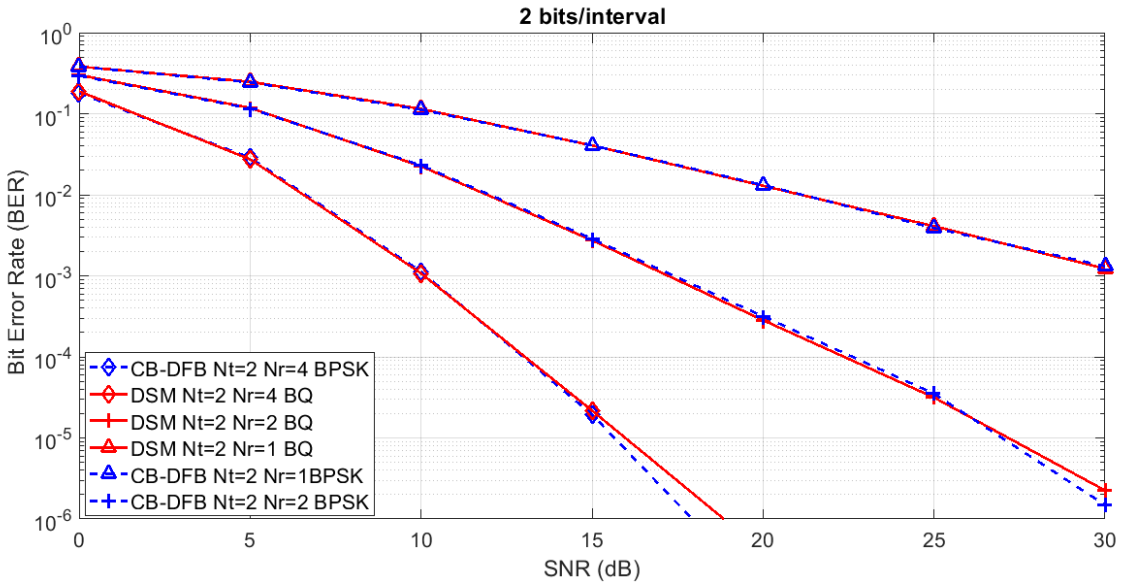

Fig. 3.8: BER performance of decision feedback scheme versus differential spatial modulation at 2 bits/interval transmission rate with $N_t = 2$. CB-DFB uses BPSK whereas DSM uses BPSK and QPSK for the two time instants respectively

Fig. 3.9 provides a detail breakdown of the BERs of CB-DFB in Fig. 3.8 into separate BERs for the antenna/spatial bits and the modulation bits. It is observed that the modulation bits consistently have a lower BER than the antenna/spatial bits. This probably is due to the fact that the entire decision feedback mechanism is kick-started by first detecting the antenna/spatial bits via non-linear processing and that's why they are less reliable.

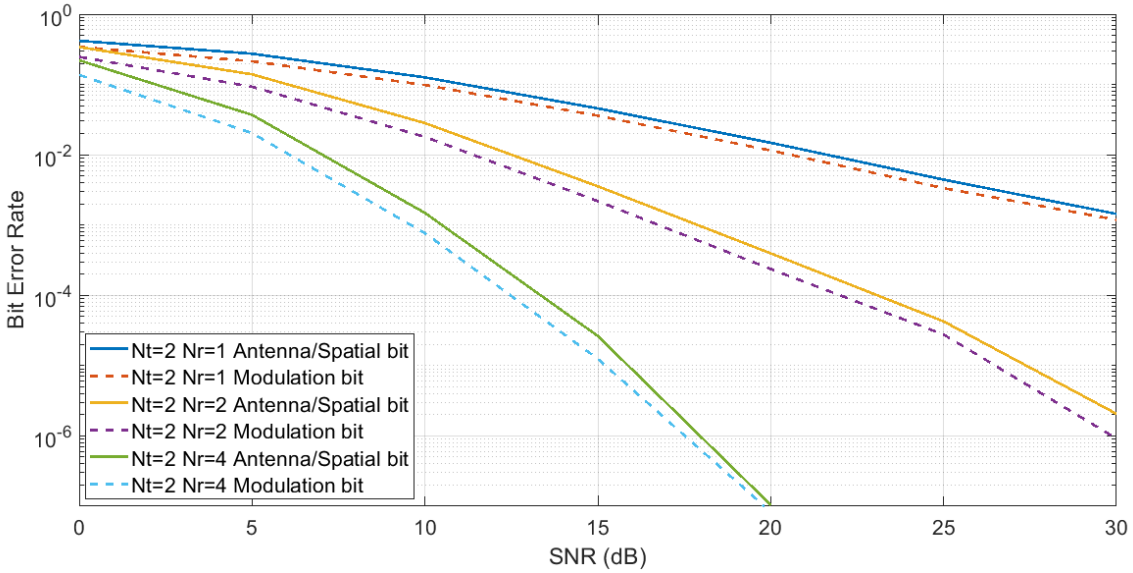

Fig. 3.9: BER performance of spatial bits and modulation bits detection shown separately for the CB-DFB scheme with $N_t = 2$ and BPSK modulation

The case of a transmission rate of 3 bits/interval is considered in Fig. 3.10. The number of transmit antennas is $N_t = 4$ (2 antenna/spatial bits per interval) while the numbers of receive antennas are $N_r = 1, 2, 4$. For CB-DFB, the modulation format was BPSK while for DSM, the modulation was QPSK in all the 4 intervals within an encoding period. The BER results show that for $N_r = 1$, CB-DFB performs a tad better than DSM. Whereas for $N_r = 2$ and $N_r = 4$ DSM performs slightly better than CB-DFB. In the worst-case scenario, CB-DFB has a performance penalty of less than 0.5 dB in the SNR for equal BER when compared with DSM.

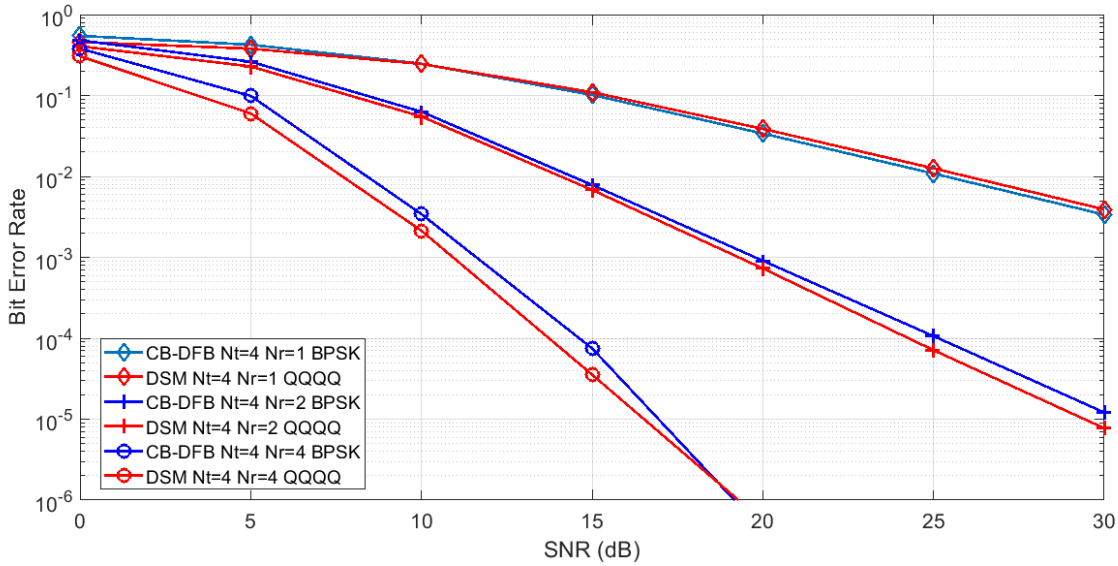

Fig. 3.10: BER performance of clustering based decision feedback scheme versus differential spatial modulation at 3 bits/interval transmission rate with $N_t = 4$. CB-DFB uses BPSK whereas DSM uses QPSK for the four time instants

Fig. 3.11 compares the BER of the proposed CB-DFB scheme for different types of antenna configurations and at various throughput. Three sets of configurations were considered: $N_t = 2, 4,$ and 8 and BPSK modulation was used throughout the 3 sets to achieve throughput of 2, 3, and 4 bits/interval respectively. For each set of configurations, the number of receive antennas was varied. In general, it is observed that the order of diversity in the BER equals to the number receive antennas. For example, when the number of receive antenna is one, we achieve a 1st order diversity; when the number of receive antennas is two, we achieve a 2nd order diversity and so on. For the same number of receive antennas, it is observed that the smaller the number of transmit antennas, the lower the BER. For example, the 2×4 configuration has a lower BER than the 4×4 configuration, which itself has a lower BER than the 8×4 configuration. This can be explained from the fact that the smaller N_t is, the less crowded is the spatial constellation, allowing the receiver to more accurately differentiate the different spatial clusters.

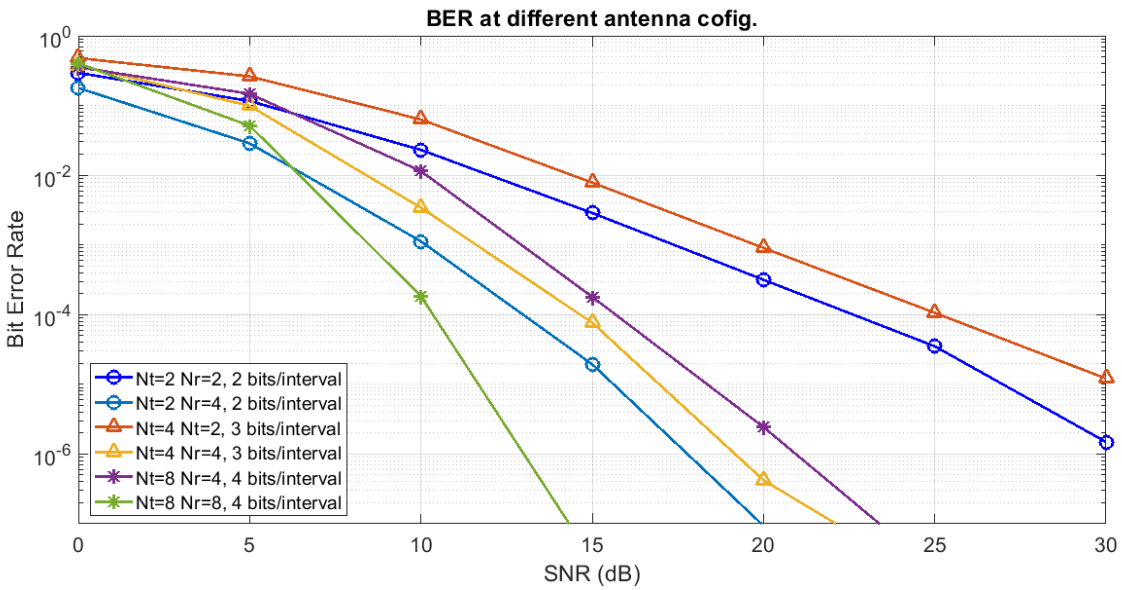

Fig. 3.11: BER comparison of CB-DFB scheme for different antenna configurations at different throughput

CB-DFB vs PSM

Fig. 3.12 compares the BER of the pilot aided spatial modulation (PSM) [24] and the proposed scheme for a $N_t = 2$, $N_r = 2$ configuration. Note that the detector for the PSM is that in Eqn. (2.9) except that the actual channel gains are replaced by their estimates provided by the pilot-aided channel estimator. In order to estimate the channel, the PSM [34] system inserts pilot symbol blocks periodically into data stream, with each block containing N_t initial reference symbols (one per transmit antenna). For the PSM in Fig. 3.12, the pilot insertion rate is 2 pilot symbols every 6 data symbols, or a 25% insertion rate. In contrast, the proposed CB-DFB requires only one block of initial reference symbols. As a result, the loss in throughput in the proposed system due to the reference symbols is almost negligible compared to that of PSM. As shown in the figure, the BER for PSM is better than the CB-DFB scheme because of its higher channel estimation accuracy. At a BER of 10^{-4}, the difference between PSM and CB-DFB is about 2 dB in SNR.

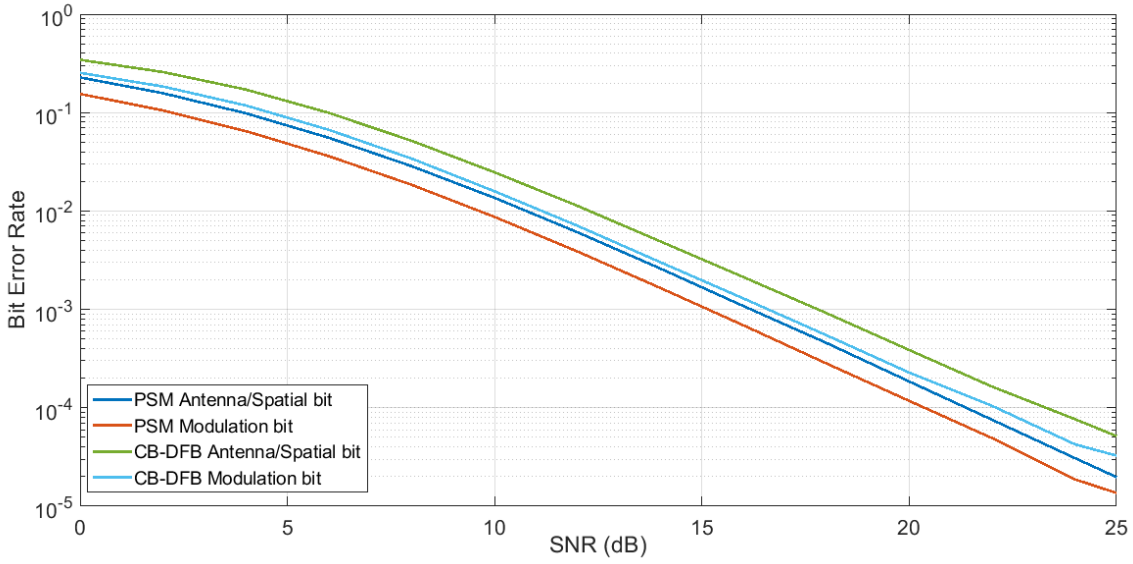

Fig. 3.12: BER comparison among pilot-aided spatial modulation, clustering based decision feedback coherent detection for a $N_t = 2, N_r = 2$ system with BPSK modulation.

3.6. Complexity comparison of CB-DFB vs DSM

As shown in the last section, the proposed CB-DFB scheme has a BER performance very similar to that of DSM. In this part, we compare the receiver complexity of the two schemes. In our presentation, we quantify complexity by the number of multiply-and-add (MAD) required in the detection process of each information bit at the receiver.

For DSM, it had already been shown in Eqn. (2.22) that the complexity per encoding block is

$$N_{total,DSM} = M^{N_t} 2^{\lfloor \log_2(Nt!) \rfloor} N_t^2 (N_t + N_r) = 2^B N_t^2 (N_t + N_r), \tag{3.19}$$

or the complexity per information bit is

$$N_{total,DSM} / bit = \frac{2^B N_t^2 (N_t + N_r)}{B} = \frac{2^{\eta N_t} N_t (N_t + N_r)}{\eta} \tag{3.20}$$

where according to (2.15) and (2.16), $B = \lfloor \log_2(N_t!) \rfloor + N_t \log_2(M)$ is the total number of bits per encoding block and $\eta = B / N_t$ is the throughput. The last equation suggests that for a fixed throughput, the receiver complexity grows exponentially with the number of transmit antennas. As for the proposed CB-DFB scheme, the complexity per encoding block is

$$N_{total,CB-DFB} = N_B \times (N_r \times N_t) \times N_I + N_B \times (N_r \times M) \times N_I + N_B \times (N_r \times M) \times N_t \qquad (3.21)$$

where N_B is the block size and N_I is the number of iterations in the clustering algorithms. This complexity per information bit can be expressed as

$$N_{total,CB-DFB} / bit = (N_r \times N_t) \times N_I + (N_r \times M) \times N_I + (N_r \times M) \times N_t \qquad (3.22)$$

Eqn. (3.22) suggests that the per bit receiver complexity of the proposed scheme is linear in the number of iterations in the clustering algorithm, and linear in the product of the numbers of transmit and receive antennas.

The complexity of DSM and CB-DFB for different system configurations and different throughput are summarized in Table 3.2. Except for the case of 2 bits/interval, the complexity of DSM is much higher than the proposed CB-DFB scheme. As a matter of fact, the complexity of DSM is prohibitively large when $N_t = 8$. The complexity of CB-DFB, on the other hand remains low even at high throughput and with a large number of transmit antennas. The conclusion is reached that DSM is impractical for large antenna arrays while the proposed CB-DFB delivers good performance with low complexity for all system configurations of practical interest.

Throughput, η	**Number of Transmit Antennas, N_t**	**Number of Receive Antennas, N_r**	**Size of Mod., DSM, M_{DSM}**	**Size of Mod., CB-DFB, M_{CB-DFB}**	**Number of MADs DSM,**	**Number of MADs CB-DFB**
2 bits/interval	2	2	2,4	2	64	32
3 bits/interval	4	4	4	2	4.37×10^{4}	104
4 bits/interval	4	4	8	4	5.24×10^{5}	160
3 bits/interval	8	8	2,4	-	7.16×10^{8}	-
4 bits/interval	8	8	4,8	2	1.37×10^{11}	368

Table 3.2: Per-bit receiver complexity comparison DSM vs CB-DFB for different throughput with different set of antenna configurations. Number of iterations in case of CF-DFB was considered as $N_I = 3$.

Chapter 4.

Generalized Clustering Based Decision Feedback Coherent Detection for Spatial Modulation

In this chapter, we generalize the CB-DFB SM scheme discussed in the last chapter by allowing more than one antenna to be activated at a time. The resultant scheme will be referred to as a Clustering Based Generalized Decision Feedback (CB-GDFB) scheme. Without loss of generality, the case of 2 activated antennas is considered. In any interval, the activated antennas transmit the same modulation symbol and the total transmitted power is divided among them equally. It should be emphasized that even though two transmit antennas are activated at the same time, only single-RF chain is required as both the antennas send the same data symbol. The detail explanations can be found in [18], [35]–[37]. The CB-GDFB scheme overcomes the constraints of traditional SM while maintaining all the advantages of traditional SM. In particular, the number of transmit antennas is no longer restricted to a power of two.

4.1. System Model

The system model of the proposed CB-GDFB SM is comparable to CB-DFB SM except that it activates α out of N_t antennas at a time, and all the α antennas selected transmit the same modulation symbol. As a result, the number of antenna/spatial bits that will be supported by this generalized scheme per signalling interval is

$$N_{a,CB-GDFB} = \left\lfloor \log_2 \binom{N_t}{\alpha} \right\rfloor, \tag{4.1}$$

where $\binom{N_t}{\alpha}$ stands for number of combinations of N_t transmit antennas taken α at a time. When $\alpha = 1$, Eqn. (4.1) degenerates into the number of the antenna bits in the CB-DFB scheme in the previous chapter. For demonstration purpose, we consider only the

case of $\alpha = 2$, meaning out of N_t transmit antennas, two transmit antennas are activated at any time instant. As an example, when $N_t = 5$ and $\alpha = 2$, the number of antenna bits supported by this generalized scheme is 2 bits per interval, or double that of the $N_t = 4$ and $\alpha = 1$ configuration in Chapter 3. It should be pointed out that while we are now activating 2 antennas at a time during the data transmission phase, the number of initial reference symbols remains at N_t and we are still activating only one antenna at a time during this initial start up phase. Maintaining this structure for the start up phase is crucial to identifying not only the individual antennas, but also their pairwise combinations. We will elaborate on this when we discuss the clustering algorithm for this generalized scheme later on. Another point worth noting is that one RF-chain is needed despite two antennas are activated at a time. This is because both selected antennas are sending the same modulation symbols [18], [35]-[37]. The only additional requirement is that two RF-switches are required to send the same modulation symbol through two transmit antennas.

Fig. 4.1 illustrates the antenna activation process of a $\alpha = 2$ out of $N_t = 6$ transmit antenna system. As mentioned above, two RF switches are needed, and they are denoted as RF_{SW1} and RF_{SW2} in the figure. The positions of the two RF switches in the picture will be determined by the input antenna bits during that interval. An encoding table for this system that supports a throughput of $\eta_{CB-GDFB} = 4$ bits/interval with BPSK modulation is shown in Table 4.1. The notations in this table are identical to that used in Table 1.2. Note that there are 15 combinations of pairs of antennas. This means without any sophisticated source coding, we can use 8 out of these 15 combinations to transport 3 antenna/spatial bits of information per interval. As shown in the figure, the first antenna/spatial bit b_1 is used to select one of the last two antennas through RF_{SW1} while the remaining two antenna/spatial bits, b_2 and b_3, are used to select one of the first four antennas via RF_{SW2}. As multiple antennas transmit at the same time instant, transmit antenna synchronization is required. Fortunately, synchronizing the transmit antenna is a simple process and can be done by driving the two RF switches from the same reference

clock [38]. The 3 antenna/spatial bits, together with the BPSK bit b_4, gives a total throughput of 4 bits/interval. If we were to use DSM or the earlier CB-DBF scheme instead (while keeping BPSK modulation), the number of transmit antennas required to achieve the same throughput are 20 and 8 respectively. In general, the throughput of CB-GDFB with $\alpha = 2$ is,

$$\eta_{CB-GDFB} = \left\lfloor \log_2 \binom{N_t}{2} \right\rfloor + \log_2(M) \qquad (\alpha = 2) \qquad (4.2)$$

where $\binom{N_t}{2}$ stands for number of combinations of all transmit antennas taken 2 at a time.

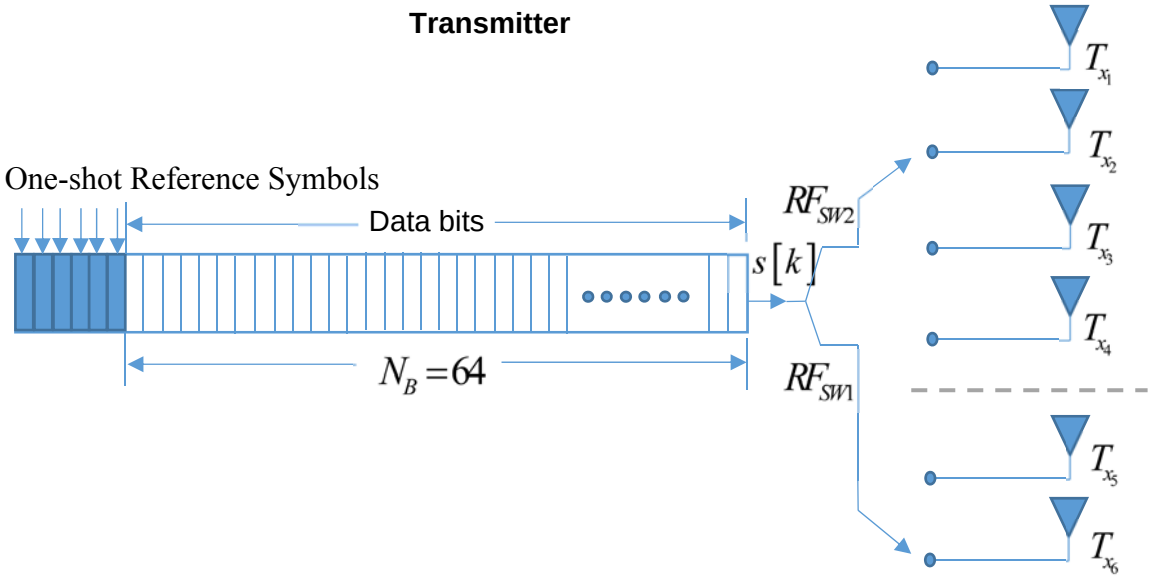

Fig. 4.1: **Clustering based generalized decision feedback scheme with single-RF chain, two RF switches and $N_t = 6$ transmit antennas**

Incoming Bits, $[b_1 \quad b_2 \quad b_3 \quad b_4]$	**Antenna/Spatial Bits,** $[b_1 \quad b_2 \quad b_3]$	**Active Antenna Indices**	**Mod Bit,** b_4	**Mod Sym.**	**Equivalent Signal Vector**
$[0 \quad 0 \quad 0 \quad 0]$	$[0 \quad 0 \quad 0]$	Ant 5, Ant 1	0	-1	$[-1 \quad 0 \quad 0 \quad 0 \quad -1 \quad 0]^T$
$[0 \quad 0 \quad 0 \quad 1]$	$[0 \quad 0 \quad 0]$	Ant 5, Ant 1	1	+1	$[+1 \quad 0 \quad 0 \quad 0 \quad +1 \quad 0]^T$
$[0 \quad 0 \quad 1 \quad 0]$	$[0 \quad 0 \quad 1]$	Ant 5, Ant 2	0	-1	$[0 \quad -1 \quad 0 \quad 0 \quad -1 \quad 0]^T$
$[0 \quad 0 \quad 1 \quad 1]$	$[0 \quad 0 \quad 1]$	Ant 5, Ant 2	1	+1	$[0 \quad +1 \quad 0 \quad 0 \quad +1 \quad 0]^T$
$[0 \quad 1 \quad 0 \quad 0]$	$[0 \quad 1 \quad 0]$	Ant 5, Ant 3	0	-1	$[0 \quad 0 \quad -1 \quad 0 \quad -1 \quad 0]^T$
$[0 \quad 1 \quad 0 \quad 1]$	$[0 \quad 1 \quad 0]$	Ant 5, Ant 3	1	+1	$[0 \quad 0 \quad +1 \quad 0 \quad +1 \quad 0]^T$
$[0 \quad 1 \quad 1 \quad 0]$	$[0 \quad 1 \quad 1]$	Ant 5, Ant 4	0	-1	$[0 \quad 0 \quad 0 \quad -1 \quad -1 \quad 0]^T$
$[0 \quad 1 \quad 1 \quad 1]$	$[0 \quad 1 \quad 1]$	Ant 5, Ant 4	1	+1	$[0 \quad 0 \quad 0 \quad +1 \quad +1 \quad 0]^T$
$[1 \quad 0 \quad 0 \quad 0]$	$[1 \quad 0 \quad 0]$	Ant 6, Ant 1	0	-1	$[-1 \quad 0 \quad 0 \quad 0 \quad 0 \quad -1]^T$
$[1 \quad 0 \quad 0 \quad 1]$	$[1 \quad 0 \quad 0]$	Ant 6, Ant 1	1	+1	$[+1 \quad 0 \quad 0 \quad 0 \quad 0 \quad +1]^T$
$[1 \quad 0 \quad 1 \quad 0]$	$[1 \quad 0 \quad 1]$	Ant 6, Ant 2	0	-1	$[0 \quad -1 \quad 0 \quad 0 \quad 0 \quad -1]^T$
$[1 \quad 0 \quad 1 \quad 1]$	$[1 \quad 0 \quad 1]$	Ant 6, Ant 2	1	+1	$[0 \quad +1 \quad 0 \quad 0 \quad 0 \quad +1]^T$
$[1 \quad 1 \quad 0 \quad 0]$	$[1 \quad 1 \quad 0]$	Ant 6, Ant 3	0	-1	$[0 \quad 0 \quad -1 \quad 0 \quad 0 \quad -1]^T$
$[1 \quad 1 \quad 0 \quad 1]$	$[1 \quad 1 \quad 0]$	Ant 6, Ant 3	1	+1	$[0 \quad 0 \quad +1 \quad 0 \quad 0 \quad +1]^T$
$[1 \quad 1 \quad 1 \quad 0]$	$[1 \quad 1 \quad 1]$	Ant 6, Ant 4	0	-1	$[0 \quad 0 \quad 0 \quad -1 \quad 0 \quad -1]^T$
$[1 \quad 1 \quad 1 \quad 1]$	$[1 \quad 1 \quad 1]$	Ant 6, Ant 4	1	+1	$[0 \quad 0 \quad 0 \quad +1 \quad 0 \quad +1]^T$

Table 4.1: Example of CB-GDFB antenna mapping for $N_t = 6$ transmit antennas with BPSK modulation at 4 bits/interval

The transmitted and received signal structures in CB-GDFB is similar to that of the original CB-DFB scheme in Chapter 3. The modulation symbol transmitted by the two selected antennas in the k-th interval is denoted as $s[k]$, where each $s[k]$ is a MPSK symbol chosen from the set $S \triangleq \{S_1, S_2, ..., S_M\}$. The corresponding received CB-

GDFB signal is similar to that shown in (3.1) except that we have to modify it for two transmit antennas. First, let

$$N_a = 2^{\left\lfloor \log_2 \binom{N_t}{2} \right\rfloor} \tag{4.3}$$

denotes the total number of antenna pairs available for selection by the

$$\eta_A = \left\lfloor \log_2 \binom{N_t}{2} \right\rfloor \tag{4.4}$$

antenna bits. Furthermore, let I_ℓ and J_ℓ be the two antenna indices in the ℓ^{th} pair, where $I_\ell, J_\ell \in \{1,2,...,N_t\}$. The ℓ^{th} effective channel/spatial symbol is subsequently defined as

$$\mathbf{h}_{\ell,eff} = \mathbf{h}_{I_\ell} + \mathbf{h}_{J_\ell}, \qquad \ell = 1,2,...,N_a, \tag{4.5}$$

where $\mathbf{H} \triangleq \{\mathbf{h}_1, \mathbf{h}_2, ..., \mathbf{h}_{N_t}\}$ is the original set of channel/spatial symbols defined in Chapter 3. With these new definitions, the received signal structure in (3.1) can be modified for two transmit antennas according to

$$\mathbf{y}[k] = \mathbf{h}_{eff}[k]s[k] + \mathbf{n}[k];\ k = 0,1,2,...,N_B - 1 \ \text{ (data symbols)} \tag{4.6}$$

where $\mathbf{h}_{eff}[k] \in \mathbf{H}_{eff} \triangleq \{\mathbf{h}_{1,eff}, \mathbf{h}_{2,eff}, ..., \mathbf{h}_{N_{a,eff}}\}$ is the effective channel/spatial symbol in the k-th interval, $\mathbf{n}[k]$ is the noise vector of the k-th signalling interval, and N_B is the block size used in the CB-GDFB scheme. The effective channel gains of $\mathbf{H}_{eff}$ are iid complex Gaussian random variable with zero mean and a variance of σ_h^2. The different components of $\mathbf{n}$ are iid complex Gaussian random variables with zero mean and unit variance, i.e. $\sigma_n^2 = 1$.

As stated earlier even though we are activating two transmit antennas during the data transmission period, only one transmit antenna is activated at any interval during the "initial reference symbols" period and thus the number of initial reference symbols are

still equal to the number of transmit antennas, N_t. The initial reference symbols are unmodulated similar to CB-DFB method, i.e. the values of $s[k]$ is equal to 1 for the initial reference symbols and the reference symbols are transmitted from antenna 1 to N_t at times $-N_t$ to -1 in that order and is expressed as in (3.2)

$$\mathbf{y}[k] = \mathbf{h}_{k+N_t+1} + \mathbf{n}_\circ[k]; k = -N_t, -1 \text{ (initial reference symbols)} \qquad (4.7)$$

where $\mathbf{h} \in \mathbf{H} \triangleq \{\mathbf{h}_1, \mathbf{h}_2, ..., \mathbf{h}_{N_t}\}$, the original set of antenna/spatial symbols as defined in Chapter 3, has zero mean and a variance of $\frac{\sigma_h^2}{2}$ and the noise vector $\mathbf{n}_\circ$ has zero mean and a variance of $\frac{\sigma_n^2}{2}$.

4.2. Clustering Based Channel Estimation and Coherent Detection

In order to detect the antenna/spatial symbol, $\mathbf{h}_{eff}[k]$ and the modulations symbol $s[k]$ accurately from the received signal in (4.6), it is necessary to have knowledge of the channel gains, $\mathbf{h}_{eff}[k] \in \mathbf{H}_{eff} \triangleq \{\mathbf{h}_{1,eff}, \mathbf{h}_{2,eff}, ..., \mathbf{h}_{N_a,eff}\}$. The initial reference symbols received from $-N_t$ to -1 intervals give us approximate information about the channel state information but those are also corrupted with noise and thus are not accurate enough. The effective channel gains are estimated using the clustering algorithms introduced in Chapter 3. The modified clustering algorithm for the generalized scheme is discussed in this section.

4.2.1. Non-linear Processing to remove Modulation

The first step in the clustering algorithm (CA) based detection process is to remove modulation information from the received signal vectors. Let the l-th component of the received signal at the k-th time period be

$$y[l,k] = h_{eff}[l,k]s[k] + n[l,k] \tag{4.8}$$

where $h_{eff}[l,k]$ and $n[l,k]$ are respectively the l-th component of $\mathbf{h}_{eff}[k]$ and $\mathbf{n}[k]$. Since $s[k] = e^{j2\pi m/M}$; $m = 1,2,...,M$, it implies that $s^M[k] = 1$ no matter what the value of $s[k]$ is. Thus, taking M-th power of Eqn. (4.8) we can write

$$y^M[l,k] \approx h_{eff}^M[l,k], \tag{4.9}$$

when $n[l,k]$ is small. Hence, $\mathbf{y}^M[0], \mathbf{y}^M[1], ..., \mathbf{y}^M[N_B - 1]$ are just the noisy versions of

$$\mathbf{h}_{1,eff}^M, \mathbf{h}_{2,eff}^M, ..., \mathbf{h}_{N_a,eff}^M \tag{4.10}$$

where $N_a = 2^{\left\lfloor \log_2 \binom{N_t}{2} \right\rfloor}$ as in Eqn. (4.3). When the block size, N_B, is sufficiently large, there will be multiple noisy copies of $\mathbf{h}_{\ell,eff}^M$ in the set of $\mathbf{y}^M[k]; k = 0,1,...,N_B - 1$. This implies if we form individual clusters of the M-th power of each of the effective channel, $\mathbf{h}_{\ell,eff}^M$, we will have the

1. effective channel/spatial symbol information of the k-th interval, by the knowledge of $\mathbf{y}^M[k]$ belonging to a particular cluster as in Eqn. (4.9)

2. modulation bit information by recognizing that the received vectors in those intervals detected in step 1 are just the noisy versions of the ℓ-th effective channel such as

$$\mathbf{h}_{\ell,eff} s[1], \mathbf{h}_{\ell,eff} s[2], ..., \mathbf{h}_{\ell,eff} s[M] \tag{4.11}$$

The CA algorithm that is used in step 1 to detect the antenna/spatial bits, is used again in step 2 to detect the modulation bits. Similar to the CB-DFB method, CB-GDFB method is also a decision feedback scheme as the decisions on the antenna/spatial symbols in step 1 are used to determine the modulation bits in step 2. Additionally, decision feedback is

again used to derive fine channel estimates for final coherent detection as discussed in Section 4.3.

4.2.2. The Clustering Algorithms for the CB-GDFB scheme

There are two clustering algorithms in the receiver of the proposed CB-GDFB scheme. Clustering Algorithm 1 detects the active antenna pairs, or the effective channel/spatial symbol as defined in Eqn. (4.5) at any k -th interval. The modulation bits associated with the detected effective channels are then detected using Clustering Algorithm 2. Finally, these decisions are then used to perform decision aided channel estimation which is shown in the later part of Clustering Algorithm 2.

Algorithm 1: (Initial) Detection of the Active Antenna Pairs

1. The iteration counter, I , is set to 0. The initial reference symbols are received as in Eqn. (4.7). Let us denote the received initial reference symbols as $\mathbf{c}_1[I], \mathbf{c}_2[I], ..., \mathbf{c}_{N_t}[I]$, where

$$\mathbf{c}_n[I] = \mathbf{y}[n - N_t - 1]; \quad n = 1, 2, ..., N_t \ . \tag{4.12}$$

These are simply noisy estimates of the individual channel symbols, the $\mathbf{h}_n,\ n = 1, 2, ..., N_t$. Since pairs of antennas will be activated during the data transmission phase, the effective centroids, $\mathbf{c}_{1,eff}[I], \mathbf{c}_{2,eff}[I], ..., \mathbf{c}_{N_a,eff}[I]$, of the clustering algorithm are formed according to the mapping rule from antenna/spatial bits to antenna pairs as follows:

$$\mathbf{c}_{\ell,eff}[I] = \left(\mathbf{c}_{I_\ell}[I] + \mathbf{c}_{J_\ell}[I]\right)^M = \left(\mathbf{y}[I_\ell - N_t - 1] + \mathbf{y}[J_\ell - N_t - 1]\right)^M \tag{4.13}$$

where $I_\ell, J_\ell \in \{1, 2, ..., N_t\}$ are the antenna indices associated with the $\ell - th$ antenna pair, $\ell = 1, 2, ..., N_a$, and N_a is the total number of antenna pairs avalilable for selection.

2. The distance between each $\mathbf{y}^M[k];\ k = 0,1,2,...,N_B - 1$, and all the initial centroids defined by (4.13) is measured using the Euclidean distance norm. The membership sets are then updated as

$$\mathbf{y}^M[k] \to \omega_j \quad iff \quad j = \arg\min_{\ell=1,2,...,N_a} \left\{ \left| \mathbf{y}^M[k] - \mathbf{c}_{\ell,eff}[I] \right|^2 \right\} \tag{4.14}$$

where $\mathbf{y}^M[k] \to \omega_j$ denotes assigning $\mathbf{y}^M[k]$ to the cluster ω_j.

3. Once all the $\mathbf{y}^M[k]$s are placed under respective clusters, the iteration counter I is increased by 1 and the centroids are updated as per

$$\mathbf{c}_{\ell,eff}[I] = avg\{\omega_\ell\} \tag{4.15}$$

where $avg\{\omega_\ell\}$ denotes taking average of all the members belonging to ℓ-th centroid.

4. Step 3 is repeated until a fixed number of iterations. After that, if it is found that $\mathbf{y}^M[k]$ belongs to the ℓ-th cluster, ω_ℓ, the receiver decides that the ℓ-th antenna pair was activated in interval k.

5. Given that $\mathbf{y}^M[k]$ belongs to ω_ℓ from Step 4, $\mathbf{y}[k]$ itself will be placed under the companion set of *M*-th roots Ω_ℓ, i.e. the members in Ω_ℓ are the M-th roots of the corresponding members in ω_ℓ.

It is important to mention that the initial unmodulated reference symbols received in (4.7) enables the receiver to link different clusters to its respective transmit antenna pairs. The initial reference symbols have a one to one relation with respective individual antennas. The clusters defined in Eqn. (4.13) is thus able to associate different clusters to their respective active antenna pairs by exploiting the initial reference symbols.

Algorithm 2: (Initial) Detection of the Modulation Symbols

After the detection of the effective antenna/spatial symbols, the receiver detects the modulation symbols associated with those antenna/spatial symbols. The CA algorithm is applied again for this purpose.

1. The first step is to set the antenna cluster number to $\ell = 1$. The antenna pair associated with this cluster is formed of antenna I_ℓ and antenna J_ℓ.

2. The iteration counter is set to $I = 0$ and the initial centroids are chosen as

$$\mathbf{p}_m[I] = (\mathbf{y}[I_\ell - N_t - 1] + \mathbf{y}[J_\ell - N_t - 1])S_m; \qquad m = 1,2,...,M \tag{4.16}$$

   where $S_m = e^{j2\pi m/M}$. In the absence of noise, these initial centroids are the summation of active channel vectors, $\mathbf{h}_{l,eff}$ as in (4.5) multiplied with different modulation symbols. Initially, all the clusters $\gamma_1, \gamma_2, ..., \gamma_M$ associated with these centroids are empty sets.

3. The distance between each member $\mathbf{y}[k]$ of the antenna cluster Ω_ℓ and all the centroids in (4.16) is calculated using the squared Euclidean norm and the membership sets are updated as

$$\mathbf{y}[k] \to \gamma_K \ \ iff \ \ K = \arg\min_{m=1,2,...,M} \left\{ \left| \mathbf{y}[k] - \mathbf{p}_m[I] \right|^2 \right\} \tag{4.17}$$

   where $\mathbf{y}[k] \to \gamma_K$ denotes assigning $\mathbf{y}[k]$ to cluster γ_K.

4. Once all the members of the antenna cluster Ω_ℓ are placed under respective modulation symbol clusters γ_m-s, the iteration counter is increased by 1 and centroids are updated as

$$\mathbf{p}_m[I] = avg\{\gamma_m\}; \ m = 1,2,...,M \tag{4.18}$$

where $avg\{\gamma_m\}$ means taking the average of all the members in the cluster γ_m .

5. Step 3 and step 4 are repeated for a fixed number of iterations. Then if it is found out that the received $\mathbf{y}[k]$ (which was found earlier by Algorithm 1 to belong to Ω_ℓ) belongs to γ_m, the receiver decides that m-th modulation PSK symbol was transmitted in interval k (by the $\ell - th$ antenna pair)

6. Finally, the channel is estimated as

$$\hat{\mathbf{h}}_{\ell,eff} = \frac{\sum_{m=1}^{M}\left(\sum_{i=1}^{n_m}\boldsymbol{\upsilon}_{m,i}\right)S_m^*}{n_1 + n_2 + ... + n_m} \tag{4.19}$$

where $\boldsymbol{\upsilon}_{m,i};\ i = 1,2,...,n_m,$ are the members of cluster γ_m, and the multiplication of γ_m by S_m^* represents modulation removal.

7. The antenna cluster number, ℓ is increased by 1 and all the steps from 2 to 6 are repeated until all the antenna clusters are exhausted.

The channel estimates obtained in (4.19) are later used in a decision-aided coherent detector for making final decisions on both the antenna/spatial symbols and modulation symbols.

To illustrate, let us consider a $N_t = 6$ transmit antenna CB-GDFB system with a block size of $N_B = 64$ and a modulation size of $M = 2$ (i.e. BPSK). The encoding rule is presented in Table 4.1. According to Clustering Algorithm 1, the steps in detecting the effective channel/spatial symbols are the following.

I. Iteration counter I is set to 0, and $N_a = 2^{\left\lfloor \log_2\binom{6}{2} \right\rfloor} = 8$ initial centroids are formed as in (4.13)

$$\mathbf{c}_{1,eff}[I]=\left(\mathbf{y}[-2]+\mathbf{y}[-6]\right)^2,\ \mathbf{c}_{2,eff}[I]=\left(\mathbf{y}[-2]+\mathbf{y}[-5]\right)^2,$$

$$\mathbf{c}_{3,eff}[I]=\left(\mathbf{y}[-2]+\mathbf{y}[-4]\right)^2,\ \mathbf{c}_{4,eff}[I]=\left(\mathbf{y}[-2]+\mathbf{y}[-3]\right)^2,$$

$$\mathbf{c}_{5,eff}[I]=\left(\mathbf{y}[-1]+\mathbf{y}[-6]\right)^2,\ \mathbf{c}_{6,eff}[I]=\left(\mathbf{y}[-1]+\mathbf{y}[-5]\right)^2,$$

$$\mathbf{c}_{7,eff}[I]=\left(\mathbf{y}[-1]+\mathbf{y}[-4]\right)^2,\ \mathbf{c}_{8,eff}[I]=\left(\mathbf{y}[-1]+\mathbf{y}[-3]\right)^2.$$

The clusters $\omega_1,\omega_2,...,\omega_8$ associated with these centroids are empty set at this point.

II. The distance between each $\mathbf{y}^2[k];k=0,1,...,63$ and all the centroids are measured as per Eqn. (4.14) and the clusters $\omega_1,\omega_2,...,\omega_8$ are updated accordingly.

III. Once all the $\mathbf{y}^2[k]$s are placed under respective clusters, the iteration counter I is increased by 1 and the centroids are updated to $\mathbf{c}_{\ell,eff}[I]=avg\{\omega_\ell\};\ell=1,2,...,8$ as per Eqn. (4.15)

IV. Step III is repeated until a fixed number of iterations. The receiver decides which antenna pair from Table 4.1 was active in interval k depending on the cluster, ω_ℓ ; $\ell=1,2,...,8$, where $\mathbf{y}^2[k]$ belongs to.

V. Assuming $\mathbf{y}^2[k]$ belongs to ω_ℓ, $\mathbf{y}[k]$ is placed under Ω_ℓ. For example, if $\mathbf{y}^2[k]$ belongs to clusters ω_5, $\mathbf{y}[k]$ is assigned to Ω_5.

For the sake of clarity, let us assume after completion of step IV and V in the above procedure, $\mathbf{y}^2[0],\mathbf{y}^2[1],...,\mathbf{y}^2[7]$ were found to belong to cluster ω_1; $\mathbf{y}^2[8],\mathbf{y}^2[9],...,\mathbf{y}^2[15]$ were found to belong to cluster ω_2; $\mathbf{y}^2[16],\mathbf{y}^2[17],...,\mathbf{y}^2[23]$ were found to belong to cluster ω_3, and so on, up to $\mathbf{y}^2[56],\mathbf{y}^2[57],...,\mathbf{y}^2[63]$ which were found to belong to cluster ω_8. Based on these clusters, the receiver makes initial decisions on which antenna pairs that were activated, and the antenna/spatial bits

associated with them based on Table 4.1. In this example, in the first 8 intervals, $\mathbf{y}^2[0], \mathbf{y}^2[1], ..., \mathbf{y}^2[7]$ were found to belong to ω_1. Thus the antenna/spatial bits in each of the first 8 intervals are $[0 \quad 0 \quad 0]$ and the square root set Ω_1 contains the received $\mathbf{y}[0], \mathbf{y}[1], ..., \mathbf{y}[7]$. Similarly in the second 8 intervals, $\mathbf{y}^2[8], \mathbf{y}^2[9], ..., \mathbf{y}^2[15]$ were found to belong to ω_2 and thus antenna/spatial bits for each of these 8 intervals are $[0 \quad 0 \quad 1]$, and the square root set Ω_2 contains the received vectors $\mathbf{y}[8], \mathbf{y}[9], ..., \mathbf{y}[15]$. At this point, the receiver proceeds to detect the modulation bits according to Clustering Algorithm 2 as follows.

I. Consider the first antenna pair (Antenna 5 and Antenna 1) and its cluster Ω_1 provided by Clustering Algorithm 1.

II. The iteration counter I is set to 0 and the initial centroids are chosen as $\mathbf{p}_1[I] = (\mathbf{y}[-2] + \mathbf{y}[-6])S_1$ and $\mathbf{p}_2[I] = (\mathbf{y}[-2] + \mathbf{y}[-6])S_2$ as per Eqn. (4.16), where $S_1 = -1$ and $S_2 = +1$. The clusters, γ_1 and γ_2, associated with these centroids are empty at this stage.

III. The distance between each member $\mathbf{y}[k]$ of the antenna cluster Ω_1 and the centroids $\mathbf{p}_1$ and $\mathbf{p}_2$ is calculated using squared Euclidean norm and the clusters γ_1 and γ_2 are updated as per Eqn. (4.17).

IV. Once all the members of the antenna cluster Ω_1 are placed into their respective modulation symbol clusters, the iteration counter I is increased by 1 and the centroids are updated to $\mathbf{p}_1 = avg\{\gamma_1\}$ and $\mathbf{p}_2 = avg\{\gamma_2\}$ as per (4.18)

V. Step III and step IV are repeated for a fixed number of iterations. At this point the receives decides on the modulation bits. Explicitly, if $\mathbf{y}[k]$ belongs to γ_1, the receiver decides that -1 was transmitted in the k-th interval through the first antenna pair (Antenna 5 and Antenna 1). Similarly, if $\mathbf{y}[k]$ belongs to γ_2 the

receiver decides that +1 was transmitted through the first antenna pair (Antenna 5 and Antenna 1). Recalling our assumption for this example, it was assumed that the first antenna pair was activated in the first 8 intervals. If we assume that out of those 8 intervals, $\mathbf{y}[0],\mathbf{y}[1],...,\mathbf{y}[3]$ belong to γ_1 while $\mathbf{y}[4],\mathbf{y}[5],...,\mathbf{y}[7]$ belong to γ_2, it means through the first antenna pair (Antenna 5 and Antenna 1), -1 was transmitted during the first 4 intervals and $+1$ was transmitted during the next 4 intervals.

VI. Once all the modulation bits in the antenna cluster Ω_1 is detected, decision aided channel estimation is performed as per Eqn. (4.19). Thus, the channel estimate for the first effective channel is, $\hat{\mathbf{h}}_{1,eff} = \frac{\left(\sum_{k=0}^{3}\mathbf{y}[k]\right).(-1)+\left(\sum_{k=4}^{7}\mathbf{y}[k]\right).(+1)}{4+4}$ where $\upsilon_{1,i}=\mathbf{y}[i-1]; i=1,2,...,4$, $\upsilon_{2,i}=\mathbf{y}[i+3]; i=1,2,...,4$, and $n_1=4, n_2=4$.

VII. All the steps from 2 to 6 are repeated for the rest of the antenna pairs and their clusters $\Omega_2,\Omega_3,...,\Omega_7$. Hence, the receiver makes initial decisions of the modulation symbols transmitted by the active antenna pairs and the corresponding effective antenna/channel estimates $\hat{\mathbf{h}}_{2,eff},\hat{\mathbf{h}}_{3,eff},...,\hat{\mathbf{h}}_{8,eff}$.

4.3. Coherent Detection of CB-GDFB

In the previous section two clustering algorithms were presented namely initial detection of active antenna pairs and initial detection of modulation symbols. Algorithm 1 detects the active antenna pairs at any time instant after a non-linear processing of the received signals while Algorithm 2 performs decision feedback detection of the modulation symbols by considering all different rotations of the detected effective channel vectors. Just like the CB-DFB scheme in Chapter 3, the CB-GDFB scheme requires only N_t initial reference symbols at the beginning to provide raw channel estimates and does not require any periodic insertion of the training symbols. However, it is worth noting that the CB-GDFB scheme actually requires lesser number of transmit

antennas to achieve the same antenna/spatial constellation size of a CB-DFB scheme. This is explained by Eqn. (4.1) where it says the number of antenna/spatial bits varies with the number of active antennas α according to $N_{a,CB-GDFB} = \left\lfloor \log_2 \binom{N_t}{\alpha} \right\rfloor$ (where $\alpha = 2$ for the CB-GDFB scheme, and $\alpha = 1$ for the CB-DFB scheme for). Since the number of antennas is less in the generalized scheme, it also requires less number of initial reference symbols. The gap between the numbers of initial reference symbols requirement for the two schemes broadens with the increase in throughput and this will be shown later in Table 4.2. Meanwhile the receiver's computational complexity of CB-GDFB scheme is alike that of CB-DFB scheme.

The CA algorithm of the CB-GDFB scheme retains the feature of calculating fine effective channel estimates. The effective channel estimates obtained as in Eqn. (4.19) is very accurate as long as the initial decision on the antenna/spatial symbols and modulation symbols are reasonably accurate. These fine channel estimates are then used to perform coherent ML detection. The receiver makes joint detection of the antenna/spatial symbol $\mathbf{h}_{eff}[k]$ and the modulation symbol $s[k]$ using the channel estimates $\hat{\mathbf{H}}_{eff} \triangleq \{\hat{\mathbf{h}}_{1,eff}, \hat{\mathbf{h}}_{2,eff}, ..., \hat{\mathbf{h}}_{N_a,eff}\}$ derived as per Eqn. (4.19) based on the ML principle. Thus, the final decisions on the antenna/spatial symbol and modulation symbol are made as follows:

$$(\hat{\mathbf{h}}_{eff}[k], \hat{s}[k]) = \underset{\substack{\hat{\mathbf{h}}_{eff} \in \hat{\mathbf{H}}_{eff} \\ S_m \in S}}{\arg\min} \left\| \mathbf{y}[k] - \hat{\mathbf{h}}_{\ell,eff} S_m \right\|_F^2 \tag{4.20}$$

This coherent ML detector is identical to the coherent ML detector used in CB-DFB case as in (3.14) except that it uses effective channel estimates instead of individual channel estimates. For the $N_t = 6,$ or $N_a = 2^{\left\lfloor \log_2 \binom{N_t}{2} \right\rfloor} = 8$ and $M = 2$ example in the Section 4.2, the receiver computes the matrices

$$M_{1,\pm1} = \left\| \mathbf{y}[k] \mp \hat{\mathbf{h}}_{1,eff} \right\|_F^2,\ M_{2,\pm1} = \left\| \mathbf{y}[k] \mp \hat{\mathbf{h}}_{2,eff} \right\|_F^2,\ M_{3,\pm1} = \left\| \mathbf{y}[k] \mp \hat{\mathbf{h}}_{3,eff} \right\|_F^2,$$

$$M_{4,\pm1} = \left\| \mathbf{y}[k] \mp \hat{\mathbf{h}}_{4,eff} \right\|_F^2,\ M_{5,\pm1} = \left\| \mathbf{y}[k] \mp \hat{\mathbf{h}}_{5,eff} \right\|_F^2,\ M_{6,\pm1} = \left\| \mathbf{y}[k] \mp \hat{\mathbf{h}}_{6,eff} \right\|_F^2,$$

$$M_{7,\pm1} = \left\| \mathbf{y}[k] \mp \hat{\mathbf{h}}_{7,eff} \right\|_F^2, \text{ and } M_{8,\pm1} = \left\| \mathbf{y}[k] \mp \hat{\mathbf{h}}_{8,eff} \right\|_F^2$$

for the 16 combination of antenna/spatial symbol (1 to 8) and modulation symbol (-1 or +1), and selects the one which is smallest. For example, if $M_{7,+1}$ is the smallest among the 16, then the data aided coherent detector decides that $\hat{\mathbf{h}}_{eff}[k] = \mathbf{h}_{7,eff}$, $\hat{s}[k] = +1$.

4.4. Channel Estimation Error Compared with CB-DFB

In this section we compare the channel estimation error of the CB-GDFB scheme with that of CB-DFB for several modulation and antenna configurations. The MSE of data aided channel estimator in (4.19) is

$$MSE_{CB-GDFB} = E\left[\left\| \mathbf{H}_{eff} - \hat{\mathbf{H}}_{eff} \right\|_F^2 \right] \tag{4.21}$$

where $\mathbf{H}_{eff} = \{\mathbf{h}_{1,eff}, \mathbf{h}_{2,eff}, ..., \mathbf{h}_{N_a,eff}\}$ and $\hat{\mathbf{H}}_{eff} = \{\hat{\mathbf{h}}_{1,eff}, \hat{\mathbf{h}}_{2,eff}, ..., \hat{\mathbf{h}}_{N_a,eff}\}$ are the effective channel matrix and its estimates respectively, $E[\cdot]$ is the expected value operator and $\|\cdot\|_F$ stands for the Frobenius norm. The normalized MSE, on the other hand is defined as MSE divided by the actual effective channel power, $\left\| \mathbf{H}_{eff} \right\|_F^2$ and is expressed as

$$NMSE_{CB-GDFB} = \frac{E\left[\left\| \mathbf{H}_{eff} - \hat{\mathbf{H}}_{eff} \right\|_F^2 \right]}{\left\| \mathbf{H}_{eff} \right\|_F^2} \tag{4.22}$$

Due to the non-linear processing applied before Clustering Algorithm 1 and the decision feedback mechanism in clustering algorithm 2, it is not possible to obtain any analytical expressions for the MSE and NMSE. As such only simulated results are presented in this section.

The MSE and NMSE comparison between CB-DFB and CB-GDFB schemes are shown in Fig. 4.2 and Fig. 4.3 respectively for a throughput of 5 bits/interval. As mentioned in the last section, CB-GDFB can achieve a higher throughput with a smaller number of transmit antennas when compared to traditional SM schemes; refer to Eqn. (4.2). For example, the $N_t = 16, N_r = 8$ (16×8), $M = 2$ CB-DFB system in Fig. 4.2 has the same throughput of 5 bits/interval as the $N_t = 7, N_r = 8$ (7×8), $M = 2$ CB-GDFB system shown in the same figure. Note that in the simulation of the MSEs in Fig. 4.2, the variance of each complex gain term $h_{l,k}$ in $\mathbf{H}$ was set to σ_h^2 and the variance of each component in the noise vector $\mathbf{n}[k]$ was set to 1 as in (3.1) for the CB-DFB case. However, for the CB-GDFB scheme, the variance of each $h_{l,k}$ is halved to make the variance of each effective gain of the form $h_{l,k,eff} = h_{l,k_1} + h_{l,k_2}$ to stay at σ_h^2. There is no change to the noise variance in $\mathbf{n}[k]$. As a result, the SNR in both cases is $10 \log \sigma_h^2$ (dB).

It is observed in Fig. 4.2 that the MSE values of the 16×8 CB-DFB scheme and the 7×8 CB-GDFB scheme almost overlaps with each other and reach their steady state of 10^{-1} at around 10 dB. The slightly higher MSE in CB-GDFB in the lower SNR range can be attributed to the way the initial centroids in the generalized scheme are formed. Note that in CB-GDFB, the initial centroids were the sums of two received reference symbols while those in CB-DFB were the received reference symbols themselves. The steady state MSE of 10^{-1} is appealing because it is one-tenth of the noise power. This means at large SNR, the NMSE in (4.22) should vary inversely with the SNR.

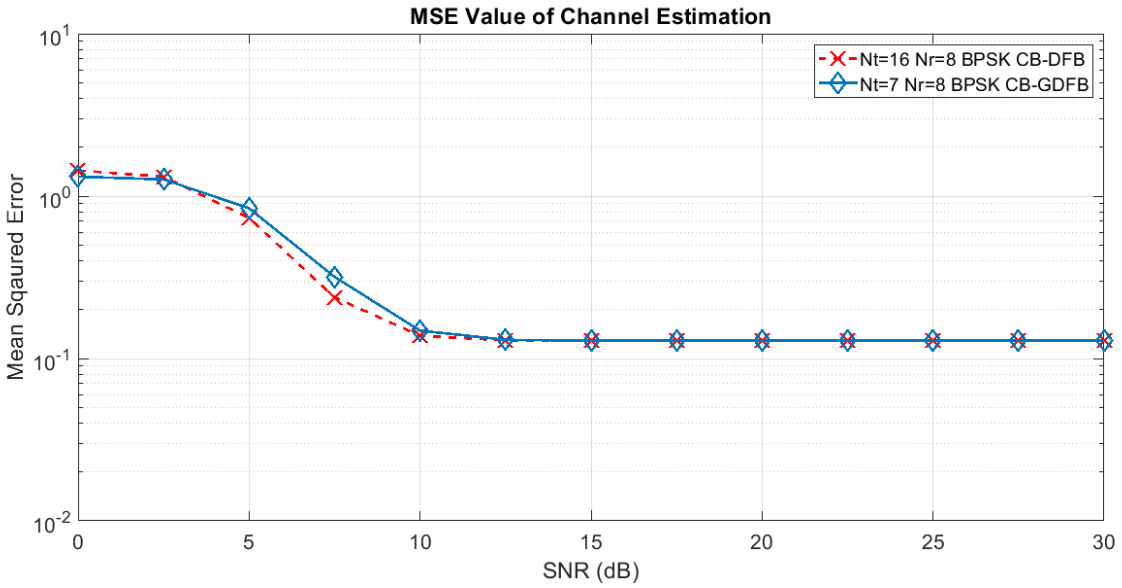

Fig. 4.2: Mean Squared Error Comparisons for CB-DFB vs CB-GDFB for the same throughput of 5 bits/interval at different antenna configurations

The NMSE of the two schemes in Fig. 4.2 are shown in Fig. 4.3. As analyzed earlier, the NMSE varies inversely with the SNR asymptotically, i.e. decreases by 1 decade per 10 dB increase in the SNR.

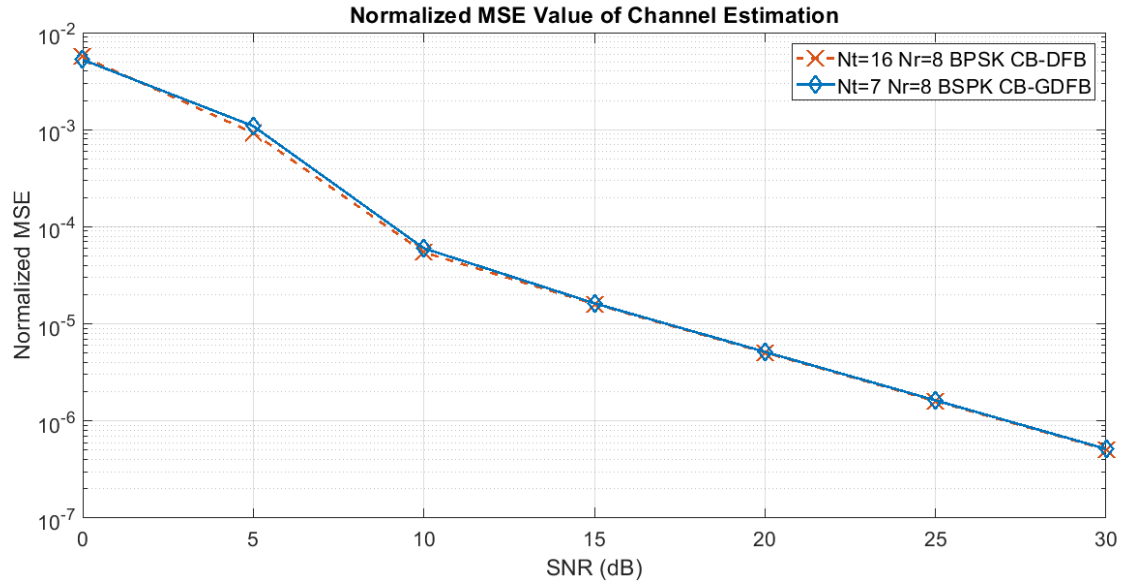

Fig. 4.3: Normalized MSE value comparison of CB-DFB vs CB-GDFB with different antenna configurations with throughput of 5 bits/interval

Fig. 4.4 further compares the channel estimation errors of a CB-DFB scheme with a $N_t = 8, N_r = 8\left(8 \times 8\right)$ configuration and a CB-GDFB scheme with a $N_t = 5, N_r = 8\left(5 \times 8\right)$ configuration. Both schemes use BPSK modulation and both have a throughput of 4 bits/interval. From the figure, it can be observed that the channel estimation error for the CB-DFB scheme is slightly less than that of CB-GDFB for SNR values up to 10 dB and after that both schemes' MSE values converge. The poorer estimation error for CB-GDFB is again explained by the way how the initial centroids are obtained. Finally, the normalized MSEs of both schemes are provided in Fig. 4.5. As in Fig. 4.3, it is observed that at large SNR, the NMSE decreases at a rate of one decade per 10 dB increase in SNR, which indicates that the decision feedback channel estimator is working properly.

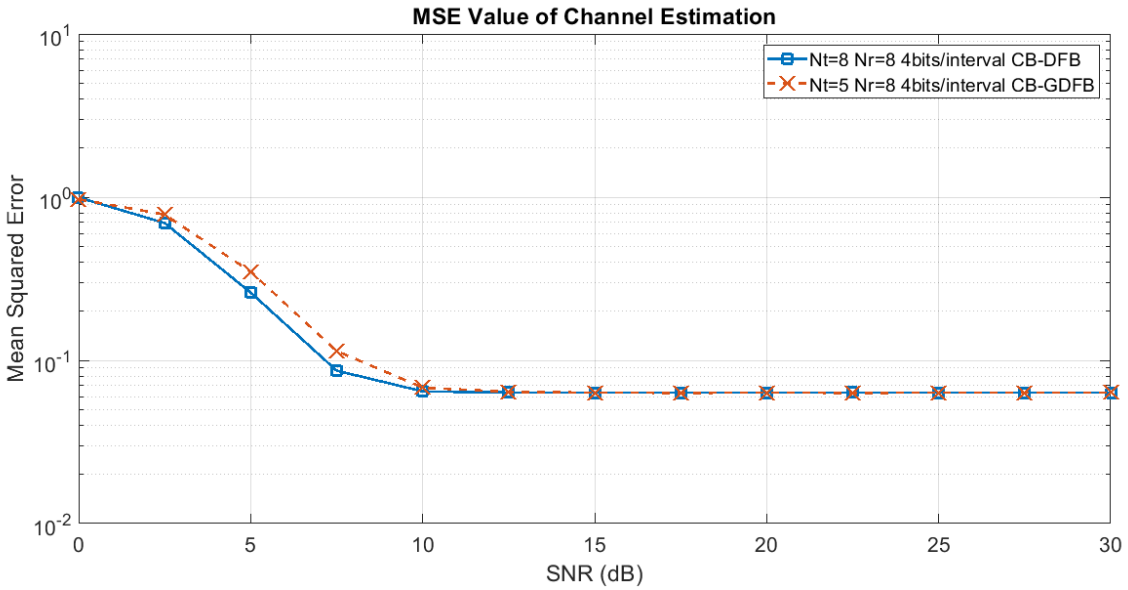

Fig. 4.4: Mean Squared Error comparisons of channel estimation between CB-DFB and CB-GDFB for a throughput of 4 bits/interval

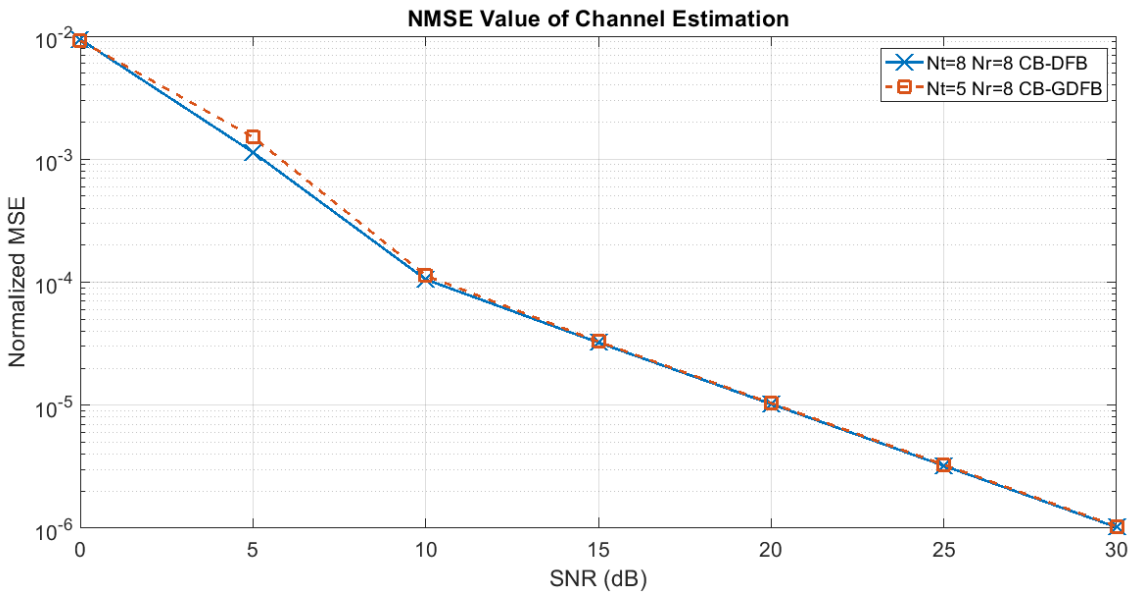

Fig. 4.5: Normalized MSE value comparison of channel estimation between CB-DFB and CB-GDFB for a throughput of 4 bits/interval

4.5. Throughput and BER Results Compared with CB-DFB

In this section we will compare the throughput of the CB-DFB scheme discussed in Chapter 3 with the CB-GDFB scheme proposed in this chapter. It will be shown that the CB-GDFB scheme has a higher throughput compared to that of traditional SM, DSM, and CB-DFB scheme. The throughput formula for CB-GDFB is expressed as in (4.2) as $\eta_{CB-GDFB} = \left\lfloor \log_2 \binom{N_t}{2} \right\rfloor + \log_2(M)$, where $\binom{N_t}{2}$ means that out of N_t antennas two antennas remain active at any time instant. Thus, CB-GDFB increases the overall throughput by base-two logarithm of the number of antenna combinations.

To illustrate, for a $N_t = 5$ transmit antenna system with BPSK modulation in case of traditional SM and CB-DFB, the throughput as per (2.1) or (3.18) is $\eta_{SM/CB-DFB} = 3$ bits/interval. In case of DSM the throughput for the same $N_t = 5$ transmit antenna system with BPSK modulation as per (2.16) is $\eta_{DSM} = 2.2$ bits/interval. On the other hand, if we consider CB-GDFB for the same system model with $N_t = 5, M = 2$, the throughput, as per (4.2), is $\eta_{CB-GDFB} = 4$ bits/interval. Thus, for the same antenna array size and

modulation constellation, traditional SM and CB-DFB scheme has a higher throughput compared to DSM; and CB-GDFB has a higher throughput compared to all of them. This is one of the major advantages of CB-GDFB over the aforementioned schemes. Equivalently, CB-GDFB can attain the same throughput as the other schemes with a smaller number of transmit antennas, N_t. For example, to achieve the same throughput of $\eta_{CB-GDFB} = 4$ bits/interval as the above $N_t = 5$ BPSK CB-GDFB scheme, traditional SM and CB-DFB require 8 antennas while DSM requires 20. These additional antenna requirements translate directly into extra reference symbols and hence reduce the effective throughput of these systems. Table 4.2 compares the reference symbol requirement and the receiver complexity (measured in number of MAD) of CB-DFB and CB-GDFB at different throughput during the data transmission phase. It should be evident from the table at high throughput (during the data transmission phase), the number of initial reference symbols in CB-DFB can become excessive, significantly reducing the overall effectiveness of the scheme.

4.5.1. BER Results Comparison

In this section, we compare the CB-GDFB scheme's performance with CB-DFB and PSM [24]. All results consider flat Rayleigh fading channel with AWGN noise. The BER results are plotted as function of SNR (dB). The total transmit power is constrained and is divided among the active antennas. As two transmit antennas remain active at any given time in the case of CB-GDFB, the per-antenna power constraint equals to half of the total transmit power constraint. As mentioned above, CB-GDFB uses less initial reference symbols compared to CB-DFB and neither of them requires any periodic insertion of the training symbols as in the PSM scheme.

CB-GDFB vs CB-DFB

CB-GDFB is compared with CB-DFB for various antenna and modulation configurations and at several throughput. Before doing that though, lets first establish concrete rationales for introducing the generalized scheme by revisiting the original CB-DFB scheme. Fig. 4.6 compares three CB-DFB schemes with different modulation

constellations and different numbers of transmit antennas. The number of received antennas is 4 for all three schemes. From the figure we can observe that the two BPSK schemes performs significantly better than the $N_t = 2$ QPSK scheme. Their error curves exhibit a 4-th order diversity while that of the QPSK scheme exhibits only a second-order diversity despite the fact that there are 4 receive antennas. The better performance in BPSK can be explained by the non-linear processing in the CA algorithm as defined by Eqn. (3.4) as it implies that a higher order modulation goes through a higher order non-linear processing. When 4 -th order non-linear processing is applied in case of QPSK, it amplifies the noise compared to the 2 -nd order non-linear processing of BPSK. As a result, for equal throughput, the BER performance is better when BPSK is used instead of QPSK. Although the QPSK scheme has the poorest BER performance, its throughput is higher than the $N_t = 2$ BPSK scheme. It also requires less transmit antennas than $N_t = 4$ BPSK scheme. In the following, we will see how the proposed CB-GDFB scheme in this Chapter can achieve a high throughput and good error performance without employing QPSK modulation and without using a large number of transmit antennas.

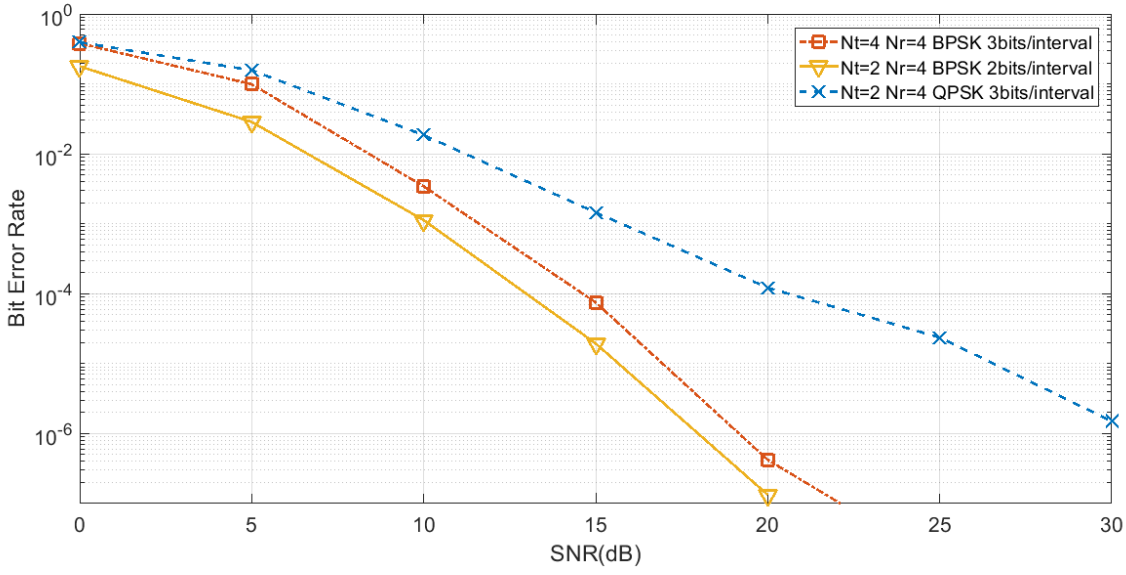

Fig. 4.6: BER performance comparison between CB-DFB schemes for different modulation orders and different throughput

Fig. 4.7 compares the BER performance between CB-GDFB and CB-DFB at a throughput of 4 bits/interval; refer to (4.3) and (3.18) for the throughput of the two approaches. The CB-GDFB scheme in the figure uses 5 transmit antennas and BPSK modulation while the CB-DFB scheme uses 4 transmit antennas and QPSK modulations. Both schemes employ 8 receive antennas. Note that in case of CB-DFB, the number of transmit antennas can actually vary from 4 to 7 without any change in the throughput for the same modulation scheme. It is because of the constraint in the CB-DFB scheme which requires the number of transmit antennas to be a power of 2[1]. This is why we adopt a "$N_t = 4/5$" notation in the legend for the CB-DFB scheme to emphasize that the result is valid for both 4 or 5 transmit antennas. In contrast, CB-GDFB overcomes this constraint and can adopt in principle a random number of transmit antennas to meet the throughput requirement, like $N_t = 5$ for the CB-GDFB scheme in Fig. 4.7 . The results in the figure shows that CB-GDFB achieves a much higher order diversity than the CB-DFB scheme for the same number of transmit to receive antennas. As explained earlier, this is because it uses BPSK (instead of QPSK) and antenna pairing to achieve a higher spatial constellation.

[1] If a sophisticated source-coding scheme is employed, this constraint can be removed.

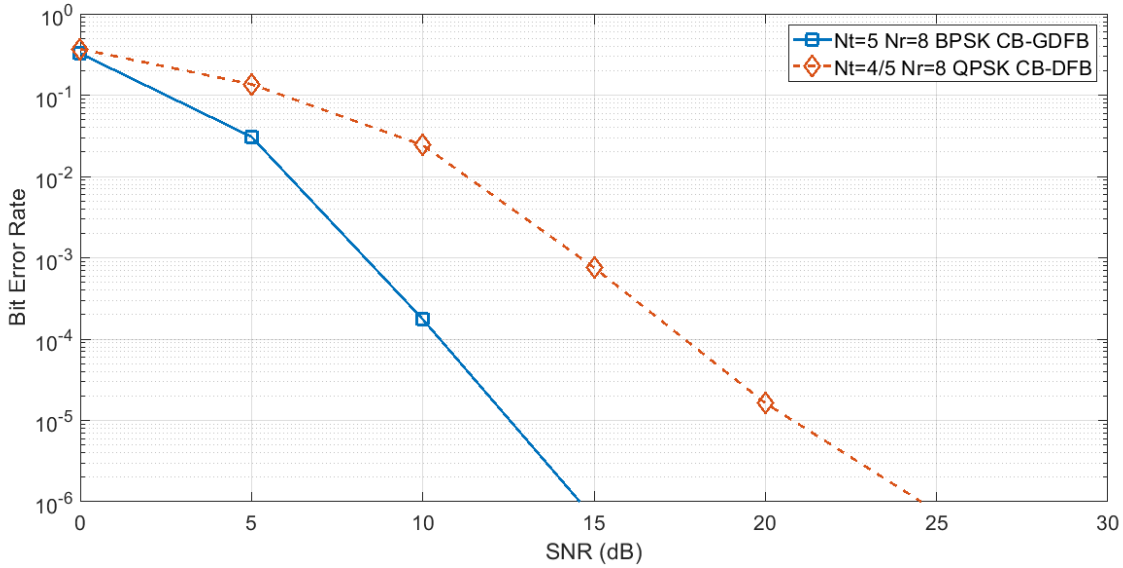

Fig. 4.7: BER performance of CB-GDFB Scheme versus CB-DFB Scheme at 4 bits/interval. CB-GDFB requires BPSK whereas CB-DFB requires QPSK to achieve the same throughput as of CB-GDFB.

Next, we compare the $N_t = 5$ CB-GDFB BPSK scheme with a $N_t = 8$ CB-DFB BPSK scheme. Both schemes have the same throughput of 4 bits/interval and both employ 8 receive antennas. The results are shown in Fig. 4.8. It is observed that the CB-GDFB scheme has a higher BER at larger SNRs. This can be explained from the fact that with 8 eight transmit antennas activated twice at a time, the spatial constellation in the CB-GDFB scheme is denser than the CB-DFB scheme with the same number of antennas but activated only one at a time. However, one advantage the CB-GDFB scheme has is that it requires only 5 initial reference symbols as opposed to 8 in the CB-DFB case.

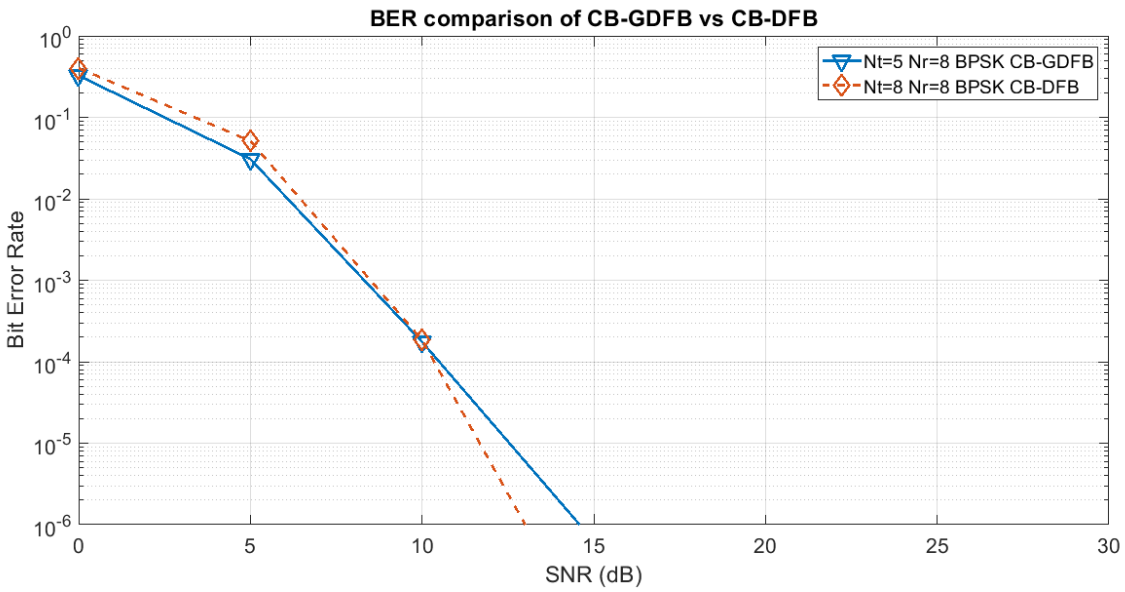

Fig. 4.8: BER comparison between CB-DFB and CB-GDFB at 4bits/interval. CB-DFB requires $N_t = 8$ whereas CB-GDFB requires $N_t = 5$ transmit antennas to achieve the same throughput.

In Fig. 4.9, we compare CB-DFB and CB-GDFB at a throughput of 5 bits/interval: a $N_t = 7$ CB-GDFB BPSK scheme , a $N_t = 16$ CB-DFB BPSK scheme, and a $N_t = 8$ CB-DFB QPSK scheme. Consistent with previous two figures, the QPSK scheme has the worst performance while the two BPSK schemes have similar BER. Amongst the two BPSK schemes, the CB-GDFB scheme has a higher BER than the CB-DFB scheme for the reason explained earlier in Fig. 4.8. The difference is 2 dB at a BER of 10^{-6}. However, it requires 9 less initial reference symbols, where 9 is the difference between the number of transmit antennas in the two systems. As will be shown in Section 4.6, that the number of reference symbols requirement gap between CB-DFB and CB-GDFB broadens substantially with the increase of throughput.

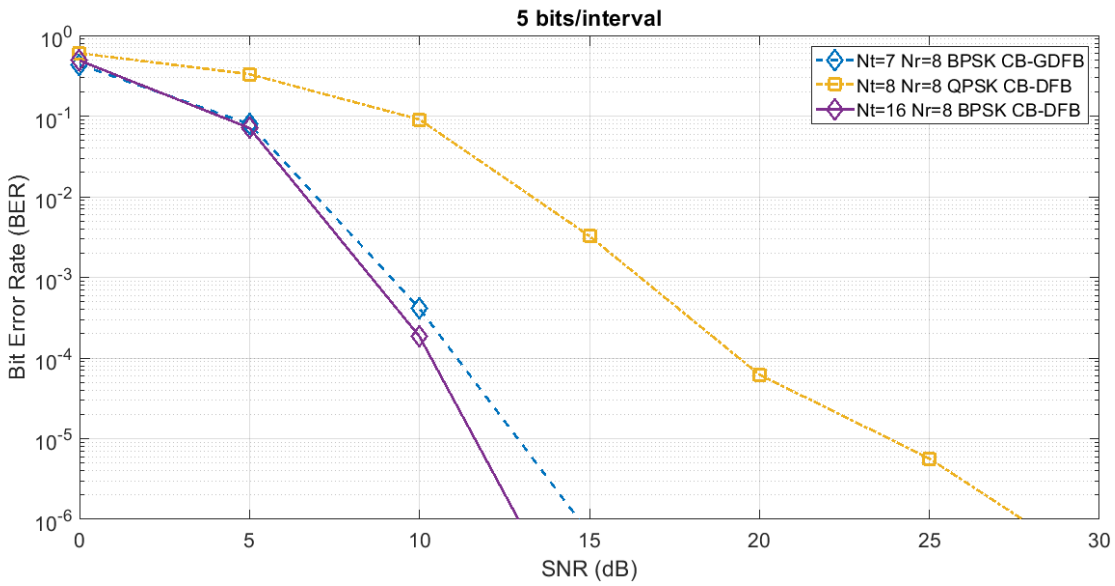

Fig. 4.9: BER comparison between CB-DFB and CB-GDFB at 5 bits/interval. CB-DFB requires $N_t = 16$ initial reference symbols whereas CB-GDFB requires only $N_t = 7$ initial reference symbols to achieve the same throughput for the same modulation constellation.

CB-DFB vs CB-GDFB vs PSM

Fig. 4.10 compares the BER among the CB-DFB, CB-GDFB and conventional PSM method. All of the schemes have a throughput of 4 bits/interval and use BPSK modulation. The bit error rate of antenna/spatial bits and modulation bits are shown separately for each case. PSM has the least BER because a higher number of pilot symbols are sent periodically throughout the data block. CB-DFB performs slightly worse than PSM, because in case of CB-DFB reference symbols are used only at the beginning of the data stream. As mentioned before, the number of initial reference symbols in CB-DFB and CB-GDFB equals the number of transmit antennas. As a result, the CB-GDFB in the figure uses only 5 initial reference symbols while the CB-DFB scheme uses 8. As for PSM scheme in Fig. 4.10, the pilot insertion rate is 8 pilot symbols every 24 data symbols, or a 25% insertion rate. So, its effective throughput is actually lower than 4 bits/interval.

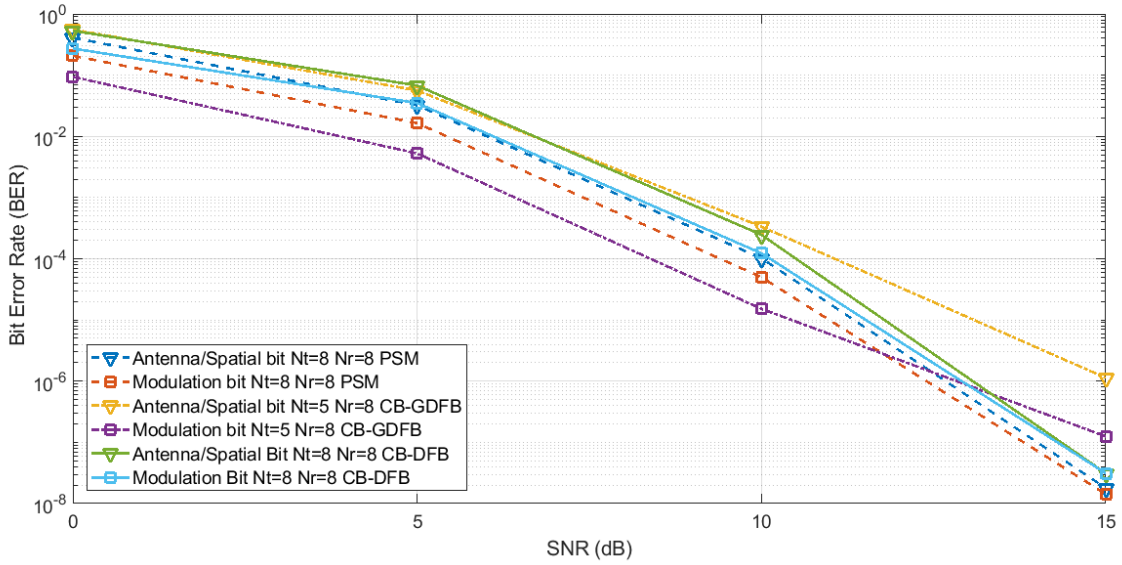

Fig. 4.10: BER comparison among conventional PSM, CB-DFB and CB-GDFB at 4 bits/interval

4.6. Complexity Comparison and Transmit Antenna Reduction of CB-GDFB vs CB-DFB

The computational complexity of the CB-GDFB receiver is calculated in this section. As shown in last section, the CB-GDFB scheme overcomes the need of using higher modulation constellation for the same transmit antenna array and thus resulting in better BER compared to the CB-DFB scheme. In other words, in CB-GDFB scheme a higher throughput is achieved with a smaller number of transmit antennas (and hence a smaller number of initial reference symbols) and a smaller modulation constellation. We have compared CB-DFB scheme with DSM in Section 3.6 and shown that the complexity grows exponentially in case of the DSM scheme. Now we will see how well CB-GDFB performs compared to CB-DFB in terms of complexity.

Similar to DSM and CB-DFB complexity calculations, we quantify complexity by the number of MADs required in the detection process of each information bit at the receiver. The complexity of the CB-GDFB receiver per encoding block is

$$N_{total,CB-GDFB} = N_B \times N_r \times 2^{\left\lfloor \log_2 \binom{N_t}{2} \right\rfloor} \times N_I + N_B \times N_r \times M \times N_I + N_B \times N_r \times M \times 2^{\left\lfloor \log_2 \binom{N_t}{2} \right\rfloor} \quad (4.23)$$

where N_B is the block size, $2^{\left\lfloor \log_2 \binom{N_t}{2} \right\rfloor}$ is the size of antenna/spatial constellation, and N_I is the number of iterations in the clustering algorithms. The complexity per information bit is expressed as

$$N_{total,CB-GDFB} / bit = N_r \times 2^{\left\lfloor \log_2 \binom{N_t}{2} \right\rfloor} \times N_I + N_r \times M \times N_I + N_r \times M \times 2^{\left\lfloor \log_2 \binom{N_t}{2} \right\rfloor} \quad (4.24)$$

Eqn. (4.24) suggests that the per bit receiver complexity of the CB-GDFB scheme is linear in the number of iterations in the clustering algorithm, and linear in the product of number of receive antennas and the size of antenna/spatial constellation.

The following Table 4.2 compares the receiver complexity of CB-GDFB with that of CB-DFB for different system configurations and different throughput. The minimum number of transmit antenna/initial reference symbols requirement between the two systems is also compared in Table 4.2. From the comparison of Table 4.2 we can see that the receiver computational complexity is linear in both cases and with just a slight increase in CB-GDFB for the cases where CB-DFB uses higher modulation constellation to achieve the same throughput. However, the number of antennas and the initial reference symbols required to achieve the same throughput increases exponentially in case CB-DFB whereas in case of CB-GDFB number of required antennas and initial reference symbols increases linearly with the increase of throughput. As an example, to achieve a throughput of 10 bits/interval, traditional SM, and CB-DFB requires minimum 512 transmit antennas/512 initial reference symbols, while to achieve the same throughput CB-GDFB requires only 33 transmit antennas/33 initial reference symbols or in other words 479 less transmit antennas/less reference symbols for the same modulation constellation. Thus, for higher throughput CB-GDFB performs even better than CB-DFB considering it significantly reduces the number of required transmit antennas as well as initial reference symbols resulting in higher effective throughput compared to CB-DFB.

Throughput, η	**No. of Receive Ants, N_r**	**Size of Mod. Order, M**		**Min No. of required TX / Number of Initial Reference symbols**		**Number of MADs**	
CB-DFB/CB-GDFB	CB-DFB/CB-GDFB	CB-DFB	CB-GDFB	CB-DFB	CB-GDFB	CB-DFB	CB-GDFB
4 bits/interval	4	4	2	4	5	160	184
4 bits/interval	8	2	2	8	5	368	368
5 bits/interval	8	4	2	8	7	544	688
5 bits/interval	16	2	2	16	7	1376	1376
6 bits/interval	32	2	2	32	9	5312	5312
7 bits/interval	64	2	2	64	12	2.1×10^4	2.1×10^4
8 bits/interval	128	2	2	128	17	8.3×10^4	8.3×10^4
10 bits/interval	512	2	2	512	33	1.3×10^6	1.3×10^6

Table 4.2: Per-bit receiver complexity and minimum number of antenna/initial reference symbols requirement comparisons for the same throughput between CB-DFB and CB-GDFB. Number of iterations in both cases was considered as $N_I = 3$.

Chapter 5.

Conclusion and Future Works

Spatial Modulation considers an innovative approach to tackle previous challenges of MIMO. In SM, a new spatial constellation diagram is added and utilized to enhance the throughput while conserving energy resources and receiver computational complexity. The traditional spatial modulation technique was discussed in this thesis along with the differential SM technique. In addition, two novel special modulation techniques were proposed based on clustering algorithm and decision feedback, namely CB-DFB and CB-GDFB.

In traditional coherent SM techniques pilots are transmitted periodically to estimate the channel at the receiver input. However, this leads to a reduction in the effective throughput. To mitigate this issue, DSM, a non-coherent technique, was proposed to avoid the need of channel estimation and periodic pilot transmission. However, the computational complexity of DSM becomes impractical even for a moderate antenna array. The CB-DFB scheme proposes a novel channel estimation method based on clustering and decision feedback. It has been shown that this method of channel estimation performs similar to that of non-coherent spatial modulation technique, DSM, in terms of bit error rate and outperforms it by a significant margin in terms of the receiver complexity. When compared to conventional pilot-aided spatial modulation technique, our proposed method performs to some extent poorer and that is because a reduced number of reference symbols are used in case of CB-DFB. But, that also means more available slots to convey information-carrying symbols for the CB-DFB scheme resulting in a much higher effective throughput.

The second proposed technique generalizes the CB-DFB and overcomes some of the constraints of traditional SM techniques. In traditional SM techniques it is necessary for the number of transmit antennas to be power of two. CB-GDFB overcomes that by activating more than one antenna at any time instant while also maintaining the single-RF property of the SM. Additionally, CB-GDFB increases the overall throughput by base-

two logarithm of the number of antenna combinations. Thus, the number of transmit antennas required to achieve any particular throughput is reduced. As a result, the number of initial reference symbols required for the CB-GDFB scheme also gets reduced, meaning even more available slots in the data block to convey information-carrying symbols and thus resulting in a higher effective throughput compared to CB-DFB scheme. It has also been shown that the gap between the number of required transmit antennas for CB-GDFB, and traditional SM transmission techniques widens significantly with the increase of throughput.

Future Works

A lot of theoretical analysis of the spatial modulation techniques have been conducted so far. However, a major promise made by the spatial modulation technique is to simplify hardware designs which leads to reduced energy consumption, computation power, and hardware cost. Until now hardware designs and practical implementations of SM techniques have not been realized in literature. Recently, some analysis of hardware cost for different spatial modulation techniques was addressed in [38]. This literature also proved by practical implementation that all the SM techniques can indeed operate with a maximum of only one RF-chain. However, the impact of the hardware components on the performance of the SM techniques needs to be addressed yet. Besides, it is also necessary to design RF components tailored to the specific needs of some of the spatial modulation techniques such as QSSK, so that its practical implementation with just single-RF is possible.

References

[1] G. Li *et al.*, “Energy-efficient wireless communications: tutorial, survey, and open issues,” *IEEE Wirel. Commun.*, vol. 18, no. 6, pp. 28–35, Dec. 2011.

[2] J. G. Andrews *et al.*, “What Will 5G Be?,” *IEEE J. Sel. Areas Commun.*, vol. 32, no. 6, pp. 1065–1082, Jun. 2014.

[3] H. Huang, C. B. Papadias, and S. Venkatesan, *MIMO Communication for Cellular Networks*, Boston, MA: Springer US, 2012.

[4] Z. Hasan, H. Boostanimehr, and V. K. Bhargava, “Green Cellular Networks: A Survey, Some Research Issues and Challenges,” *IEEE Commun. Surv. Tutor.*, vol. 13, no. 4, pp. 524–540, Nov. 2011.

[5] D. Persson, T. Eriksson, and E. G. Larsson, “Amplifier-Aware Multiple-Input Multiple-Output Power Allocation,” *IEEE Commun. Lett.*, vol. 17, no. 6, pp. 1112–1115, Jun. 2013.

[6] A. Mohammadi and F. M. Ghannouchi, “Single RF Front-End MIMO Transceivers,” *IEEE Commun. Mag.*, vol. 49, no. 12, pp. 104-109, Dec. 2011.

[7] J. Jeganathan, A. Ghrayeb, L. Szczecinski, and A. Ceron, “Space shift keying modulation for MIMO channels,” *IEEE Trans. Wirel. Commun.*, vol. 8, no. 7, pp. 3692–3703, Jul. 2009.

[8] R. Bohnke, D. Wubben, V. Kuhn, and K.-D. Kammeyer, “Reduced complexity MMSE detection for BLAST architectures,” *IEEE Global Telecom.Conf.,* San Francisco, pp. 2258–2262, 1-5 Dec. 2003.

[9] S. M. Alamouti, “A Simple Transmit Diversity Technique for Wireless Communications,” *IEEE Journal on Selec. Areas in Commun.,* vol. 16, no. 8, pp. 1451-1458, Oct 1998.

[10] R. Mesleh, H. Haas, Yeonwoo. Lee, and Sangboh Yun, “Interchannel Interference Avoidance in MIMO Transmission by Exploiting Spatial Information,” IEEE *19th Int. Symp. On Per., Ind., and Mob. Rad. Commun.*, Berlin, 11-14 Sept. 2005.

[11] A. F. Molisch and M. Z. Win, “MIMO systems with antenna selection,” *IEEE Microw. Mag.*, vol. 5, no. 1, pp. 46–56, Aug. 2004.

[12] A. Kalis, A. Kanatas, and C. Papadias, “A Novel Approach to MIMO Transmission Using a Single RF Front End,” *IEEE J. Sel. Areas Commun.*, vol. 26, no. 6, pp. 972–980, Aug. 2008.

[13] M. Di Renzo, H. Haas, A. Ghrayeb, S. Sugiura, and L. Hanzo, “Spatial Modulation for Generalized MIMO: Challenges, Opportunities, and Implementation,” *Proc. IEEE*, vol. 102, no. 1, pp. 56–103, Jan. 2014.

[14] M. Renzo, H. Haas, and P. Grant, “Spatial modulation for multiple-antenna wireless systems: a survey,” *IEEE Commun. Mag.*, vol. 49, no. 12, pp. 182–191, Dec. 2011.

[15] Yuli Yang and Bingli Jiao, “Information-guided channel-hopping for high data rate wireless communication,” *IEEE Commun. Lett.*, vol. 12, no. 4, pp. 225–227, Apr. 2008.

[16] R. Mesleh, H. Haas, Sinan Sinanovic, Chang Wook Ahn, and Sangboh Yun, “Spatial Modulation,” *IEEE Trans. On Vehic. Technol.*, vol. 57, no. 4, pp. 2228-2241, Jul. 2008

[17] J. Jeganathan, A. Ghrayeb, and L. Szczecinski, “Spatial modulation: optimal detection and performance analysis,” *IEEE Commun. Lett.*, vol. 12, no. 8, pp. 545–547, Aug. 2008.

[18] R. Mesleh, S. S. Ikki, and H. M. Aggoune, “Quadrature Spatial Modulation,” *IEEE Trans. Veh. Technol.*, vol. 64, no. 6, pp. 2738–2742, Jun. 2015.

[19] E. Basar, U. Aygolu, E. Panayirci, and H. V. Poor, "Space-Time Block Coded Spatial Modulation," *IEEE Trans. Commun.*, vol. 59, no. 3, pp. 823–832, Mar. 2011.

[20] Y. Bian, X. Cheng, M. Wen, L. Yang, H. V. Poor, and B. Jiao, "Differential Spatial Modulation," *IEEE Trans. Veh. Technol.*, pp. 1, Jul. 2015.

[21] M. Di Renzo, D. De Leonardis, F. Graziosi, and H. Haas, "Space Shift Keying (SSK—) MIMO with Practical Channel Estimates," *IEEE Trans. Commun.*, vol. 60, no. 4, pp. 998–1012, Apr. 2012.

[22] M. D. Renzo and H. Haas, "Space Shift Keying (SSK) MIMO over Correlated Rician Fading Channels: Performance Analysis And a New Method for Transmit-Diversity," *IEEE Trans. Commun.*, vol. 59, no. 1, pp. 116–129, Jan. 2011.

[23] R. Mesleh, H. Haas, C. W. Ahn, and S. Yun, "Spatial Modulation - A New Low Complexity Spectral Efficiency Enhancing Technique," *First Int. Conf. on Commun. and Net.,* Beijing, pp. 1–5, 25-27 Oct. 2006.

[24] X. Wu, H. Claussen, M. Di Renzo, and H. Haas, "Channel Estimation for Spatial Modulation," *IEEE Trans. Commun.*, vol. 62, no. 12, pp. 4362–4372, Dec. 2014.

[25] Yuyang Bian, Miaowen Wen, Xiang Cheng, H. V. Poor, and Bingli Jiao, "A differential scheme for Spatial Modulation," *IEEE Global Commun. Conf.,* Atlanta, pp. 3925–3930, 9-13 Dec. 2013.

[26] S. Sugiura, S. Chen, and L. Hanzo, "Coherent and Differential Space-Time Shift Keying: A Dispersion Matrix Approach," *IEEE Trans. Commun.*, vol. 58, no. 11, pp. 3219–3230, Nov. 2010.

[27] J. Mietzner, R. Schober, L. Lampe, W. Gerstacker, and P. Hoeher, "Multiple-antenna techniques for wireless communications - a comprehensive literature survey," *IEEE Commun. Surv. Tutor.*, vol. 11, no. 2, pp. 87–105, Jun. 2009.

[28] P. W. Wolniansky, G. J. Foschini, G. D. Golden, and R. A. Valenzuela, "V-BLAST: an architecture for realizing very high data rates over the rich-scattering wireless

channel," *URSI Inter. Sym. on Sig., Sys., and Electron. Conf., Pisa,* Italy, pp. 295–300, 2 Oct. 1998

[29] G. Auer *et al.*, "Cellular Energy Efficiency Evaluation Framework," *IEEE 73rd Vehic. Technol. Conf.*, pp. 1–6, Yokohama, Japan, 15-18 May 2011.

[30] F. Heliot, M. A. Imran, and R. Tafazolli, "On the Energy Efficiency-Spectral Efficiency Trade-off over the MIMO Rayleigh Fading Channel," *IEEE Trans. Commun.*, vol. 60, no. 5, pp. 1345–1356, May 2012.

[31] E. Larsson, O. Edfors, F. Tufvesson, and T. Marzetta, "Massive MIMO for next generation wireless systems," *IEEE Commun. Mag.*, vol. 52, no. 2, pp. 186–195, Feb. 2014.

[32] Q. Li and Y. P. Zhang, "CMOS T/R Switch Design: Towards Ultra-Wideband and Higher Frequency," *IEEE J. Solid-State Circuits*, vol. 42, no. 3, pp. 563–570, Mar. 2007.

[33] V. Tarokh, "A Differential Detection Scheme for Transmit Diversity," *IEEE J. Sel. AREAS Commun.*, vol. 18, no. 7, p. 6, Jul. 2000.

[34] M. Biguesh and A. B. Gershman, "Training-based MIMO channel estimation: a study of estimator tradeoffs and optimal training signals," *IEEE Trans. Signal Process.*, vol. 54, no. 3, pp. 884–893, Mar. 2006.

[35] A. Younis, N. Serafimovski, R. Mesleh, and H. Haas, "Generalised spatial modulation,"44th Asilomar Conf. on Sig., Sys., and Comp., pp. 1498–1502, 7-10 Nov. 2010.

[36] J. Jeganathan, A. Ghrayeb, and L. Szczecinski, "Generalized space shift keying modulation for MIMO channels," IEEE *19th Int. Symp. on Per., Ind., and Mob. Rad. Commun*., Cannes, France, pp. 1–5, 15-18 Sept. 2008.

[37] J. Wang, S. Jia, and J. Song, “Generalised Spatial Modulation System with Multiple Active Transmit Antennas and Low Complexity Detection Scheme,” *IEEE Trans. Wirel. Commun.*, vol. 11, no. 4, pp. 1605–1615, Apr. 2012.

[38] R. Mesleh, O. Hiari, A. Younis, and S. Alouneh, “Transmitter Design and Hardware Considerations for Different Space Modulation Techniques,” *IEEE Trans. Wirel. Commun.*, vol. 16, no. 11, pp. 7512–7522, Nov. 2017.

[39] J. G. Proakis and M. Salehi, *Digital communications*, 5th ed. Boston: McGraw-Hill, 2008.

[40] M. Simon and M.-S. Alouini, *Digital Communication over Fading Channels.* Somerset: Wiley, 2000.

[41] M.-S. Alouini and A. J. Goldsmith, “A Unified Approach for Calculating Error Rates of Linearly Modulated Signals over Generalized Fading Channels,” *IEEE Trans. Commun.*, vol. 47, no. 9, pp. 1324 - 1334, Sept. 1999.

[42] I. S. Gradshteĭn, I. M. Ryzhik, and A. Jeffrey, *Table of integrals, series, and products*, 7th ed. Amsterdam ; Boston: Academic Press, 2007.

[43] R. Mesleh; A. Alhassi, *Space Modulation Techniques*, 1st ed. Wiley Telecom, John Wiley & Sons, Inc., 2018.

Appendix.

Average Bit Error Probability Analysis

The derivation of the average bit error probability for the spatial modulation technique can be computed by deriving the pairwise error probability (PEP). The PEP can be defined as the error probability that transmitted antenna/spatial and modulation symbols, $\mathbf{h}_l$ and s_t are received as another antenna/spatial and modulation symbols, $\mathbf{h}_{\hat{l}}$ and $s_{\hat{t}}$ respectively, and is given by $PEP((\mathbf{h}_l, s_t) \rightarrow (\mathbf{h}_{\hat{l}}, s_{\hat{t}}))$ [39].

The assumption of perfect channel knowledge at the receiver is impractical. In practical wireless systems, pilots are transmitted to estimate the channel at the receiver input. Similar to the transmitted data, transmitted pilots are corrupted by the additive white Gaussian noise (AWGN) at the receiver input, which leads to mismatch between exact channel and estimated channel. The difference between these two is generally called channel estimation errors (CSE). In the presence of CSE, the ML-optimum receiver for SM is given by

$$[\hat{\tilde{\mathbf{h}}}_l, \hat{s}_t] = \arg \min_{\substack{\tilde{\mathbf{h}}_{\hat{l}} \in \tilde{\mathbf{h}} \\ s_{\hat{t}} \in s}} \left\| \mathbf{y} - \tilde{\mathbf{h}}_{\hat{l}} s_{\hat{t}} \right\|_F^2 \tag{A.1}$$

where $\tilde{\mathbf{h}}_l$ is the l -th element of the N_t -length channel vector $\tilde{\mathbf{h}}$. Thus, PEP for SM in the presence of CSE is given by

$$
\begin{aligned}
\Pr_{Error} &= \Pr((\tilde{\mathbf{h}}_l, s_t) \to (\tilde{\mathbf{h}}_{\hat{l}}, s_{\hat{t}}) \mid \tilde{\mathbf{h}}) \\
&= \Pr(\left| y - \tilde{\mathbf{h}}_l s_t \right|^2 > \left| y - \tilde{\mathbf{h}}_{\hat{l}} s_{\hat{t}} \right|^2 \left| \tilde{\mathbf{h}} \right.) \\
&= \Pr(\left| (\mathbf{h}_l s_t + \mathbf{n}) - \tilde{\mathbf{h}}_l s_t \right|^2 > \left| (\mathbf{h}_l s_t + \mathbf{n}) - \tilde{\mathbf{h}}_{\hat{l}} s_{\hat{t}} \right|^2 \left| \tilde{\mathbf{h}} \right.) \\
&= \Pr(\left| ((\tilde{\mathbf{h}}_l + e) - \tilde{\mathbf{h}}_l) s_t + \mathbf{n} \right|^2 > \left| ((\tilde{\mathbf{h}}_l + e) s_t + \mathbf{n}) - \tilde{\mathbf{h}}_{\hat{l}} s_{\hat{t}} \right|^2 \left| \tilde{\mathbf{h}} \right.) \\
&= \Pr(\left| e s_t + \mathbf{n} \right|^2 > \left| (\tilde{\mathbf{h}}_l s_t - \tilde{\mathbf{h}}_{\hat{l}} s_{\hat{t}}) + (e s_t + \mathbf{n}) \right|^2 \left| \tilde{\mathbf{h}} \right.) \\
&= \Pr(\left| \bar{\mathbf{n}} \right|^2 > (\left| \tilde{\mathbf{h}}_l s_t - \tilde{\mathbf{h}}_{\hat{l}} s_{\hat{t}} \right|^2 - 2\,\mathrm{Re}\{\bar{\mathbf{n}}^* (\tilde{\mathbf{h}}_l s_t - \tilde{\mathbf{h}}_{\hat{l}} s_{\hat{t}})\} + \left| \bar{\mathbf{n}} \right|^2) \left| \tilde{\mathbf{h}} \right.) \\
&= \Pr(2\,\mathrm{Re}\{\bar{\mathbf{n}}^* (\tilde{\mathbf{h}}_l s_t - \tilde{\mathbf{h}}_{\hat{l}} s_{\hat{t}})\} > \left| \tilde{\mathbf{h}}_l s_t - \tilde{\mathbf{h}}_{\hat{l}} s_{\hat{t}} \right|^2 \left| \tilde{\mathbf{h}} \right.) \\
&= \mathbf{Q}(\sqrt{\frac{\sigma_h{}^2 \left| \tilde{\mathbf{h}}_l s_t - \tilde{\mathbf{h}}_{\hat{l}} s_{\hat{t}} \right|^2}{2(\sigma_e^2 \left| s_t \right|^2 + 1)}}) = Q(\sqrt{\gamma_e^{SM}})
\end{aligned}
\tag{A.2}
$$

where $\bar{\mathbf{n}} = e s_t + \mathbf{n}$ is complex Gaussian random variable with zero mean and variance $(\sigma_e^2 \left| s_t \right|^2 + 1)$. Moreover,

$$
\gamma_e^{SM} = \frac{\sigma_h{}^2 \left| \tilde{\mathbf{h}}_\mathbf{l} s_t - \tilde{\mathbf{h}}_{\hat{l}} s_{\hat{t}} \right|^2}{2(\sigma_e^2 \left| s_t \right|^2 + 1)} \tag{A.3}
$$

is an exponential random variable with a mean value

$$
\bar{\gamma}_e^{SM} = \frac{\sigma_h{}^2 + \sigma_e^2}{2(\sigma_e^2 \left| s_t \right|^2 + 1)} \times \begin{cases} \left| s_t - s_{\hat{t}} \right| & if\ \ \hat{l} = l \\ \left| s_t \right|^2 + \left| s_{\hat{t}} \right|^2 & if\ \ \hat{l} \neq l \end{cases} \tag{A.4}
$$

Therefore, the average PEP is

$$
\Pr((\tilde{\mathbf{h}}_l, s_t) \to (\tilde{\mathbf{h}}_{\hat{l}}, s_{\hat{t}})) = \frac{1}{2}(1 - \sqrt{\frac{\bar{\gamma}_e^{SM}}{1 + \bar{\gamma}_e^{SM}}}) \tag{A.5}
$$

The above formula is obtained for an exponential random variable form [40], [41] as

$$E_{\gamma_e}\left\{Q(\sqrt{\gamma_e}\right\} = \int_{\gamma_e} P_{\gamma_e}(\gamma_e)Q(\sqrt{\gamma_e})d\gamma_e = \int_{\gamma_e} \frac{1}{\overline{\gamma}_e}\exp(-\frac{\gamma_e}{\overline{\gamma}_e})Q(\sqrt{\gamma_e})d\gamma_e$$
$$= \frac{1}{2}\left(1 - \sqrt{\frac{\overline{\gamma}_e/2}{1+\overline{\gamma}_e/2}}\right) \tag{A.6}$$

The above PEP is calculated assuming $N_r = 1$, receive antenna. For an arbitrary number of receive antennas N_r, the PEP is given by

$$\Pr_{error} = Q\left(\sqrt{\sum_{r=1}^{N_r}\gamma_{e,r}^{SM}}\right) = Q(\sqrt{v_e^{SM}}) \tag{A.7}$$

where $v_e^{SM} = \sum_{r=1}^{N_r}\gamma_{e,r}^{SM}$ is a chi-squared random variable RV with a PDF

$$P_{v_e^{SM}}(v_e^{SM}) = \frac{1}{\Gamma(N_r)(\overline{\gamma}_e^{SM})^{N_r}}(v_e^{SM})^{N_r-1}\exp(-\frac{v_e^{SM}}{\overline{\gamma}_e^{SM}}) \tag{A.8}$$

and

$$\gamma_{e,r}^{SM} = \frac{\sigma_h{}^2\left|\tilde{\mathbf{h}}_{l,r}s_t - \tilde{\mathbf{h}}_{\hat{l},r}s_{\hat{t}}\right|^2}{2(\sigma_e^2\left|s_t\right|^2+1)} \tag{A.9}$$

where $\tilde{\mathbf{h}}_{l,r}$ is the r th element of the N_r -length channel vector $\tilde{\mathbf{h}}_l$, and $\tilde{\mathbf{h}}_l$ is the lth vector of the $N_r \times N_t$ estimated channel matrix $\tilde{\mathbf{H}}$. Thus, the average PEP is given by [40], [42],

$$\Pr((\mathbf{h}_l, s_t) \to (\tilde{\mathbf{h}}_{\hat{l}}, s_{\hat{t}})) = (\alpha_{a,e}^{SM})^{N_r}\sum_{i=0}^{N_r-1}\binom{N_r-1+i}{i}[1-\alpha_{a,e}^{SM}]^i \tag{A.10}$$

where

$$\alpha_{a,e}^{SM} = \frac{1}{2}(1 - \sqrt{\frac{\overline{\gamma}_e^{SM}/2}{1+\overline{\gamma}_e^{SM}/2}})$$

Finally, the ABER for SM over MIMO Rayleigh fading channels in the presence of CSE can be computed using the union bounding technique as [39]

$$\begin{aligned} ABER &\le \sum_{l=1}^{N_t}\sum_{t=1}^{M}\sum_{\hat{l}=1}^{N_t}\sum_{\hat{t}=1}^{M}\frac{e_{\hat{l},\hat{t}}^{l,t}\Pr((\mathbf{h}_l, s_t)\to(\tilde{\mathbf{h}}_{\hat{l}}, s_{\hat{t}}))}{N_t M} \\ &= \sum_{l=1}^{N_t}\sum_{t=1}^{M}\sum_{\hat{l}=1}^{N_t}\sum_{\hat{t}=1}^{M}\frac{e_{\hat{l},\hat{t}}^{l,t}(\alpha_{a,e}^{SM})^{N_r}\sum_{i=0}^{N_r-1}\binom{N_r-1+i}{i}[1-\alpha_{a,e}^{SM}]^i}{N_t M} \end{aligned} \tag{A.11}$$

where $e_{\hat{l},\hat{t}}^{l,t}$ is the number of bits in error between the symbol $\mathbf{h}_l, s_t$ and $\mathbf{h}_{\hat{l}}, s_{\hat{t}}$.